University of California
Santa Barbara

Structuring light to manipulate multipolar resonances for metamaterial applications

A dissertation submitted in partial satisfaction
of the requirements for the degree

Doctor of Philosophy
in
Electrical and Computer Engineering

by

Tanya Das

Committee in charge:

Professor Jon Schuller, Chair
Professor John Bowers
Professor Nadir Dagli
Professor Ania Jayich

September 2017

The Dissertation of Tanya Das is approved.

Professor John Bowers

Professor Nadir Dagli

Professor Ania Jayich

Professor Jon Schuller, Committee Chair

June 2017

Structuring light to manipulate multipolar resonances for metamaterial applications

For my parents.

Acknowledgements

There are many people without whose help and support this work would not be possible. First and foremost, I want to thank my advisor, Professor Jon Schuller, for his patience and guidance throughout the last five years. I especially want to thank him for giving me freedom to pursue my interests and for teaching me to think critically. I want to thank every one of the members of my research group, Nikita, Ryan, Prasad, Steve, and Tomer, for making my time at UCSB extremely enjoyable. I could not have asked for a better group of people to see every day. I also want to thank Professor Luke Theogarajan for being a wonderful mentor to me during my first years at UCSB.

I would never have gotten to where I am today without the amazing people at the Center for Science and Engineering Partnerships who seamlessly enfolded me into their warm and supportive group. I especially want to thank two people at CSEP. Arica, for being the first person who made me believe that I could take my career interests seriously, and for consistently reminding me of that throughout my time at UCSB. And Lubi, for helping me actually realize those dreams, and for being an incredible boss, mentor, and friend.

I want to thank the many friends I have made at UCSB for the unforgettable memories they have given me over the last few years. I also want to thank all my friends from Michigan, especially the Butts.

Of course, I want to thank my parents and my sister. I am grateful to my parents for their continuous support of me since age zero and I am grateful to my sister for always keeping me grounded.

And, lastly, I want to thank Advait. Starting from that first quantum mechanics class through to the end of my PhD, he has been a consistent best friend.

Thank you to all of you.

Curriculum Vitæ

Tanya Das

Education

2017	Ph.D. in Electrical and Computer Engineering University of California, Santa Barbara
2013	M.S. in Electrical and Computer Engineering University of California, Santa Barbara
2011	B.S. in Electrical Engineering University of Michigan, Ann Arbor

Publications

1. **Tanya Das** and Jon A. Schuller, "Dark modes and field enhancements in dielectric dimers illuminated by cylindrical vector beams," *Physical Review B*, 95 (20), 201111, (2017).
2. Tyler Susko, Ilan Ben-Yaacov, **Tanya Das**, Francesco Bullo, Lubi Lenaburg, "A coupled course design to strengthen multidisciplinary engineering capstone design projects," *ASEE Annual Conference*, (2016)
3. **Tanya Das**, Lubi Lenaburg, Tyler Susko, "Assessment of an Undergraduate Engineering Design Capstone Course," *ASEE Pacific Southwest Conference*, (2016)
4. **Tanya Das**, Prasad P. Iyer, Ryan A. DeCrescent, and Jon A. Schuller, "Beam engineering for selective and enhanced coupling to multipolar resonances," *Physical Review B*, 92 (24), 241110, (2015).
5. Justin M. Foley, Anne M. Itsuno, **Tanya Das**, Silviu Velicu, and Jamie D. Phillips, "Broadband long-wavelength infrared Si/SiO_2 subwavelength grating reflector," *Optics Letters*, 37 (9), 1523-1525, (2012).

Research Experience

- Graduate student researcher at University of California, Santa Barbara, Schuller Research Group, March 2012 – June 2017: Developed a new fundamental understanding of multipolar light-matter interactions based on the illuminating beam
- Graduate student intern at Jet Propulsion Laboratory, Infrared Research Group, July – Sept. 2012: Developed computer code to experimentally test and characterize infrared cameras
- Graduate student intern at NASA Ames, Robotics Academy, June – Aug. 2011: Designed, built, and tested electronics system for lunar exploration robot with a team of interns

- Undergraduate student researcher at University of Michigan, Ann Arbor, Phillips Research Group, May 2010 – Sept. 2011: Modeled effects of structural imperfections on performance of interferometer, a device used to optically characterize materials
- Undergraduate student intern at NASA Ames, Robotics Academy, June – Aug. 2009: Designed, built, and tested electronics system for lunar exploration robot with a team of interns
- Undergraduate student researcher at University of Michigan, Ann Arbor, Roger DeRoo Research Group, Sept. 2008 – May 2009: Programmed a microprocessor to wirelessly report atmospheric data to a host computer

Selected Extracurricular Activities

- Graduate student evaluator at University of California, Santa Barbara, Center for Science and Engineering Partnerships, May 2015 – May 2017: Evaluated engineering curricula and programs
- Beyond Academia conference planning committee, Mar. 2015 – June 2016: Organized conference aimed at helping graduate students explore and pursue careers outside of academia
- Poetry workshop founder at Santa Barbara Juvenile Probation Center, Mar. – June 2014: Founded program and led weekly workshops to help criminal teens use poetry to work through personal issues
- Graduate Students for Diversity in Science, Nov. 2014 – June 2017: Developed introductory GRE course for California State University students pursuing STEM Ph.D. degrees

Selected Honors and Awards

- SIPE/OSA (AAAS) Arthur H. Guenther Congressional Fellowship 2017
- Michael Pate Optical Sciences Memorial Scholarship 2016
- UCSB Broida-Hirschfelder Disseratation Fellowship 2016
- AAAS Meeting Student Poster Award in Education 2016
- MRS Spring Meeting Student Poster Award in Resonant Optics 2014
- California Space Grant Award 2012
- Michigan Space Grant Award 2010
- Cisco Internet Generation Award 2009
- Sharon Postnieks Scholarship for Women in Science and Engineering 2007

Abstract

Structuring light to manipulate multipolar resonances for metamaterial applications

by

Tanya Das

Multipolar electromagnetic phenomena in sub-wavelength resonators are at the heart of metamaterial science and technology. Typically, researchers engineer multipolar light-matter interactions by modifying the size, shape, and composition of the resonators. Here, we instead engineer multipolar interactions by modifying properties of the incident radiation. In this dissertation, we propose a new framework for determining the scattering response of resonators based on properties of the local excitation field.

First, we derive an analytical theory to determine the scattering response of spherical nanoparticles under any type of illumination. Using this theory, we demonstrate the ability to drastically manipulate the scattering properties of a spherical nanoparticle by varying the illumination and demonstrate excitation of a longitudinal quadrupole mode that cannot be accessed with conventional illumination. Next, we investigate the response of dielectric dimer structures illuminated by cylindrical vector beams. Using finite-difference time-domain simulations, we demonstrate significant modification of the scattering spectra of dimer antennas and reveal how the illumination condition gives rise to these spectra through manipulation of electric and magnetic mode hybridization. Finally, we present a simple and efficient numerical simulation based on local field principles for extracting the multipolar response of any resonator under illumination by structured light. This dissertation enhances the understanding of fundamental light-matter interactions in metamaterials and lays the foundation for researchers to identify, quantify, and manipulate multipolar light-matter interactions through optical beam engineering.

Contents

List of Figures

List of Tables

Chapter 1

Introduction

The word *metamaterial* comes from the Greek word *meta* meaning "beyond." Hence, metamaterials refer to materials that have light manipulating properties that go beyond those of naturally-occurring materials. Metamaterials enable unique applications such as invisibility cloaks [3, 4, 5], optical antennas [6, 7, 8], negative refractive index materials [9], and superlenses capable of imaging beyond the diffraction limit [10].

Metamaterials derive their unique properties from the collective interference of electromagnetic fields in arrays of sub-wavelength particles. Such particles, when excited by light, exhibit a series of resonances in wavelength space, called multipolar resonances, that can be characterized as electric and magnetic in nature, along with a mode order (dipole, quadrupole, hexapole, etc.). In order to engineer the response of these particles, researchers typically focus on manipulating their physical properties such as their size, shape, and composition [11, 10, 12]. However, the other part of this interaction – the light – is typically completely ignored, and researchers exclusively use plane wave illumination for metamaterial design. The focus of this thesis is instead to manipulate the properties of the illumination beam to uncover new metamaterial phenomena that are inaccessible by conventional plane wave illumination. Existing work in exploring the effects of illu-

mination are limited in scope to plasmonic antennas [13, 14, 15, 16], with a few studies on single dielectric particles [2, 17, 18]. However, much remains to be explored on the utility and scope of engineering the illumination beam in designing new metmaterials.

This dissertation explores the use of exotic illumination schemes in exposing new metamaterial phenomena. First, chapter 2 introduces a new analytical framework for determining the multipolar response of a spherical particle under illumination by any arbitrary illumination beam, known as the local field theory. Chapter 3 applies the local field expressions to uncover the scattering response of a spherical particle under illumination by cylindrical vector beams, and shows how engineering of the illumination beam can achieve selective excitation of individual multipolar modes. Chapter 4 explores the response of a dimer antenna to cylindrical vector beams, and shows that such systems can be used to generate unprecedented magnetic field enhancement and coupling to dark modes. Finally, chapter 5 presents a numerical implementation of the analytical local field theory as a method for efficiently and quickly determining the scattering response of arbitrary particles under any type of illumination.

Chapter 2

Analytical local field theory

In this chapter, we rigorously derive a simplified, analytical method to quantify multipolar light absorption and scattering for a spherical nanoparticle (NP) illuminated by any light source of interest, deemed the local field theory. We prove that dipolar and quadrupolar interactions depend only on local fields or field gradients respectively. The expressions derived in this chapter describe the scattering, absorption, and extinction of a spherical nanoparticle of any size and composition within a homogenous medium, under illumination by any kind of beam.

2.1 Background

The basis for metamaterial design centers on an analytical theory known as Mie theory, formulated by Gustav Mie in 1908 [19]. Mie theory analytically describes the interaction between a linearly polarized plane wave and a spherical particle of any size and composition within a homogenous medium. First, the plane wave is expanded into spherical vector harmonics (SVHs), a complete basis set for

Conventionally, scattering and absorption of spherical nanoparticles (NPs) under arbitrary types of illumination are calculated with Generalized Lorenz Mie theory (GLMT) [20], which involves expressing an incident beam as a plane wave or spherical wave expansion [21]. These expansions require knowing the electric field everywhere on a planar $[\mathbf{E}(x, y, z = z_0)]$ or spherical $[\mathbf{E}(\theta, \phi, r = r_0)]$ surface respectively. This approach is complete, and can be used to describe interactions with spherical NPs of any size or composition. However, NPs used in plasmonics or metamaterials are typically in a size regime where only dipolar and quadrupolar modes contribute to the optical response. For these cases, we derive a greatly simplified approach for calculating scattering and absorption in inhomogeneous fields, inspired by the multipolar interaction Hamiltonian [22, 23, 24, 25, 26, 27], given as,

$$H = \underbrace{-\mathbf{p} \cdot \mathbf{E}(\mathbf{r}_p)}_{\text{ED}} - \underbrace{\mathbf{m} \cdot \mathbf{H}(\mathbf{r}_p)}_{\text{MD}} - \underbrace{[\overleftrightarrow{\mathbf{Q}} \nabla] \cdot \mathbf{E}(\mathbf{r}_p)}_{\text{EQ}} - \underbrace{[\overleftrightarrow{\mathbf{G}} \nabla] \cdot \mathbf{H}(\mathbf{r}_p)}_{\text{MQ}} ... \tag{2.1}$$

The light-matter interaction energy is described by a collection of multipolar terms, corresponding to electric dipole (ED), magnetic dipole (MD), electric quadrupole (EQ), and magnetic quadrupole (MQ) interactions. Each interaction term depends on a light-independent multipole moment ($\mathbf{p}$ for ED, $\mathbf{m}$ for MD, etc.), as well as a matter-independent electromagnetic field quantity ($\mathbf{E}$ is the electric field, and $\mathbf{H}$ is the magnetic field) that

only depends on the local field at the NP center ($\mathbf{r}_p$), which can be placed at any point of interest within the inhomogeneous field distribution. These principles are combined with Mie Theory [28] to rigorously derive simple local-field relations that fully describe the dipolar and quadrupolar scattering interaction of NPs in inhomogeneous fields. These derivations are given in the next section.

2.2 Electromagnetic fields radiated by a sphere under arbitrary illumination

In this section, expressions are derived for the internal and scattered electric and magnetic fields of a spherical particle under illumination by an arbitrary incident beam. Expressions for the electric and magnetic fields of the arbitrary incident beams are also derived, and are expressed both as a summation plane waves (plane wave spectrum, or PWS), and a subsequent expansion into SVHs.

2.2.1 Incident electric and magnetic fields

Any arbitrary incident beam can be expressed as a summation of plane waves, as is the convention in the plane wave spectrum technique [29, 21]. The angular spectrum representation [30] of such a beam is given as,

$$\mathbf{E}_{inc}(\mathbf{r}) = \int_0^{2\pi} \int_0^{\alpha} \widehat{E}(\theta,\phi) e^{i\mathbf{k}\cdot\mathbf{r}} \sin\theta d\theta d\phi \tag{2.2}$$

Here, $\widehat{E}(\theta,\phi)$ is the angular spectrum for the incident beam, $\mathbf{k}\cdot\mathbf{r} = k(\sin\theta\cos\phi x + \sin\theta\sin\phi y + \cos\theta z)$ where k is the wavenumber of the wave in the medium, and α is the collection angle of a lens for a focused wave. The vector $\mathbf{r}$ describes the position of the nano particle (NP) within the beam. This integral may be consequently converted to a

summation as,

$$\mathbf{E}\ (\mathbf{r}) = \lim_{N_\theta, N_\phi \to \infty} \sum_{i=1}^{N_\theta} \sum_{j=1}^{N_\phi} \widehat{E}(\theta_i, \phi_i) e^{i\mathbf{k}\cdot\mathbf{r}} d\theta_i d\phi_i \tag{2.3}$$

where $d\theta_i = \frac{\alpha}{N_\theta}$ and $d\phi_i = \frac{2\pi}{N_\phi}$. Taking a finite number of plane waves N_θ and N_ϕ, the integral in equation (2.2) is approximated by a discrete summation of plane waves with varying polarization, angle of incidence, and complex amplitude, each given by a pair of rotation angles θ_i and ϕ_j. By fixing the location of the NP within the beam $\mathbf{r}$, this discrete summation becomes a summation of plane waves with varying polarization and complex amplitude.

The convention in Mie theory, which fully describes the interaction between a plane wave and a spherical NP, is that the plane wave be x-polarized and incident along the z-axis [28]. Here, we describe the incident beam with as a collection of plane waves with arbitrary polarization and angle of incidence. We treat each incident plane wave as if, in a local coordinate system which is specific to each wave, it is x-polarized and incident along the z-axis. Then, using rotation angles, each plane wave in the angular spectrum may be expressed using rotation angles about the y- (θ_p) and z- (ϕ_p) axes, to translate each wave from being polarized along the x-axis and incident along the z-axis in a local coordinate system, to being arbitrarily polarized in a main coordinate system, as depicted in Fig. 2.1. For simplicity, we only consider rotations about the y- and z-axes, but a rotation about the x-axis can be included for completeness.

Using this convention, the the electric field due to the p^{th} plane wave in the summation is given by equation (2.4), in which $\mathbf{k_p}$ is the rotated wave vector expressed in the main coordinate system, defined as $k\left(\sin\theta_p\cos\phi_p\hat{e}_x + \sin\theta_p\sin\phi_p\hat{e}_y + \cos\theta_p\hat{e}_z\right)$ and $E_p^{'}$ is the

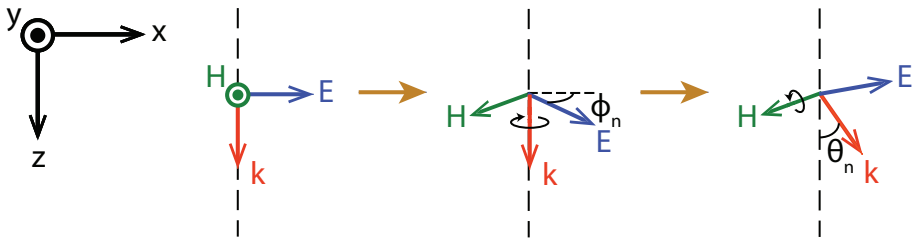

Figure 2.1: In order to translate waves from being polarized along the x-axis and incident along the z-axis in a local coordinate system, to being oriented in some arbitrary direction in a main coordinate system, each plane wave in angular spectrum is described by two rotation angles about the y- and z-axes.

amplitude of the incident plane wave.

$$\mathbf{E}_p = E_p^{'} \left(\cos\theta_p \cos\phi_p \hat{e}_x + \cos\theta_p \sin\phi_p \hat{e}_y - \sin\theta_p \hat{e}_z\right) e^{i\mathbf{k_P}\cdot\mathbf{r}} \tag{2.4}$$

The particle may be located at any point in the incident beam. By fixing this location $\mathbf{r}$, equation (2.4) can be rewritten as,

$$\mathbf{E}_p(\mathbf{r}) = E_p \left(\cos\theta_p \cos\phi_p \hat{e}_x + \cos\theta_p \sin\phi_p \hat{e}_y - \sin\theta_p \hat{e}_z\right) \tag{2.5}$$

where the amplitude of the incident plane wave changes from $E_p^{'}$ to E_p when the location within the beam is fixed. Thus, for a total number of plane waves P, the electric field of the incident beam is given by,

$$\mathbf{E}_{inc}^{PWS} = \sum_{p=1}^{P} E_p \left(\cos\theta_p \cos\phi_p \hat{e}_x + \cos\theta_p \sin\phi_p \hat{e}_y - \sin\theta_p \hat{e}_z\right) \tag{2.6}$$

Alternatively, the plane waves in (2.6) could be expanded into SVHs, and the resulting expression for the electric field of the incident beam is given by,

$$\mathbf{E}_{inc}^{SVH} = \sum_{p=1}^{P} \sum_{l=1}^{\infty} E_l E_p \left(R_{li}^{M} \mathbf{M}_{o1l}^{p} - i R_{li}^{N} \mathbf{N}_{e1l}^{p}\right) \tag{2.7}$$

which is adapted from equation (4.37) in reference [28]. Here, $E_l = i^l \frac{2l+1}{l(l+1)}$, where l refers to the mode order, in the context of Mie Theory. R_{li}^N describes the radial dependence, and is defined as,

$$R_{li,s}^N = \begin{cases} \psi_l'(\rho)/\rho \text{ for incoming } (i) \text{ fields} \\ \xi_l'(\rho)/\rho \text{ for scattered } (s) \text{ fields} \end{cases} \quad R_{li,s}^M = \begin{cases} \psi_l(\rho)/\rho \text{ for incoming } (i) \text{ fields} \\ \xi_l(\rho)/\rho \text{ for scattered } (s) \text{ fields} \end{cases} \tag{2.8}$$

where ψ_l and ξ_l are the Riccati-Bessel functions, and $\rho = kr$. The p superscripts on $\mathbf{M}_{o1l}$ and $\mathbf{N}_{e1l}$ indicate that these SVHs include rotation information, which are defined explicitly in later sections. We ignore the radial vector component of the $\mathbf{N}$ SVHs for simplicity, since only the $\hat{e}_{theta}$ and $\hat{e}_{phi}$ components of the SVHs are needed for our derivations.

Similarly, the magnetic field of the incident beam can be expressed as a summation of plane waves and as a subsequent expansion into SVHs, given by,

$$\mathbf{H}_{inc}^{PWS} = \sum_{p=1}^{P} H_p \left(-\sin\phi_p \hat{e}_x + \cos\phi_p \hat{e}_y\right) \tag{2.9}$$

$$\mathbf{H}_{inc}^{SVH} = -\frac{k}{\omega\mu} \sum_{p=1}^{P} \sum_{l=1}^{\infty} E_l E_p \left(R_{li}^M \mathbf{M}_{e1l}^p + i R_{li}^N \mathbf{N}_{o1l}^p\right) \tag{2.10}$$

2.2.2 Internal and scattered electric and magnetic fields

Using the formulation provided in section 2.2.1, the electric and magnetic fields internal to the particle are given by,

$$\mathbf{E}_{int} = \sum_{p=1}^{P} \sum_{l=1}^{\infty} E_l E_p \left(c_l R_{li}^M \mathbf{M}_{o1l}^p - i d_l R_{li}^N \mathbf{N}_{e1l}^p\right) \tag{2.11}$$

$$\mathbf{H}_{int} = -\frac{k_{np}}{\omega\mu_{np}} \sum_{p=1}^{P} \sum_{l=1}^{\infty} E_l E_p \left(d_l R_{li}^{M} \mathbf{M}_{e1l}^{p} + i c_l R_{li}^{N} \mathbf{N}_{o1l}^{p} \right) \tag{2.12}$$

where k_{np} refers to the wave number inside the particle and μ_{np} refers to the magnetic permeability inside the particle.

Similarly, the scattered electric and magnetic fields are given by,

$$\mathbf{E}_{sca} = \sum_{p=1}^{P} \sum_{l=1}^{\infty} E_l E_p \left(i a_l R_{ls}^{N} \mathbf{N}_{e1l}^{p} - b_l R_{ls}^{M} \mathbf{M}_{o1l}^{p} \right) \tag{2.13}$$

$$\mathbf{H}_{sca} = \frac{k}{\omega\mu} \sum_{p=1}^{P} \sum_{l=1}^{\infty} E_l E_p \left(i b_l R_{ls}^{N} \mathbf{N}_{o1l}^{p} + a_l R_{ls}^{M} \mathbf{M}_{e1l}^{p} \right) \tag{2.14}$$

The coefficients a_l, b_l, c_l and d_l refer to the appropriate Mie coefficients obtained by applying the Maxwell boundary conditions, and are defined in [28]. Using these expressions, the scattered, extinction, and absorbed power may be derived for the dipole and quadrupole modes, given in section 2.3, and are shown to depend on specific field properties for each type of mode.

2.3 Power absorbed and radiated by a sphere under arbitrary illumination

In this section, expressions are provided for the scattered, extinction, and absorbed power of the electric and magnetic dipole and quadrupole modes. The expressions are derived for the electric modes explicitly, while the derivations for the magnetic modes follow straightforwardly from the information contained within. These expressions demonstrate an explicit dependence upon the properties of the illuminating field, where the illuminating field magnitudes are shown to drive the dipole mode interactions, and the illuminating

field gradients are shown to drive the quadrupole mode interactions.

2.3.1 Scattered power: dipole modes

As mentioned previously, the power scattered by the electric dipole mode is derived explicitly, and the expression for the power scattered by the magnetic dipole mode is provided. In order to calculate the power scattered by the electric dipole mode, the scattered electric and magnetic fields for the electric dipole mode are required. These may be obtained from equations (2.13) and (2.14), in which the mode order is chosen as $l = 1$, as these correspond to the dipole modes, and the a_n Mie coefficients are chosen, as these correspond to the electric modes. The resulting expressions for the scattered electric and magnetic fields are given by,

$$\mathbf{E}_{sca}^{ED} = \sum_{p=1}^{P} E_{l=1} E_p \left(i a_1 R_{1s}^N \mathbf{N}_{e11}^p \right) = E_{EDs} \sum_{p=1}^{P} E_p \mathbf{N}_{e11}^p \tag{2.15}$$

$$\mathbf{H}_{sca}^{ED} = \frac{k}{\omega\mu} \sum_{p=1}^{P} E_{l=1} E_p \left(a_1 R_{1s}^M \mathbf{M}_{e11}^p \right) = H_{EDs} \sum_{p=1}^{P} E_p \mathbf{M}_{e11}^p \tag{2.16}$$

where $E_{EDs} = i a_1 E_{l=1} R_{1s}^N = -a_1 \frac{3}{2} \frac{\xi_1'(kr)}{kr}$ and $H_{EDs} = a_1 \frac{k}{\omega\mu} E_{l=1} R_{1s}^M = i a_1 \frac{k}{\omega\mu} \frac{3}{2} \frac{\xi_1(kr)}{kr}$. The notation here differs from [28] in that the radial dependence of the SVHs is expressed independently. The scattered power is then calculated from the scattered electric and magnetic fields as,

$$P_{sca} = \frac{1}{2} \mathrm{Re} \int_0^{2\pi} \int_0^{\pi} (E_{s\theta} H_{s\phi}^* - E_{s\phi} H_{s\theta}^*) r^2 \sin\theta d\theta d\phi \tag{2.17}$$

Using equations (2.15) and (2.16) in (2.17) gives (2.18),

$$P_{sca}^{ED} = \frac{1}{2}\text{Re } E_{EDs}H_{EDs}^{*}\int_{0}^{2\pi}\int_{0}^{\pi}\left[\left(E_1 N_{e11\theta}^{1} + ... + E_P N_{e11\theta}^{P}\right)\left(E_1^{*} M_{e11\phi}^{1*} + ... + E_P^{*} M_{e11\phi}^{P*}\right)\right.$$
$$\left. - \left(E_1 N_{e11\phi}^{1} + ... + E_P N_{e11\phi}^{P}\right)\left(E_1^{*} M_{e11\theta}^{1*} + ... + E_P^{*} M_{e11\theta}^{P*}\right)\right] r^2 \sin\theta d\theta d\phi \tag{2.18}$$

Explicitly performing the multiplications in (2.18) gives,

$$\begin{aligned} P_{sca}^{ED} = \text{Re } W_{EDs}\int_{0}^{2\pi}\int_{0}^{\pi}\Big[&|E_1|^2\left(N_{e11\theta}^{1}M_{e11\phi}^{1*} - N_{e11\phi}^{1}M_{e11\theta}^{1*}\right) + ... \\ &+|E_P|^2\left(N_{e11\theta}^{P}M_{e11\phi}^{P*} - N_{e11\phi}^{P}M_{e11\theta}^{P*}\right) + \\ &E_1E_2^{*}\left(N_{e11\theta}^{1}M_{e11\phi}^{2*} - N_{e11\phi}^{1}M_{e11\theta}^{2*}\right) + ... \\ &+E_{P-1}E_P^{*}\left(N_{e11\theta}^{P-1}M_{e11\phi}^{P*} - N_{e11\phi}^{P-1}M_{e11\theta}^{P*}\right) + \\ &E_2E_1^{*}\left(N_{e11\theta}^{2}M_{e11\phi}^{1*} - N_{e11\phi}^{2}M_{e11\theta}^{1*}\right) + ... \\ &+E_PE_{P-1}^{*}\left(N_{e11\theta}^{P}M_{e11\phi}^{P-1*} - N_{e11\phi}^{P}M_{e11\theta}^{P-1*}\right)\Big]\sin\theta d\theta d\phi \end{aligned} \tag{2.19}$$

where $W_{EDs} = \frac{1}{2}E_{EDs}H_{EDs}^{*}r^2$. This integral is composed of two types, each of which can be solved explicitly. In order to do so, we now introduce the explicit expressions for $\mathbf{N}_{e11}^{p}$ and $\mathbf{M}_{e11}^{q}$, given by,

$$\mathbf{N}_{e11}^{p} = \left(\cos\theta_p\cos\left(\phi_p+\phi\right)\cos\theta + \sin\theta_p\sin\theta\right)\hat{e}_\theta - \cos\theta_p\sin\left(\phi_p+\phi\right)\hat{e}_\phi \tag{2.20}$$

$$\mathbf{M}_{e11}^{p} = \cos\theta_p\sin\left(\phi_p+\phi\right)\hat{e}_\theta + \left(\cos\theta_p\cos\left(\phi_p+\phi\right)\cos\theta + \sin\theta_p\sin\theta\right)\hat{e}_\phi \tag{2.21}$$

As such, the first type of integral in (2.19) is given by equation (2.22), and can be solved to give,

$$|E_p|^2 \int_0^{2\pi} \int_0^{\pi} \left(N^p_{e11\theta} M^{p*}_{e11\phi} - N^p_{e11\phi} M^{p*}_{e11\theta} \right) \sin\theta d\theta d\phi = -\frac{8\pi}{3} |E_p|^2 \tag{2.22}$$

Due to the spherical symmetry of this scattering problem, equation (2.22) is true for any value of p, i.e., for every plane wave in the summation. The second type of integral is given by,

$$\int_0^{2\pi} \int_0^{\pi} \left[E_p E_q^* \left(N^q_{e11\theta} M^{p*}_{e11\phi} - N^p_{e11\phi} M^{q*}_{e11\theta} \right) + E_q E_p^* \left(N^q_{e11\theta} M^{p*}_{e11\phi} - N^q_{e11\phi} M^{p*}_{e11\theta} \right) \right] \sin\theta d\theta d\phi \tag{2.23}$$

Using symmetry arguments, it can be shown that $N^q_{e11\theta} M^{p*}_{e11\phi} - N^p_{e11\phi} M^{q*}_{e11\theta} = N^q_{e11\theta} M^{p*}_{e11\phi} - N^q_{e11\phi} M^{p*}_{e11\theta}$. This reduces equation (2.23) to equation (2.24), which can also be solved to give,

$$\begin{aligned} &\left(E_p E_q^* + E_q E_p^* \right) \int_0^{2\pi} \int_0^{\pi} \left(N^q_{e11\theta} M^{p*}_{e11\phi} - N^p_{e11\phi} M^{q*}_{e11\theta} \right) \sin\theta d\theta d\phi \\ &= -\frac{8\pi}{3} \left(E_p E_q^* + E_q E_p^* \right) \left(\cos\theta_p \cos\theta_q \cos\left(\phi_p - \phi_q\right) + \sin\theta_p \sin\theta_q \right) \end{aligned} \tag{2.24}$$

Thus the expression for the power scattered by the electric dipole mode (2.19) reduces to,

$$\begin{aligned} P^{ED}_{sca} = &-\text{Re } W_{EDs} \frac{8\pi}{3} \sum_{p=1}^{P} \sum_{q \neq p} |E_p|^2 + \\ &\left(E_p E_q^* + E_q E_p^* \right) \left(\cos\theta_p \cos\theta_q \cos\left(\phi_p - \phi_q\right) + \sin\theta_p \sin\theta_q \right) \end{aligned} \tag{2.25}$$

We previously defined $W_{EDs} = \frac{1}{2}E_{EDs}H^*_{EDs}r^2 = -i\frac{9}{8}|a_1|^2\frac{1}{k\omega\mu}\xi_1\xi_1'^*$. Since we are dealing with far-field expressions, we take the limit for large kr: $\lim_{kr\to\infty}\xi_1\xi_1'^* = -i$. Inserting this into equation (2.25) gives our final expression for the power scattered by the electric dipole mode to be,

$$P^{ED}_{sca} = \frac{3\pi}{k\omega\mu}|a_1|^2\sum_{p=1}^{P}\sum_{q\neq p}|E_p|^2 + \left(E_pE_q^* + E_qE_p^*\right)\left(\cos\theta_p\cos\theta_q\cos\left(\phi_p-\phi_q\right)+\sin\theta_p\sin\theta_q\right) \tag{2.26}$$

To simply this expression further we turn to our original expression for the incident electric field. Using equation (2.6), we can calculate the magnitude of the incident electric field as follows:

$$\begin{aligned}
|\mathbf{E}_{inc}|^2 &= |E_{inc,x}|^2 + |E_{inc,y}|^2 + |E_{inc,z}|^2 \\
|E_{inc,x}|^2 &= \sum_{p=1}^{P}\sum_{q\neq p}|E_p|^2\cos{\theta_p}^2\cos{\phi_p}^2 + \left(E_pE_q^* + E_p^*E_q\right)\left(\cos\theta_p\cos\theta_q\cos\phi_p\cos\phi_q\right) \\
|E_{inc,y}|^2 &= \sum_{p=1}^{P}\sum_{q\neq p}|E_p|^2\cos{\theta_p}^2\sin{\phi_p}^2 + \left(E_pE_q^* + E_p^*E_q\right)\left(\cos\theta_p\cos\theta_q\sin\phi_p\sin\phi_q\right) \\
|E_{inc,z}|^2 &= \sum_{p=1}^{P}\sum_{q\neq p}|E_p|^2\sin{\theta_p}^2 + \left(E_pE_q^* + E_p^*E_q\right)\left(\sin\theta_p\sin\theta_q\right)
\end{aligned}$$

$$\implies |\mathbf{E}_{inc}|^2 = \sum_{p=1}^{P}\sum_{q\neq p}|E_p|^2 + \left(E_pE_q^* + E_qE_p^*\right)\left(\cos\theta_p\cos\theta_q\cos\left(\phi_p-\phi_q\right)+\sin\theta_p\sin\theta_q\right) \tag{2.27}$$

We see that (2.26) is simplified by (2.27) and our final expression for the power

scattered by the electric dipole mode is directly given by the magnitude of the incident electric field as,

$$P_{sca}^{ED} = \frac{3\pi}{k\omega\mu}|a_1|^2|\mathbf{E}_{inc}|^2 \tag{2.28}$$

The power scattered by the magnetic dipole mode may be derived similarly, and is given by,

$$P_{sca}^{MD} = \frac{3\pi}{k\omega\mu}|b_1|^2 Z^2|\mathbf{H}_{inc}|^2 \tag{2.29}$$

where Z is the impedance of the medium.

2.3.2 Extinction and absorbed power: dipole modes

The extinction power for the electric dipole mode is derived explicitly and the expression for the extinction power of the magnetic dipole mode is provided. In order to calculate the extinction power of the electric dipole mode, the electric and magnetic field components of the incident beam that drive the electric dipole interaction are required, as well as the scattered electric and magnetic fields for the electric dipole mode. The latter are given in (2.15) and (2.16). The former may be obtained from (2.7) and (2.10), in which the mode order is chosen as $l = 1$ and the even SVHs are chosen ($\mathbf{N}$ for the electric field and $\mathbf{M}$ for the magnetic field), as these correspond to the electric dipole mode. The resulting expressions for the incident electric and magnetic fields driving the electric dipole interaction are given by,

$$\mathbf{E}_{inc}^{ED} = \sum_{p=1}^{P} E_{l=1} E_p \left(-iR_{1i}^{N}\mathbf{N}_{e11}^{p}\right) = E_{EDi}\sum_{p=1}^{P} E_p \mathbf{N}_{e11}^{p} \tag{2.30}$$

$$\mathbf{H}_{inc}^{ED} = -\frac{k}{\omega\mu}\sum_{p=1}^{P} E_{l=1}E_p\left(R_{1i}^{M}\mathbf{M}_{e11}^{p}\right) = H_{EDi}\sum_{p=1}^{P} E_p\mathbf{M}_{e11}^{p} \tag{2.31}$$

where $E_{EDi} = -iE_{l=1}R_{1i}^{N} = \frac{3}{2}\frac{\psi_1^{'}(kr)}{kr}$ and $H_{EDi} = -\frac{k}{\omega\mu}E_{l=1}R_{1i}^{M} = -i\frac{k}{\omega\mu}\frac{3}{2}\frac{\psi_1(kr)}{kr}$.

The extinction power is given by,

$$P_{ext} = \frac{1}{2}\mathrm{Re}\int_0^{2\pi}\int_0^{\pi}(E_{i\phi}H_{s\theta}^{*} - E_{i\theta}H_{s\phi}^{*} - E_{s\theta}H_{i\phi}^{*} + E_{s\phi}H_{i\theta}^{*})r^2\sin\theta d\theta d\phi \tag{2.32}$$

Using equations (2.15)-(2.16) and (2.30)-(2.31) in (2.32) gives,

$$\begin{aligned} P_{ext}^{ED} &= \frac{1}{2}\mathrm{Re}\ \left(E_{EDi}H_{EDs}^{*} + E_{EDs}H_{EDi}^{*}\right) \\ &\int_0^{2\pi}\int_0^{\pi}\left[\left(E_1N_{e11\theta}^{1} + ... + E_PN_{e11\theta}^{P}\right)\left(E_1^{*}M_{e11\phi}^{1*} + ... + E_P^{*}M_{e11\phi}^{P*}\right)\right. \\ &\left.-\left(E_1N_{e11\phi}^{1} + ... + E_PN_{e11\phi}^{P}\right)\left(E_1^{*}M_{e11\theta}^{1*} + ... + E_P^{*}M_{e11\theta}^{P*}\right)\right]r^2\sin\theta d\theta d\phi \end{aligned} \tag{2.33}$$

The integral in equation (2.33) is the same as that in equation (2.18), which has already been solved. Thus we can rewrite the extinction power of the electric dipole mode as,

$$\begin{aligned} P_{ext}^{ED} &= -\mathrm{Re}\ W_{EDe}\frac{8\pi}{3}\sum_{p=1}^{P}\sum_{q\neq p}|E_p|^2 + \\ &\left(E_pE_q^{*} + E_qE_p^{*}\right)\left(\cos\theta_p\cos\theta_q\cos\left(\phi_p - \phi_q\right) + \sin\theta_p\sin\theta_q\right) \end{aligned} \tag{2.34}$$

where the prefactor can be simplified as follows,

$$\begin{aligned}
&\text{Re }\left(W_{EDe}\right) = \text{Re }\frac{1}{2}\left(E_{EDi}H^*_{EDs} + E_{EDs}H^*_{EDi}\right)r^2 \\
&= \text{Re }\frac{1}{k\omega\mu}\frac{9}{8}\left(ia_1^*\psi_1^{'}\xi_1^* + ia_1\xi_1^{'}\psi_1^*\right) \\
&= \text{Re }\frac{1}{k\omega\mu}\frac{9}{8}\left(ia_1^*\psi_1^{'}\left(\psi_1^* + i\chi_1^*\right) + ia_1(\psi_1^{'} - i\chi_1^{'})\psi_1^*\right) \\
&= \frac{1}{k\omega\mu}\frac{9}{8}\text{Re}\left(i(a_1^* + a_1)\psi_1^{'}\psi_1^* - a_1^*\psi_1^{'}\chi_1^* + a_1\chi_1^{'}\psi_1^*\right) \\
&= \frac{1}{k\omega\mu}\frac{9}{8}\left(\text{Re}(a_1)\text{Im}(\psi_1^{'}\psi_1^*) - \text{Re}(a_1)\text{Re}\left(\psi_1^{'}\chi_1^* - \chi_1^{'}\psi_1^*\right)\right) \\
&= -\frac{1}{k\omega\mu}\frac{9}{8}\text{Re}(a_1)
\end{aligned} \tag{2.35}$$

Here, the last step follows since ψ_n is always real for real argument, and $\psi_n^{'}\chi_n^* - \chi_n^{'}\psi_n^* = 1$. Inserting this back into (2.34), and using the definition for the magnitude of the incident electric field in (2.27), the expression for the extinction power of the electric dipole mode simplifies to,

$$P_{ext}^{ED} = \frac{3\pi}{k\omega\mu}\text{Re}\left(a_1\right)\left|\mathbf{E}_{inc}\right|^2 \tag{2.36}$$

and once again the dipole mode is shown to be driven by the incident electric field magnitude. The extinction power of the magnetic dipole mode may be derived similarly, and is given by,

$$P_{ext}^{ED} = \frac{3\pi}{k\omega\mu}\text{Re}\left(b_1\right)\left|\mathbf{H}_{inc}\right|^2 \tag{2.37}$$

where Z is the impedance of the medium.

Correspondingly, the absorbed power for the dipole modes is obtained from the scat-

tered and extinction power equations, and is given by,

$$W_{abs} = W_{ext} - W_{sca} \tag{2.38}$$

where P_{sca} and P_{ext} are given in equations (5.1), (2.36) and (2.29), (2.37) for the electric and magnetic dipoles, respectively.

2.3.3 Scattered power: quadrupole modes

In this section, the power scattered by the electric quadrupole mode is derived explicitly, and the expression for the power scattered by the magnetic quadrupole mode is provided. Similar to the derivation for the power scattered by the electric dipole mode, we begin by obtaining expressions for the scattered electric and magnetic fields for the electric quadrupole mode. These may be obtained from equations (2.13) and (2.14), in which the mode order is chosen as $l = 2$, as these correspond to the quadrupole modes, and the a_n coefficient are chosen, as these correspond to the electric modes. The resulting expressions for the scattered electric and magnetic fields for the electric quadrupole modes are given by,

$$\mathbf{E}_{sca}^{EQ} = \sum_{p=1}^{P} E_{l=2} E_p \left(i a_2 R_{2s}^N \mathbf{N}_{e12}^p \right) = E_{EQs} \sum_{p=1}^{P} E_p \mathbf{N}_{e12}^p \tag{2.39}$$

$$\mathbf{H}_{sca}^{EQ} = \frac{k}{\omega\mu} \sum_{p=1}^{P} E_{l=2} E_p \left(a_2 R_{2s}^M \mathbf{M}_{e12}^p \right) = H_{EQs} \sum_{p=1}^{P} E_p \mathbf{M}_{e12}^p \tag{2.40}$$

where $E_{EQs} = i a_2 E_{l=2} R_{2s}^N = -i a_2 \frac{5}{6} \frac{\xi_2'(kr)}{kr}$ and $H_{EQs} = a_2 \frac{k}{\omega\mu} E_{l=2} R_{2s}^M = -a_2 \frac{k}{\omega\mu} \frac{5}{6} \frac{\xi_2(kr)}{kr}$. The scattered power is then calculated from (2.17) to give an expression very similar to equation (2.18), in which we simply replace N_{e11}, M_{e11} with N_{e12}, M_{e12}. The explicit

expressions for $\mathbf{N}^p_{e12}$ and $\mathbf{M}^q_{e12}$ are given by,

$$\begin{aligned}\mathbf{N}^p_{e12} = &\left(3\cos 2\theta_p \cos 2\theta \cos\left(\phi-\phi_p\right) + \frac{3}{4}\left(3+\sin 2\theta_p \sin 2\theta \cos 2(\phi-\phi_p)\right)\right)\hat{e}_\theta \\ &- 3\left(\cos 2\theta_p \cos\theta + \cos\left(\phi-\phi_p\right)\sin 2\theta_p \sin\theta\right)\sin\left(\phi-\phi_p\right)\hat{e}_\phi\end{aligned} \tag{2.41}$$

$$\begin{aligned}\mathbf{M}^p_{e12} = &-3\left(\cos 2\theta_p \cos\theta + \cos\left(\phi-\phi_p\right)\sin 2\theta_p \sin\theta\right)\sin\left(\phi-\phi_p\right)\hat{e}_\theta \\ &- \left(3\cos 2\theta_p \cos 2\theta \cos\left(\phi-\phi_p\right) + \frac{3}{4}\left(3+\sin 2\theta_p \sin 2\theta \cos 2(\phi-\phi_p)\right)\right)\hat{e}_\phi\end{aligned} \tag{2.42}$$

Similarly to before, we have two types of integrals to solve for, and the integrals as well as their exact solutions are given below as,

$$|E_p|^2 \int_0^{2\pi}\int_0^{\pi}\left(N^p_{e12\theta}M^{p*}_{e12\phi} - N^p_{e12\phi}M^{p*}_{e12\theta}\right)\sin\theta d\theta d\phi = -\frac{72\pi}{5}|E_p|^2 \tag{2.43}$$

$$\begin{aligned}&\left(E_pE_q^* + E_qE_p^*\right)\int_0^{2\pi}\int_0^{\pi}\left(N^q_{e12\theta}M^{p*}_{e12\phi} - N^p_{e12\phi}M^{q*}_{e12\theta}\right)\sin\theta d\theta d\phi \\ &= -\frac{18\pi}{5}\left(E_pE_q^* + E_qE_p^*\right)* \\ &\left(4\cos 2\theta_p \cos 2\theta_q \cos\left(\phi_p-\phi_q\right) + \sin 2\theta_p \sin 2\theta_q\left(3+\cos 2\left(\phi_p-\phi_q\right)\right)\right)\end{aligned} \tag{2.44}$$

Thus the expression for the power scattered by the electric quadrupole mode is given by,

$$\begin{aligned}P^{EQ}_{sca} = -\mathrm{Re}\ W_{EQs}\frac{18\pi}{5}\sum_{p=1}^{P}\sum_{q\neq p} &4|E_p|^2 + \left(E_pE_q^* + E_qE_p^*\right)\left(4\cos 2\theta_p \cos 2\theta_q \cos\left(\phi_p-\phi_q\right)\right. \\ &\left.+\sin 2\theta_p \sin 2\theta_q\left(3+\cos 2\left(\phi_p-\phi_q\right)\right)\right)\end{aligned} \tag{2.45}$$

where previously defined $W_{EQs} = \frac{1}{2} E_{EQs} H^*_{EQs} r^2 = i\frac{25}{72}|a_2|^2 \frac{1}{k\omega\mu} \xi_2 \xi_2^{'*}$. Since we are dealing with far-field expressions, we take the limit for large kr: $\lim_{kr\to\infty} \xi_2 \xi_2^{'*} = -i$. Inserting this into equation (2.45) gives our final expression for the power scattered by the electric quadrupole mode to be,

$$P_{sca}^{EQ} = -\frac{5\pi}{4}\frac{1}{k\omega\mu}|a_2|^2 \sum_{p=1}^{P}\sum_{q\neq p} 4|E_p|^2 + \left(E_p E_q^* + E_q E_p^*\right)\left(4\cos 2\theta_p \cos 2\theta_q \cos\left(\phi_p - \phi_q\right)\right.$$
$$\left. + \sin 2\theta_p \sin 2\theta_q \left(3 + \cos 2\left(\phi_p - \phi_q\right)\right)\right) \tag{2.46}$$

To simply this expression, we calculate the gradient of the incident electric field (reprinted here) along the different Cartesian directions at a fixed point in space.

$$\mathbf{E}_p = E_p^{'}\left(\cos\theta_p \cos\phi_p \hat{e}_x + \cos\theta_p \sin\phi_p \hat{e}_y - \sin\theta_p \hat{e}_z\right) e^{ik(\sin\theta_p \cos\phi_p x + \sin\theta_p \sin\phi_p y + \cos\theta_p z)} \tag{2.47}$$

The gradient components for each plane wave p in the plane wave summation are given as,

$$\begin{aligned}
\frac{\partial E_x}{\partial x} &= ikE_p \cos\theta_p \sin\theta_p \cos^2\phi_p & \frac{\partial E_x}{\partial y} &= ikE_p \cos\theta_p \sin\theta_p \cos\phi_p \sin\phi_p \\
\frac{\partial E_x}{\partial z} &= ikE_p \cos^2\theta_p \cos\phi_p & \frac{\partial E_y}{\partial x} &= ikE_p \cos\theta_p \sin\theta_p \cos\phi_p \sin\phi_p \\
\frac{\partial E_y}{\partial y} &= ikE_p \cos\theta_p \sin\theta_p \sin^2\phi_p & \frac{\partial E_y}{\partial z} &= ikE_p \cos^2\theta_p \sin\phi_p \\
\frac{\partial E_z}{\partial x} &= -ikE_p \sin^2\theta_p \cos\phi_p & \frac{\partial E_z}{\partial y} &= -ikE_p \sin^2\theta_p \sin\phi_p \\
\frac{\partial E_z}{\partial z} &= -ikE_p \cos\theta_p \cos\theta_p
\end{aligned} \tag{2.48}$$

We define Q_{ij} as the summation of these field gradients, where i, j iterate over the Cartesian components x, y, z and the expression is given by,

$$Q_{ij} = \frac{1}{2}\left(\frac{\partial E_i}{\partial j} + \frac{\partial E_j}{\partial i}\right) \tag{2.49}$$

Using this expression, each of the Q_{ij} terms are given as,

$$\begin{aligned}
Q_{xx} &= ikE_p \cos\theta_p \sin\theta_p \cos^2\phi_p \qquad & Q_{xy} &= Q_{yx} = ikE_p \cos\theta_p \sin\theta_p \cos\phi_p \sin\phi_p \\
Q_{xz} &= Q_{zx} = \frac{ik}{2} E_p \cos 2\theta_p \cos\phi_p & Q_{yy} &= ikE_p \cos\theta_p \sin\theta_p \sin^2\phi_p \\
Q_{yz} &= Q_{zy} = \frac{ik}{2} E_p \cos 2\theta_p \sin\phi_p & Q_{zz} &= -ikE_p \cos\theta_p \sin\theta_p
\end{aligned} \tag{2.50}$$

Finally, computing summation of the absolute value of Q_{ij} gives,

$$\begin{aligned}
\sum_{i,j} |Q_{i,j}|^2 &= |Q_{xx}|^2 + ... + |Q_{zz}|^2 \\
&= -\frac{k^2}{8} \sum_{p=1}^{P} \sum_{q \neq p} 4|E_p|^2 + \left(E_p E_q^* + E_q E_p^*\right) \left(4 \cos 2\theta_p \cos 2\theta_q \cos\left(\phi_p - \phi_q\right)\right. \\
&\quad \left. + \sin 2\theta_p \sin 2\theta_q \left(3 + \cos 2\left(\phi_p - \phi_q\right)\right)\right)
\end{aligned} \tag{2.51}$$

This reduces our expression for the power scattered by the electric quadrupole mode (2.46) to,

$$P_{sca}^{EQ} = \frac{10\pi}{k^3 \omega \mu} |a_2|^2 \sum_{i,j} |Q_{i,j}|^2 \tag{2.52}$$

and the power scattered by the electric quadrupole mode is directly given by the summation of the incident electric field gradients. The power scattered by the magnetic

qudrupole mode may be derived similarly, and is given by,

$$P_{sca}^{MQ} = \frac{10\pi}{k^3\omega\mu}|b_2|^2 Z^2 \sum_{i,j}|G_{i,j}|^2 \tag{2.53}$$

where G_{ij} is defined analogously to (2.49), where the electric fields are replaced with magnetic fields.

2.3.4 Extinction and absorbed power: quadrupole modes

The extinction power for the electric quadrupole mode is derived explicitly and the expression for the extinction power of the magnetic quadrupole mode is provided. The procedure is similar to that outlined in section 2.3.2, so the extinction power for the electric quadrupole mode is written directly as,

$$\begin{aligned} P_{sca}^{EQ} = -\text{Re } W_{EQe}\frac{18\pi}{5}\sum_{p=1}^{P}\sum_{q\neq p} 4|E_p|^2 + \left(E_pE_q^* + E_qE_p^*\right)\left(4\cos 2\theta_p \cos 2\theta_q \cos\left(\phi_p - \phi_q\right)\right. \\ \left. + \sin 2\theta_p \sin 2\theta_q \left(3 + \cos 2\left(\phi_p - \phi_q\right)\right)\right) \end{aligned} \tag{2.54}$$

in which $W_{EQe} = \frac{1}{2}\left(E_{EQi}H_{EQs}^* + E_{EQs}H_{EQi}^*\right)r^2$, and E_{EQi}, H_{EQi} are given as,

$$\mathbf{E}_{inc}^{EQ} = \sum_{p=1}^{P} E_{l=2}E_p\left(-iR_{2i}^N\mathbf{N}_{e12}^p\right) = E_{EQi}\sum_{p=1}^{P}E_p\mathbf{N}_{e12}^p \tag{2.55}$$

$$\mathbf{H}_{inc}^{EQ} = -\frac{k}{\omega\mu}\sum_{p=1}^{P} E_{l=2}E_p\left(R_{2i}^M\mathbf{M}_{e12}^p\right) = H_{EQi}\sum_{p=1}^{P}E_p\mathbf{M}_{e12}^p \tag{2.56}$$

Similarly to before, the prefactor can be simplified as follows,

$$\begin{aligned}
&\text{Re }\left(W_{EQe}\right) = \text{Re }\frac{1}{2}\left(E_{EQi}H^*_{EQs} + E_{EQs}H^*_{EQi}\right)r^2 \\
&= \text{Re }\frac{1}{k\omega\mu}\frac{25}{72}\left(ia_2^*\psi_2^{'}\xi_2^* + ia_2\xi_2^{'}\psi_2^*\right) \\
&= \text{Re }\frac{1}{k\omega\mu}\frac{25}{72}\left(ia_2^*\psi_2^{'}\left(\psi_2^* + i\chi_2^*\right) + ia_2(\psi_2^{'} - i\chi_2^{'})\psi_2^*\right) \\
&= \frac{1}{k\omega\mu}\frac{25}{72}\text{Re}\left(i(a_2^* + a_2)\psi_2^{'}\psi_2^* - a_2^*\psi_2^{'}\chi_2^* + a_2\chi_2^{'}\psi_2^*\right) \\
&= \frac{1}{k\omega\mu}\frac{25}{72}\left(\text{Re}(a_2)\text{Im}(\psi_2^{'}\psi_2^*) - \text{Re}(a_2)\text{Re}\left(\psi_2^{'}\chi_2^* - \chi_2^{'}\psi_2^*\right)\right) \\
&= -\frac{1}{k\omega\mu}\frac{25}{72}\text{Re}(a_2)
\end{aligned} \tag{2.57}$$

Inserting this back into (2.54), and using the definition of Q_{ij} in (2.51), the expression for the extinction power of the electric quadrupole mode simplifies to,

$$P_{sca}^{EQ} = \frac{10\pi}{k^3\omega\mu}\text{Re}\left(a_2\right)\sum_{i,j}|Q_{i,j}|^2 \tag{2.58}$$

The extinction power of the magnetic quadrupole mode may be derived similarly, and is given by equation as,

$$P_{sca}^{MQ} = \frac{10\pi}{k^3\omega\mu}Z^2\text{Re}\left(b_2\right)\sum_{i,j}|G_{i,j}|^2 \tag{2.59}$$

And again, the the absorbed power for the dipole modes is obtained from the scattered and extinction power equations, as given in equation (2.38). Building from this local-field approach, we investigate the scattering response of spherical NPs under illumination by

focused linearly, azimuthally, and radially polarized focused light beams, given in the following chapter.

Chapter 3

Manipulating multipolar resonances in a spherical particle using structured light

In this chapter, we use the expressions derived in chapter 2 to demonstrate selective suppression and enhancement of individual multipolar modes by manipulating beam symmetries and numerical apertures. These calculations reveal a longitudinal quadrupole mode, which is completely inaccessible by conventional linearly polarized light. Additionally, we achieve selective excitation of individual multipolar modes. These findings demonstrate a method for quantifying multipolar interactions in sub-wavelength particles and establish beam engineering as a powerful method for manipulating multipolar phenomena.

3.1 Validating the local field theory

As derived in chapter 2, the total power scattered via dipolar modes for a spherical NP under arbitrary illumination is given by,

$$P_{sca}^{dip} = \frac{3\pi}{k\omega\mu} \begin{cases} |a_1|^2 |\mathbf{E}_{inc}(\mathbf{r}_p)|^2, \text{ electric} & (3.1) \\ Z^2 |b_1|^2 |\mathbf{H}_{inc}(\mathbf{r}_p)|^2, \text{ magnetic} & (3.2) \end{cases}$$

where, Z, μ, and k are respectively the impedance, permeability, and wave number of the background medium. a_n and b_n are Mie coefficients, determined from standard plane wave illumination. Lastly, $|\mathbf{E}_{inc}(\mathbf{r}_p)|^2$ and $|\mathbf{H}_{inc}(\mathbf{r}_p)|^2$ are the electric and magnetic field intensity at the center of the NP, in the absence of the NP. In analogy with the multipolar interaction Hamiltonian, the scattering is proportional to a field-independent "moment", i.e., the Mie coefficient, and a particle-independent driving term, i.e., the field intensity.

Similarly, the power scattered by quadrupole modes is given by,

$$P_{sca}^{quad} = \frac{10\pi}{k^3\omega\mu} \begin{cases} |a_2|^2 \sum_{i,j} |Q_{ij}|^2, \text{ electric} & (3.3) \\ Z^2 |b_2|^2 \sum_{i,j} |G_{ij}|^2, \text{ magnetic} & (3.4) \end{cases}$$

where the driving term depends on a summation of field gradients and is defined as,

$$Q_{ij} = \frac{1}{2}\left(\frac{\partial E_i}{\partial j} + \frac{\partial E_j}{\partial i}\right) \tag{3.5}$$

and i, j refer to the Cartesian coordinates x, y, z [31]. There are nine terms in this summation, but only six unique terms, since $Q_{ij} = Q_{ji}$. The MQ field interaction term G_{ij} is defined similarly, replacing electric field gradients with magnetic field gradients.

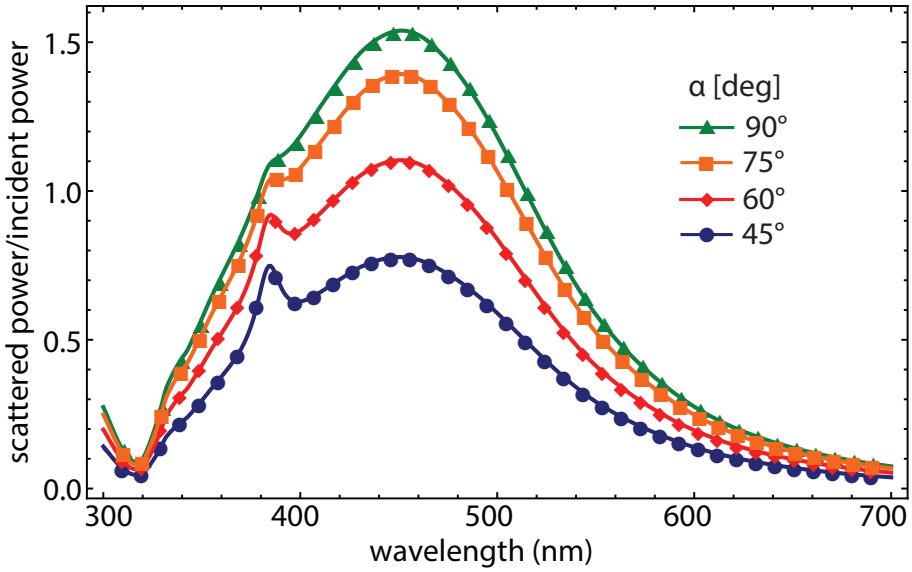

Figure 3.1: Fraction of scattered power to incident power of silver spherical NP in water with radius 100nm under focused linearly polarized illumination, as a function of wavelength. Local field results (shapes) are superimposed on GLMT results (solid lines) from ref [1] at four different focus angles, and the two show excellent agreement. The Mathematica code used to generate this figure is given in Appendix A.1.

These expressions may be used to determine the power scattered by a spherical particle at any location in an inhomogeneous illuminating field.

Local-field based expressions may also be used to describe higher order multipole interactions; here we restrict discussion to the dipole and quadrupole modes that dominate the response of typical plasmonic and metamaterial NP constituents. Although we focus on scattering cross-sections here, expressions for the electromagnetic fields and absorbed power are included in chapter 2. The local field approach confers a variety of advantages over GLMT. It is particularly useful in cases where the spatial electromagnetic field distributions are already known – the need for spherical wave or plane wave decompositions is eliminated. Additionally, the local field expressions intuitively reveal opportunities for tuning multipolar light-matter interactions via beam engineering.

To validate the expressions for the scattered power (eqns. 3.1-3.4), the ratio of the scattered to incident power is calculated for a gold particle in water under illumination

by a focused linearly polarized wave, and compared with published results from [1]. The results obtained using the local field method are given in the shapes (triangle, square, diamond, circle), while the original data, obtained using the generalized Lorenz Mie theory, is plotted in solid lines, as shown in Fig. 3.1. The two methods are shown to give excellent agreement.

Additionally, the scattering spectra obtained from an experimental work on focused azimuthally polarized illumination of a Silicon spherical particle on a glass substrate are compared with the results obtained from the local field theory, shown in Fig. 3.2. The slight deviations in the resonant wavelengths of the magnetic multipolar modes are explained by the use of a glass substrate in a) and an air medium in b). The presence of the glass substrate causes shifting of the multipolar resonances, as explained in ref [32]. Accounting for the substrate-induced shifts, the spectra match very well.

3.2 Engineering the scattering response of a sphere

Next, the validity of this local field model is demonstrated in Fig. 3.4 for the case of a Silicon NP with index n = 3.7 and radius r_{NP} = 100nm. The ratio of scattered power to incident power is plotted as a function of a normalized frequency parameter: the radius of the NP divided by the wavelength of the incident light. A focused, linearly polarized beam (LP) is expressed as a discrete summation of plane waves. Scattering spectra determined via GLMT (dashed red line) and the local field approach (blue line) are identical. The ratio of scattered to incident power sometimes exceeds 1 due to the normalization used. Because the incident beam is described as a discrete superposition of plane waves, the incident power transmitted through the xy-plane does not converge. This is because the focused incident beams are expressed as a discrete summation of plane waves. All the focused beams in the main text are described as summation of 10,000 total

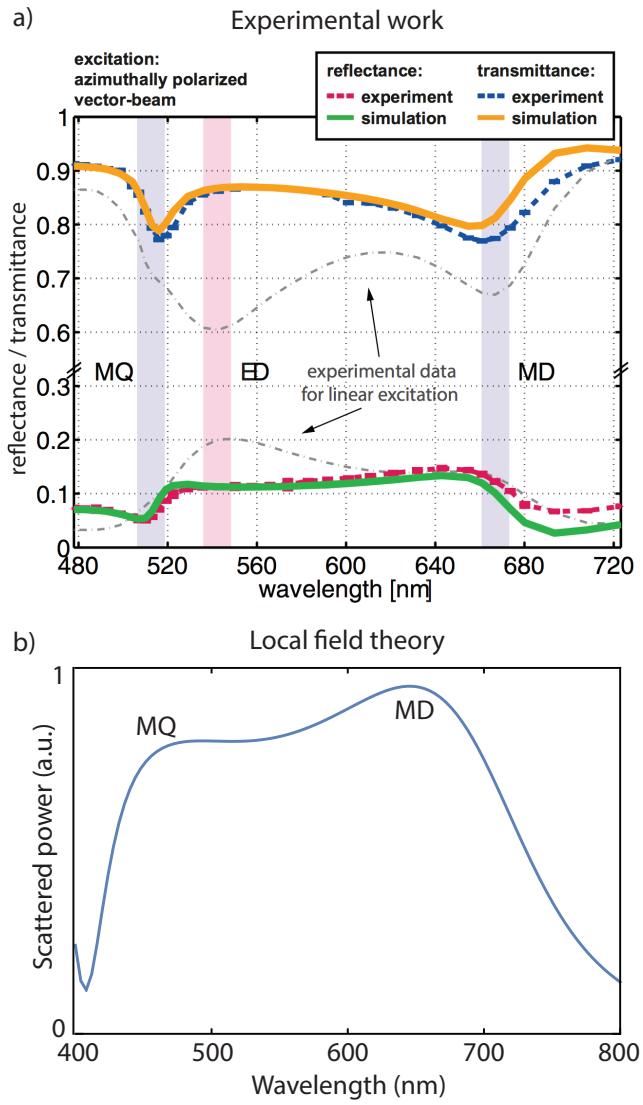

Figure 3.2: a) Experimental results of transmission/reflection of a single Si spherical particle on a glass substrate under illumination by a focused azimuthally polarized beam, reprinted from ref [2]. b) Scattered power of same Si spherical particle in air using local field theory.

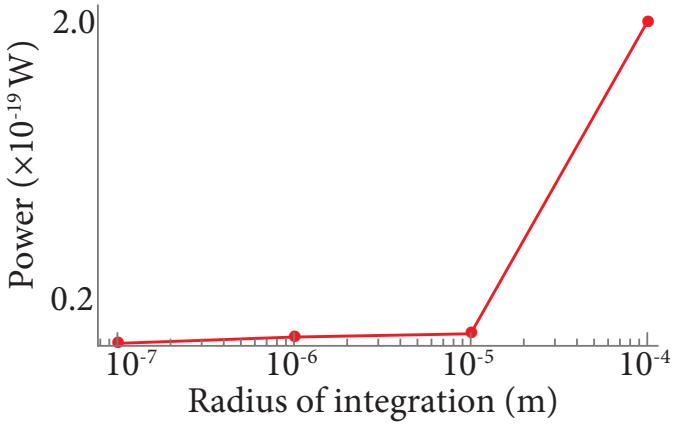

Figure 3.3: Power as a function of radius of integration for focused LP beam. Due to the discretization of the incident beam, the power does not converge, even when integrated over a large area. The Mathematica code used to generate the scattered power in this figure is given in Appendix B.3.

Table 3.1: Electric and magnetic field magnitudes and gradients, and orientations of each, under LP, AP, and RP illumination, for ED, MD, EQ, and MQ modes.

	Dipoles		Quadrupoles	
Illumination	Electric	Magnetic	Electric	Magnetic
LP	x	y	Q_{xz}	Q_{yz}
AP	z	0	Q_{xx}=Q_{yy} =-2Q_{zz}	0
RP	0	z	0	Q_{xx}=Q_{yy}=-2Q_{zz}

plane waves. The incident power of the illumination beam is calculated by integrating the z-component of the Poynting vector over a circular area, with a specified radius of integration. Even when the radius of integration is quite large (up to 0.1 cm), the incident power does not converge, as is shown in Fig 3.3. Thus the fraction of scattered to incident power sometimes exceeds 1, since the incident power does not converge even when a large number of plane waves (10,000) are included in the summation that describes the incident beam. In order to obtain the incident power we integrate the incident Poynting vector over a circular area comprising the main intensity lobe of the focused beam, as shown in the inset of Fig. 3.4.

Illumination by a LP beam results in excitation of all multipole modes, since the

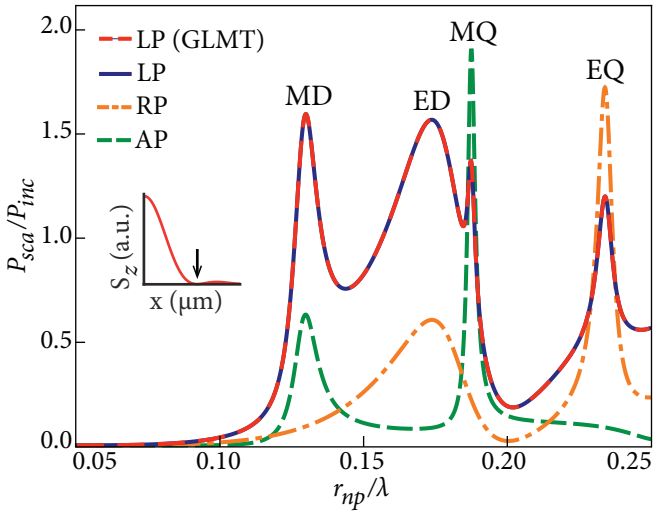

Figure 3.4: Ratio of scattered power to incident power for a spherical NP with refractive index n = 3.7 under linearly (LP, blue line), azimuthally (AP, dashed green line), and radially (RP, dot-dashed orange line) polarized illumination, as a function of normalized frequency. GLMT calculations for scattering by a LP beam (dashed red line) show excellent agreement with the local field expressions derived in this chapter. Multipolar mode peaks are labeled, with E = electric, M = magnetic, D = dipole, and Q = quadrupole. Inset depicts the normalization scheme in which the incident Poynting vector is integrated over the main intensity lobe of the illumination beam, as indicated by arrow, where Sz is the z-component of the Poynting vector plotted as a function of distance along the x-axis (shown for focused LP illumination). The Mathematica code used to generate the scattered power in this figure is given in Appendix A.3, and the incident power is given in B.3.

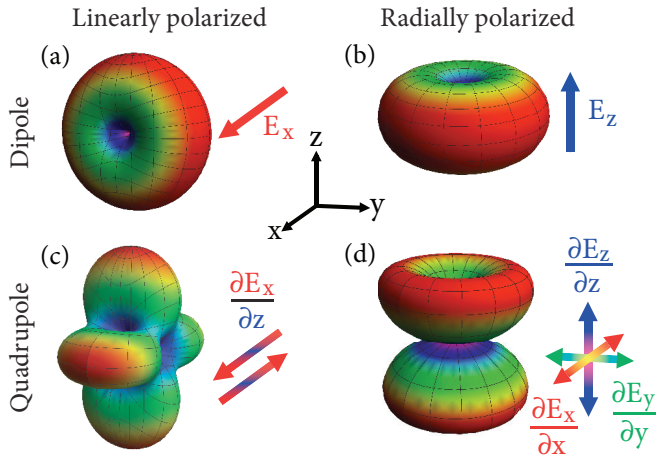

Figure 3.5: Radiation patterns of ED (top row) and EQ (bottom row) modes under LP (left column) and RP (right column) illumination, with corresponding field components that drive each excitation. LP illumination results in (a) an x-oriented dipole and RP illumination results in (b) a z-oriented dipole. Due to incident field gradients, LP illumination couples to (c) a transverse quadrupole whereas RP illumination couples to (d) a longitudinal quadrupole mode, which is typically thought to be non-radiating. The Mathematica code used to generate this figure is given in Appendix B.6.

relevant dipolar and quadrupolar driving fields are all nonzero (Table 3.1). In contrast, a focused azimuthally polarized (AP) beam exhibits a null in the electric field at the beam's focus [33]. Additionally, although individual electric field gradients are quite strong, the electric quadrupole moment depends on a sum of gradients (equation 4) that cancel each other at the beam's focus. As such, the resultant scattering spectrum (Fig. 3.4, green line) for a NP at the focus of an AP beam exhibits only magnetic modes. A focused radially polarized (RP) beam exhibits identical symmetries to that of an AP beam, except that the electric and magnetic fields are switched. Consequently, illumination by a RP wave excites only electric modes. The selective excitation of magnetic (electric) modes [34, 35] via azimuthally (radially) polarized illumination is explained here by considering the appropriate local field quantities. By changing symmetries of the illuminating radiation, scattering spectra are strongly modified.

Changing the illumination condition affects not only the scattering spectra of the

NP, but also the orientation of the excited multipolar modes. Although the individual multipole resonance frequencies are unchanged, the associated radiation patterns vary with illumination conditions. For example, an x-polarized LP beam excites an in-plane ED, with a dipole moment along the x-axis. The associated radiation pattern is shown in Fig. 3.5(a). Conversely, the RP wave excites an out-of-plane ED, with a dipole moment along the z-axis, as seen in Fig. 3.5(b). Thus, changing illumination symmetries allows rotation of the dipole orientation in space. Such modifications of the multipolar radiation patterns are more significant for the case of quadrupole modes, which are driven by field gradients (see Table 1). The x-polarized LP beam only exhibits a non-zero gradient for the x-component of the electric field along the z-direction $\left(\frac{\partial E_x}{\partial z} \neq 0\right)$; $Q_{xz} = Q_{zx}$ are the relevant driving terms. This results in a characteristic four-lobe radiation pattern, as shown in Fig. 3.5(c). We refer to this as a *transverse* quadrupole. In contrast, the RP beam has only nonzero *longitudinal* gradients: $\frac{\partial E_x}{\partial x} = \frac{\partial E_y}{\partial y} = -2\frac{\partial E_z}{\partial z}$, and $Q_{xx} = Q_{yy} = -2Q_{zz}$ (Table 1). This results in excitation of a longitudinal quadrupole mode. The associated two-lobe radiation pattern (Fig. 3.5(d)) is markedly distinct from the typical transverse quadrupole mode. Interestingly, this type of quadrupole excitation is typically referred to as a "dark" mode in plasmonic dimer antennas [36, 37]. These results highlight the fact that such modes are only "dark" because they cannot be excited by conventional linearly (or circularly) polarized sources. Thus, beam engineering allows for excitation of new classes of multipole modes.

Even when the beam symmetries are unchanged, the multipole spectra depend strongly on other beam properties such as the focused spot size, determined here by changing the numerical aperture (NA = $\sin(\alpha)$). Previously, the focusing angle was fixed to 0.86 ($\alpha = \pm 60°$). Varying the NA changes the relative weight of dipole and quadrupole driving terms. This effect is shown in plots of the fraction of incident power scattered by dipole (red) and quadrupole (green) modes, as well as their ratio, under LP (Fig. 3.6(a))

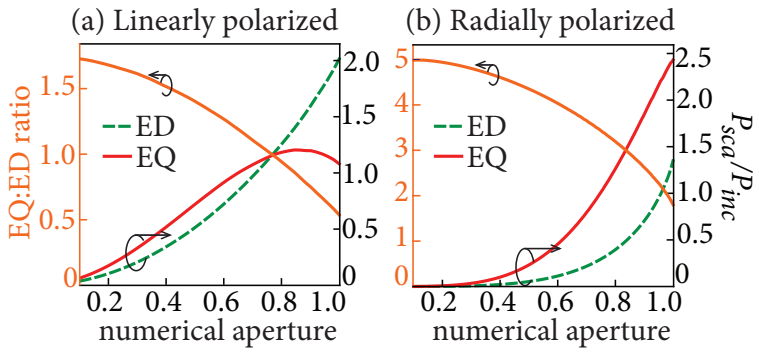

Figure 3.6: Change in fraction of scattered power to incident power (right axis) with increasing numerical aperture (i.e., focusing), for ED and EQ modes (on resonance) under (a) LP illumination, and (b) RP illumination. The ED mode generally dominates in LP beams, while the opposite is true of RP beams. The ratio of quadrupole to dipole scattering decreases in both cases (left axis). The Mathematica code used to generate this figure is given in Appendix A.6.

and RP (Fig. 3.6(b)) illumination. For the LP beam, the EQ response is generally weaker than the ED response at higher focus, and increases much more slowly with focusing. As a result, the ratio of EQ:ED scattering decreases with tighter focusing. The scaling for RP illumination is quite different: the EQ response is always larger than the ED response (EQ:ED ratio > 1), although the ratio also decreases with tighter focusing. The behavior for the magnetic modes is identical when illuminated by AP beams. Beam engineering not only allows for selective excitation of electric vs. magnetic modes, but also the tuning of the relative weight of quadrupoles vs. dipoles.

Previous methods for directly quantifying multipolar light-matter interactions have relied on decomposing output light from e.g., photoluminescence [38, 39] or Rayleigh scattering [40, 41]. More recently, researchers have proposed [42, 43, 44, 45, 34, 46, 16, 47, 48, 49] and experimentally demonstrated [13, 50, 15, 51, 2] enhancement or suppression of multipolar scattering in engineered light beams. In general, selecting out individual multipolar modes requires light beams in which all other multipole orders have been suppressed. Taking advantage of the previously discussed beam symmetries, we achieve selective excitation of individual dipole and quadrupole modes using standing

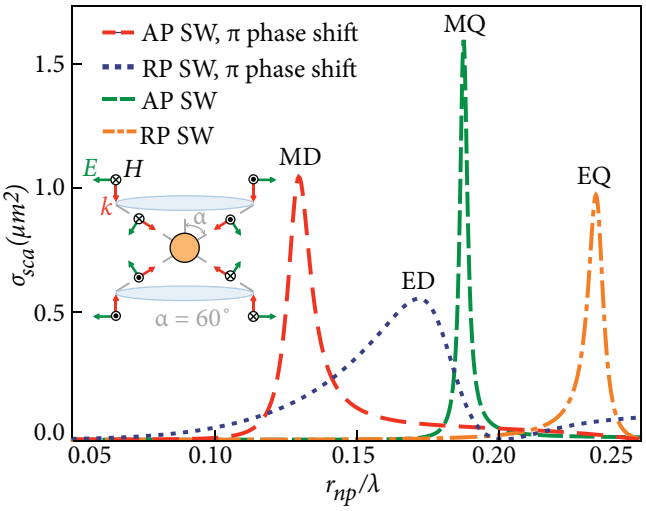

Figure 3.7: Scattering cross-section as a function of normalized frequency. Standing wave (SW) illumination by an AP with a π phase shift between the two beams (dashed red line), RP with a π phase shift (dashed blue line), AP (dashed green line), and RP beam (dashed orange line) beam results in selective excitation of the MD, ED, MQ, and EQ modes, respectively. Inset depicts illumination scheme for RP SW illumination.

wave illumination–i.e., by illuminating from both the top and bottom. Selective excitation of dipole modes requires that all field gradients in the cross terms cancel. This can be achieved by illuminating with two counter-propagating focused RP beams that are π out of phase with each other, enabling complete suppression of the magnetic field and both field gradients. A NP placed at the beam focus exhibits only a z-oriented ED mode (see Fig. 3.7). Similarly, selective excitation of a z-oriented MD mode is achieved via standing wave (SW) illumination comprising of two counter-propagating AP beams that are π out of phase with each other. Similarly, selective excitation of the quadrupole modes is achieved by removing the phase difference between two counter-propagating beams. A longitudinal EQ (MQ) mode is excited by SW illumination of two counter-propagating RP (AP) beams. The scattering spectra resulting from these SW illumination profiles is shown in Fig. 3.7, where the inset depicts the illumination condition for a RP standing-wave without any phase shift. Since these standing waves produce zero power flux (the power from one beam is canceled by the counter-propagating beam) we plot the scat-

tering cross-section: the scattered power divided by the incident intensity. As seen in Fig. 3.7, individual multipolar resonance spectra are clearly resolved by this illumination method.

In summary, we have derived a simplified method for determining the multipolar scattering of NPs in inhomogeneous beams. Our approach only requires knowing the local electromagnetic fields and their gradients at one point in space, obviating the need for plane wave or spherical wave decompositions. Using this method, we demonstrate the manipulation of multipolar spectra via beam engineering. We show selective excitation of electric and magnetic modes and the emergence of a "bright" longitudinal quadrupole. We subsequently demonstrate how to tune the relative weight of dipole and quadrupole contributions by manipulating the beam focusing conditions. We conclude by demonstrating selective excitation of individual multipole modes in standing wave configurations. This establishes beam engineering as a powerful approach for manipulating the multipolar scattering properties of nanostructures, and for studying the multipolar light-matter interactions in nanoscale elements. In the next chapter, we explore how a dimer antenna (consisting of two spherical particles) responds to different types of polarizations, and how the phenomena observed in single particles carry over to dimer antennas.

Chapter 4

Dark modes and field enhancement in dimers illuminated by cylindrical vector beams

In chapters 2 and 3, we used analytical expressions to explore the multipolar response of spherical particles. In this chapter, we use numerical simulations to investigate the response of dielectric dimer structures illuminated by cylindrical vector beams. Using FDTD simulations, we demonstrate significant modification of the scattering spectra of dimer antennas and reveal how the illumination condition gives rise to these spectra through manipulation of electric and magnetic mode hybridization. By appropriately combining dimer geometries and beam symmetries, we demonstrate coupling to high-Q dark quadrupole modes with exceptional magnetic intensity enhancements. This approach exploits structured light as a powerful framework for manipulating multipolar phenomena in multi-particle dielectric resonators.

4.1 Introduction

The optical properties of metamaterials are made possible by engineering multipolar resonances in sub-wavelength structures. The ability of dielectric particles to support magnetic modes permits a variety of useful applications including optical switching [52], efficient polarization conversion [53], and tunable beam steering [54]. The optical response of such antennas is typically engineered by modifying the size, shape, or composition of the antenna structures [55, 56, 57, 58, 32]. An alternative approach for engineering these antenna properties is to use structured light [59], such as cylindrical vector beams, Airy beams, and Laguerre Gaussian beams of varying orbital angular momentum. For instance, when applied to plasmonic antennas [60, 51, 61, 34, 46] the unique properties of azimuthally and radially polarized beams [62, 63] enable coupling to dark modes [13, 47, 14, 15, 16] and produce exceptionally high electric field enhancement [47, 34, 64].

The unique properties of radially (RP) and azimuthally polarized (AP) beams have unveiled similar effects in dielectric particles [65, 2, 17, 18, 66]. However, existing studies are limited to the response of single particles. In this chapter, we use exotic illumination schemes to modify the hybridization of electric and magnetic modes in dielectric dimer antennas. We demonstrate how the spectra and radiation patterns of dimers illuminated with RP and AP beams are significantly modified relative to conventional linearly polarized illumination. We show that such beams can produce narrow-linewidth spectral features due to high-Q magnetic resonances, enable coupling to dark electric and magnetic modes, and generate unprecedented magnetic intensity enhancements external to the dielectric resonators.

4.2 Exploring the scattering response of a dimer antenna to cylindrical vector beam illumination

Scattering spectra of spherical dimers illuminated by focused beams of varying symmetries [34, 67, 33] are calculated with Finite Difference Time Domain simulations [68]. Full details of the simulation files and post-processing scripts are given in Appendix B. First we study the response of a dimer antenna consisting of two spherical nanoparticles (NPs) in air, each with radius $r_{np} = 100$nm and index of refraction $n = 3.7$, separated along the x-axis by 10nm. We refer to this antenna as an x-dimer to highlight the separation direction relative to the illumination, which is incident along the z-axis. Scattering spectra for focused (half-angle annular aperture of the focusing lens $\alpha = 60°$) linearly polarized beams with E-field polarized parallel (x-polarized) and perpendicular (y-polarized) to the dimer axis are shown in Figs. 4.1(a) and (b) respectively. As compared to the spectra of a single sphere (see inset in Fig. 4.1(a)), dimers exhibit modified scattering spectra. The spectral location of single sphere magnetic dipole, electric dipole, and magnetic quadrupole modes are shown with dashed vertical lines. As discussed in previous studies [69, 70, 71] the x-polarized scattering spectrum exhibits significant broadening and overlap of the two lowest order resonances. The y-polarized scattering spectrum more closely matches that of a single particle, suggesting that mode hybridization is strongest when the E-field is oriented along the dimer axis.

In contrast, AP and RP beams exhibit a number of unique properties that alter the way they interact with dielectric particles. In particular, AP and RP beams exhibit zero electric and magnetic fields, respectively, along the beam axis. As a consequence, when a spherical particle is placed at the focus of an AP (RP) beam, only magnetic (electric) modes are excited. However, the underlying multipolar spectral line-shapes are unchanged; only the coupling to different modes is affected [65]. Away from the focus of

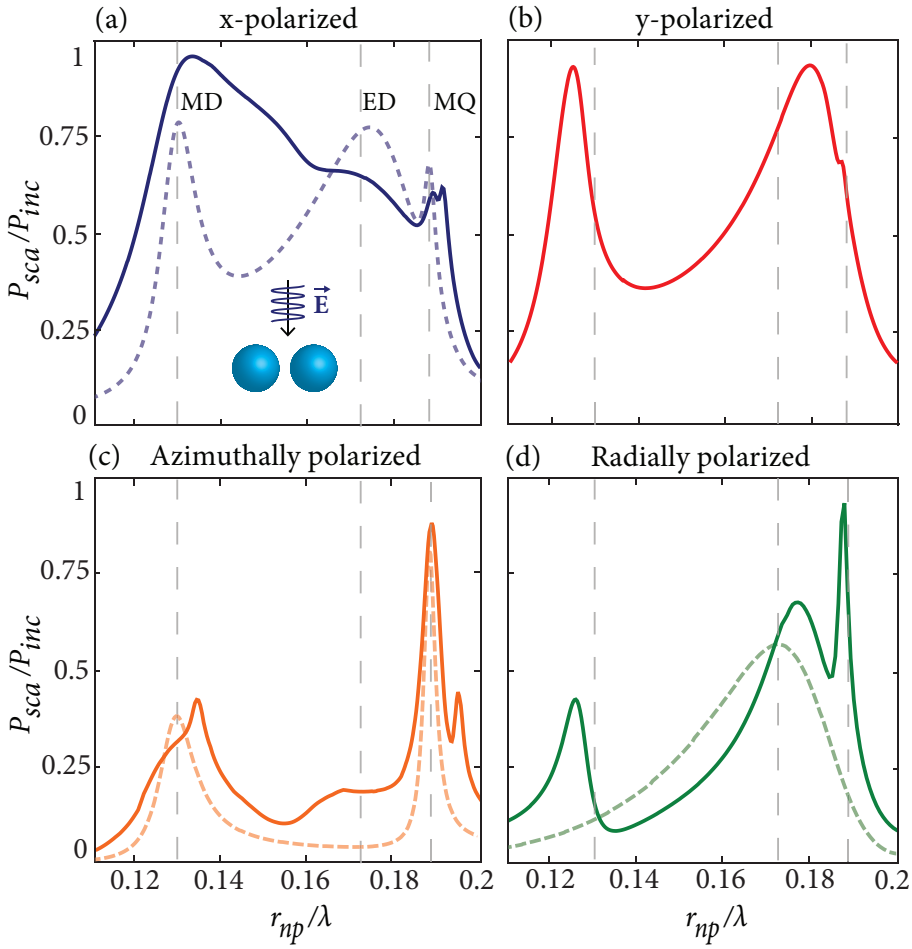

Figure 4.1: Ratio of scattered power to incident power for a dimer antenna consisting of two spherical NPs oriented along the x-axis under tightly focused (a) x-polarized, (b) y-polarized, (c) AP, and (d) RP illumination, as a function of normalized frequency. y-axes are normalized such that the largest scattering peak has unity amplitude. The dashed vertical lines indicate, from left to right, the locations of the magnetic dipole (MD), electric dipole (ED), and magnetic quadrupole (MQ) resonances in a single sphere under plane wave illumination. Dashed curves in in (a), (c), and (d) depict the spectral response of a single sphere for each type of illumination. Inset in (a) shows the illumination geometry.

an AP or RP beam, both beams have nonzero electric and magnetic field properties, resulting in excitation of both electric and magnetic modes in spheres offset from the focus. However, the different symmetries of these fields leads to different mode hybridization and modification of the scattering spectra. The scattering spectra of the x-dimer under AP and RP illumination are shown in Figs. 4.1(c) and (d) respectively. Both AP and RP illumination excite resonances with higher Q-factors than those accessible with x- or y-polarized illumination. Unlike the case of single spheres, where AP and RP beams can only change the relative coupling to different multipolar modes, dimer structures exhibit qualitatively different spectra due to the different nature of the mode hybridization.

The unique symmetries of AP and RP beams suggest that this spectral engineering may be particularly pronounced in longitudinal dimer geometries, i.e. when structures are separated along the z-axis. To probe this further, we investigate the scattering response of a z-oriented dimer (z-dimer) under LP, AP, and RP illumination. The z-dimer has the same nanoparticle radius, index, and gap size as the x-dimer, but the two constituent spheres are separated along the z-axis (see inset in Fig. 4.2(a)). Under linearly polarized (LP) illumination each sphere sees a mixture of electric and magnetic fields and the vertical z-dimer exhibits a rich series of broad resonances. In comparison, under RP and AP illumination the individual spheres see only electric and magnetic fields respectively. As expected, then, the RP beam exhibits only a single resonance in the frequency range shown, corresponding to a hybridization of the lone single-particle electric dipole mode near $r_{np}/\lambda = 0.175$ (Fig. 4.2(b)).

In contrast, the resultant AP scattering exhibits a drastically modified spectrum (Fig. 4.3(a)). The AP beam excites a series of high Q-factor magnetic modes with narrower linewidths than the underlying single-particle resonances. The narrow spectral features seen under AP illumination correspond to dark modes that are unseen under LP illumination. For instance, consider the prominent lowest order feature at r_{np}/λ

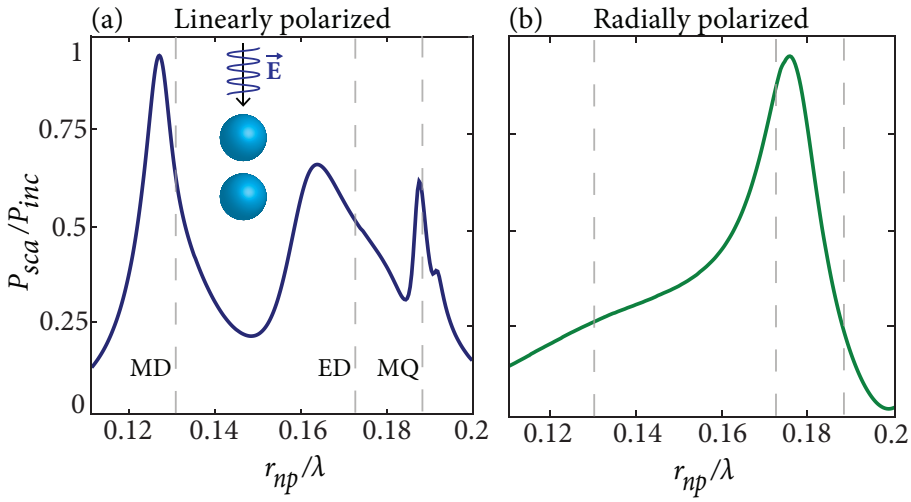

Figure 4.2: Ratio of scattered power to incident power for a dimer antenna consisting of two spherical NPs oriented along the z-axis under tightly focused (a) LP and (b) RP illumination, as a function of normalized frequency. y-axes are normalized such that the largest scattering peak has unity amplitude. The dashed lines indicate, from left to right, the locations of the magnetic dipole (MD), electric dipole (ED), and magnetic quadrupole (MQ) resonances in a single sphere under plane wave illumination. Inset in (a) depicts the illumination geometry.

= 0.126. The resonance is slightly red-shifted relative to the single-particle magnetic dipole mode (see dashed line), which is driven by the strong z-oriented magnetic fields along the beam axis. The phase of this z-oriented field evolves along the beam axis and can thus couple to both symmetric and anti-symmetric oscillations of the two dimer constituents. The prominent feature at $r_{np}/\lambda = 0.135$ corresponds to an anti-symmetric oscillation–the evolving phase provides the driving source of a longitudinal magnetic quadrupole mode [65]. The longitudinal magnetic quadrupole character is evident in the four-fold radiation pattern shown in Fig. 4.3(b). Such modes are frequently described as dark modes, accessible only through symmetry breaking structures [35, 72]. The mode hybridization becomes even more complex at higher frequencies.

Consider the two higher order modes in Fig. 4.3(a). One is red-shifted ($r_{np}/\lambda =$ 0.183) and the other blue-shifted ($r_{np}/\lambda = 0.195$) relative to the single-particle longitudinal magnetic quadrupole mode at $r_{np}/\lambda = 0.188$. In the single particle resonance

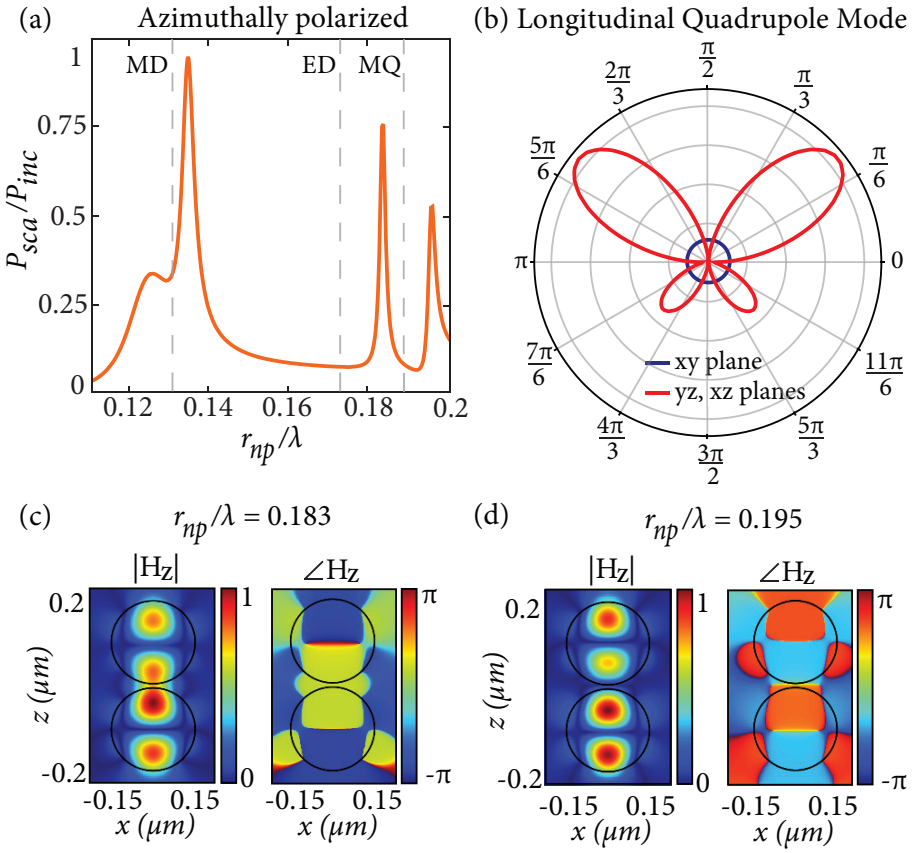

Figure 4.3: (a) Ratio of scattered power to incident power for a dimer antenna consisting of two spherical NPs oriented along the z-axis under tightly focused AP illumination, as a function of normalized frequency. y-axis is normalized such that the largest scattering peak has unity amplitude. (b) Far-field radiation pattern of longitudinal magnetic quadrupole mode under focused AP illumination at $r_{np}/\lambda = 0.135$. (c, d) Amplitude (left) and phase (right) in z-dimer antenna at (c) $r_{np}/\lambda = 0.183$ and (d) 0.195.

the z-oriented magnetic field points in opposite directions on the top and bottom of the sphere. The associated field patterns in the dimer are shown in Figs. 4.3(c, d). The two modes correspond to anti-symmetric and symmetric combinations of single-particle modes respectively. In the anti-symmetric combination, the magnetic fields in the gap region add up constructively (Fig. 4.3(c)), and the dimer resonance is red-shifted relative to the single particle mode. In the symmetric combination the z-fields in the gap must cancel. There is an additional null in the magnetic field distribution (Fig. 4.3(d)) and the mode is blue-shifted relative to the single-particle resonance. The strong longitudinal fields of the AP beam lead to longitudinal modes that in turn exhibit the unusual mode hybridization phenomena seen in Fig. 4.3(c, d).

4.3 Electric and magnetic field enhancement from a dimer antenna

A principal motivation for investigating plasmonic and dielectric dimers is the possibility of generating large electromagnetic intensity enhancements in gap regions between the particles. Dielectric dimers, in particular, can support both electric and magnetic hotspots [69, 70, 73, 74, 75]. For instance, electric intensity enhancements for x-dimers under various beams are shown in Fig. 4.4(a). Here, intensity enhancement is calculated by dividing the field intensity at the origin with the dimer in place by the field intensity at the origin with no dimer. The x-dimer exhibits a significant electric field intensity in the gap when illuminated by an x-polarized beam (blue). The enhancement peaks near the lowest order dipole mode and no significant enhancement is seen at higher frequencies. The intensity enhancement is similarly modest for y-polarized (red) and RP (orange) beams. The field enhancement is only seen when the relevant field points along

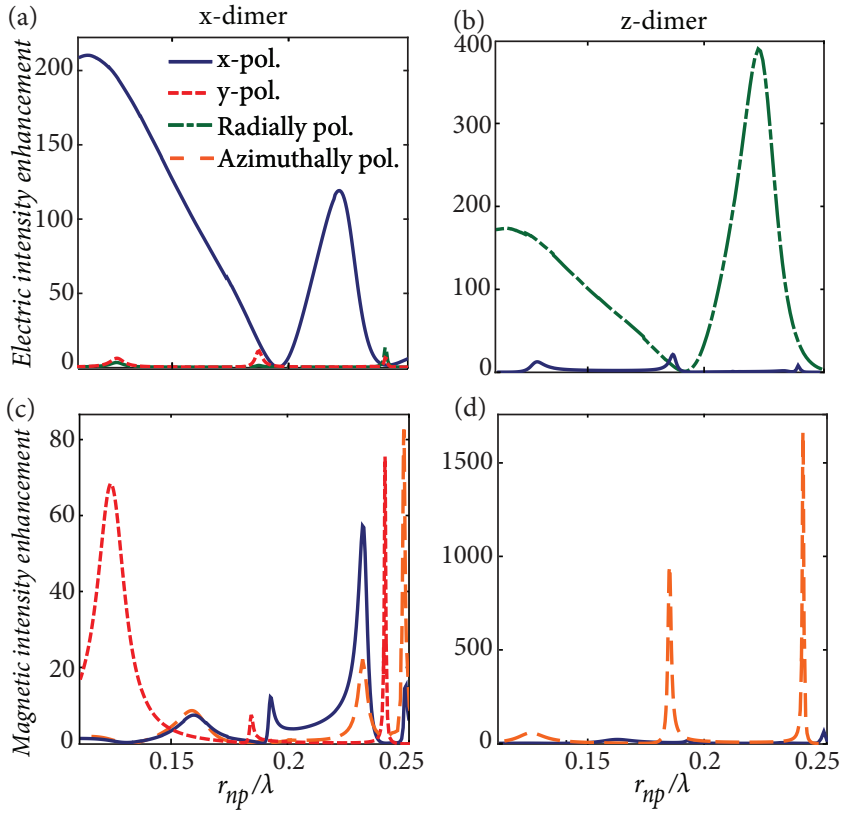

Figure 4.4: (a, b) Electric and (c, d) magnetic intensity enhancement (i.e. $|H_{tot}|^2/|H_{inc}|^2$ = total field intensity divided by incident field intensity at origin) for x-dimer (a, c) and z-dimer (b, d) under focused x-polarized, y-polarized (identical to x-polarized for z-dimer), AP, and RP illumination, as a function of normalized frequency.

the dimer axis [64]. This rule is similarly seen in the magnetic intensity enhancements of the x-dimer. The y-polarized beam generates a significant enhancement that is comparable to the enhancement produced by the AP beam (Fig. 4.4(c)). Following this trend, we can expect interesting field enhancements in RP and AP beams to emerge in the vertical dimer geometries introduced here.

Electric intensity enhancements for the z-dimer are plotted in Fig. 4.4(b). In this case x- and y-polarized beams are identical and exhibit modest enhancements. AP beams

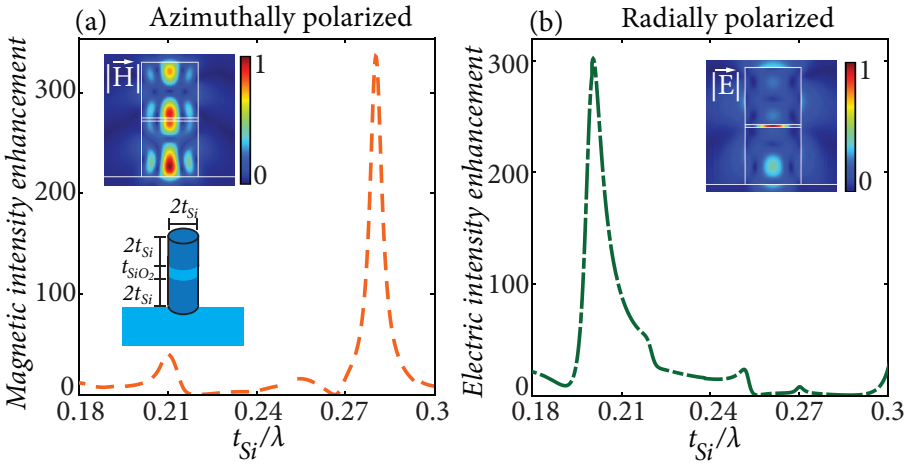

Figure 4.5: (a) Magnetic intensity enhancement of vertical disk dimer antenna under AP illumination. Insets depict (top) magnetic field profile on resonance and (bottom) structure of disk antenna on SiO_2 substrate, with dimensions of $2t_{Si} = 1\mu$m and $t_{SiO_2} = 50$nm. (b) Electric intensity enhancement of same disk antenna under RP illumination. Inset depicts electric field profile on resonance.

exhibit zero E-fields at the origin and thus no enhancement is defined, but as expected the fields in the gap are small. In RP illumination, however, the intensity enhancement is large (380) and higher than that seen in horizontal dimers illuminated with an x-polarized beam (211).

Just as horizontal dimers can generate strongly enhanced x-oriented fields, vertical dimers can strongly enhance the z-oriented fields of RP beams. The high electric intensity enhancement occurs near the wavelength of the single-particle electric quadrupole resonance. This enhancement due to hybridization of single-particle quadrupole modes is particularly striking for z-dimers illuminated by AP beams (Fig. 4.4(d)). The maximum field intensity achieved by the AP beam occurs near the single-particle magnetic quadrupole mode, and provides nearly two orders of magnitude improvement in the magnetic intensity enhancement (950) compared to that of the x-dimer (68). Structured illumination enables significantly larger field enhancements than that possible in conventionally illuminated dimer structures.

We apply these principles to a more practical dimer antenna design and demonstrate comparable magnetic intensity enhancements. We design a dielectric dimer antenna comprising of two silicon (Si) disks with a silicon dioxide (SiO_2) spacer placed on a silicon dioxide substrate, and determine the intensity enhancement of this antenna under AP and RP illumination. The diameter and height of the Si disks are $2t_{Si} = 1\mu$m, and the thickness of the SiO_2 gap is $t_{SiO_2} = 50$nm. As seen in Fig. 4.5(a), AP illumination of the Si-SiO_2 disk antenna results in a high magnetic intensity enhancement of 336 [69, 70, 73, 74]. This high magnetic intensity enhancement is made possible by the use of AP instead of LP illumination, which removes electric modes in the longitudinal antenna and allows for higher magnetic intensity enhancement. This magnetic intensity enhancement may be used to experimentally boost magnetic dipole transitions in rare earth ions [38] embedded within the SiO_2 spacer. A previous experimental work used AP illumination to excite such transitions[76], and there are many methods for experimentally generating AP and RP beams [77]. Similar to the disk antenna under AP illumination, RP illumination provides excellent confinement and enhancement of the electric field in the dimer gap (Fig. 4.5(b)). This high electric intensity enhancement (302) may be used in Surface Enhanced Raman Spectroscopy (SERS) applications [78], where dielectrics are emerging as a powerful basis for achieving sub-wavelength concentration of light.

In conclusion, structuring light significantly alters the scattering response of dielectric dimer antennas. In particular, RP and AP illumination enable coupling to dark dimer modes that cannot be accessed with linearly or circularly polarized light sources. These effects are most pronounced in vertical dimer geometries where only electric or magnetic modes hybridize. We show that RP and AP beams couple to high-Q magnetic resonances and dark quadrupole modes. In addition, the different symmetries and resultant mode hybridization enable far larger electromagnetic enhancements with RP and AP illumination, even for the same particle geometries. Building from these concepts, we design an

easily-fabricated dimer structure that leverages the unique properties of AP illumination to achieve high magnetic field enhancements within a spacer material. Thus we have used structured light to uncover the rich response of dielectric dimer antennas and highlighted the potential for using structured illumination to maximize the desired response of structured dielectric resonators. In the next chapter, we introduce a simpler method for modeling structured light using FDTD.

Chapter 5

Numerical implementation of the local field theory

In this chapter, we present a simple and efficient simulation framework, based on the local field concepts introduced in chapter 2, for extracting the multipolar response of any resonator under illumination by structured light. This method is based on the principle that each multipolar mode is driven by a specific property of the illumination beam. We present an extremely simple and efficient method for modeling structured light in FDTD that relies on local field principles, which is twenty times faster than existing simulation methods. We then apply this method to qualitatively match the scattering response of spherical and dimer antennas.

5.1 Introduction

Recently there has been growing interest in using structured light to design new metamaterials. Structuring the illumination beam completely changes the response of metamaterial resonators in ways that are impossible to access with plane wave illumination. For example, researchers have demonstrated tunable beam steering [17], controlled excitation of modes [79], and plasmonic focusing [80], all metamaterial applications that are made possible by the unique properties of the structured light that excites them.

The fundamental building blocks of metamaterials are the resonator structures that compose them. Thus the first step in engineering any metamaterial is to design a resonator that possess the appropriate scattering properties for a desired application. These properties include the spectral response, the multipolar modes of the resonator, the wavelength regime in which these modes occur, the field enhancement capabilities, the shape of its modes, etc. Typically, these resonator properties are designed using numerical simulations. The growing interest in structured light has led researchers to explore different methods for modeling the interactions between engineered beams and metamaterial resonators. Analytical formulations rely on an extension of Mie Theory based on a summation of plane waves, and are limited in scope to spherical particles [34, 67]. Some FDTD methods numerically implement the summation of waves technique [81, 82, 83, 84, 45, 85]. Other techniques involve a full two-dimensional representation of the input beam [14, 86]. The former method, similar to analytical techniques, requires expressing the incident illumination beam on a planar surface. The latter method suffers from long simulation times due to the necessity of generating the incident fields in a two-dimensional plane and propagating them through three-dimensional space, in addition to the large simulation region required for convergence.

Here, we introduce a new numerical technique for modeling the interaction between

any type of illumination beam and any resonator geometry. This technique, deemed the local field simulation, provides two orders of magnitude time speedup as compared to the full beam simulation. First, we numerically validate the analytical local field theory using FDTD full beam simulations. We then extend the principles of the local field theory to implement an extremely simple and computationally efficient method for modeling the scattering response of any arbitrary particle under illumination by an inhomogeneous beam in FDTD, based on reproducing the incident field with dipole sources. After confirming that this method accurately predicts the qualitative scattering response of a spherical particle, we apply these methods to investigate the multipolar response of a more complex resonator geometry, namely a dimer antenna, although the methodology is generalizable to arbitrary collections of particles. The local field simulation uncovers all the important features in engineering light-matter interactions for metamaterial applications, including the spectral locations of multipolar resonances, the approximate Q-factor of these resonances, and the electric and magnetic fields inside the resonators, at a fraction of the time and effort required by other simulation methods.

5.2 Developing the numerical local field theory

Introduced in chapter 2, the analytical local field theory reframes the interaction between an arbitrary light beam and a spherical particle by revealing that each multipolar mode is driven by specific field properties. For example, the dipole and quadrupole modes are directly driven by field magnitude and gradients, respectively. The exact mathematical relationship between these field components and the power scattered by these modes, is given by (where dip = dipole and quad = quadrupole):

$$P_{sca}^{dip} = \frac{3\pi}{k\omega\mu}|a_1|^2|\mathbf{E}|^2 \tag{5.1}$$

$$P_{sca}^{quad} = \frac{10\pi}{k^3\omega\mu}|a_2|^2 \sum_{i,j} \left| \frac{1}{2} \left(\frac{\partial E_i}{\partial j} + \frac{\partial E_j}{\partial i} \right) \right|^2 \tag{5.2}$$

where μ, k, and ω are respectively the permeability, wave number of the background medium, and frequency of the incident beam. a_n is the Mie coefficient, determined from standard plane wave illumination [28], $\mathbf{E}$ is the electric field at the center of the spherical nanoparticle, in the absence of the nanoparticle, and i, j refer to the Cartesian coordinates $x, y, andz$. The relevant expressions for the magnetic dipole and quadrupole modes are obtained by replacing a_n with Zb_n and $\mathbf{E}$ with $\mathbf{H}$ in Eq. (5.1-5.2), where Z is the impedance of the background medium. The analytical local field theory implies that the scattering response of a spherical particle can be reconstructed by knowing the field properties of the illumination beam at the location of the particle, without any need for mathematical reformulations for different types of beams.

This method enables quick and simple analytical extraction of the scattering response of a spherical particle under any type of structured light. We later show that these principles may be applied to numerically extract the response of any resonator illuminated by any beam of interest. First, we validate the analytical theory using Lumerical FDTD [68], a commercial FDTD solver. We implement a three-dimensional model of focused radially polarized (RP) and azimuthally polarized (AP) illumination using expressions for the full beams in a plane (see Appendix B for full details on simulation methodology). These beams are incident on a spherical particle with radius $r_{np} = 100nm$ and index of refraction $n = 3.7$, which is placed at the focus of these beams. A schematic of the full beam simulation setup is given in Fig. 5.1 (a).

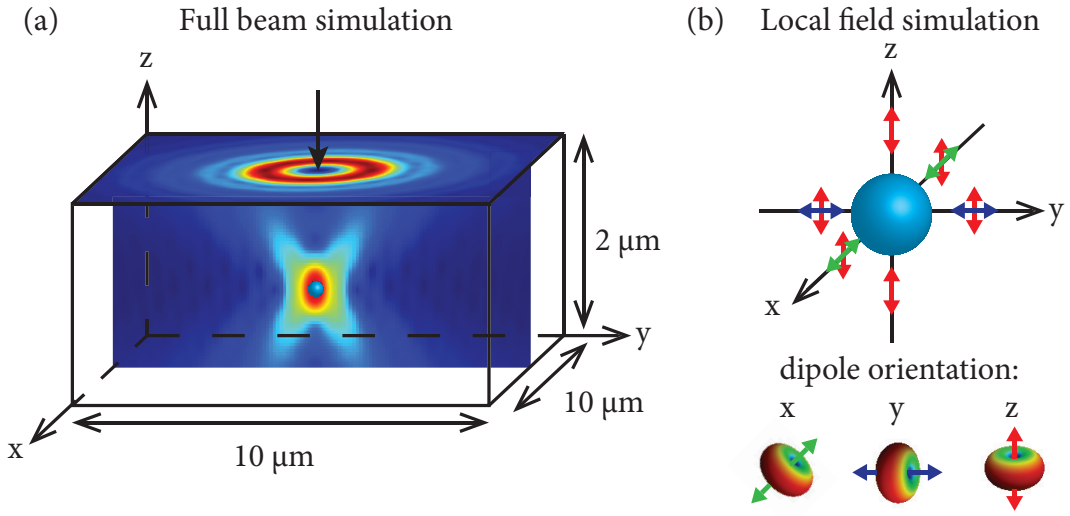

Figure 5.1: (a) Schematic of full beam FDTD simulation: In this simulation setup, the electric and magnetic fields of the incident illumination beam are calculated in a 2D plane and are injected into the 3D simulation at a plane $1\mu m$ away from the focus of the beam. The beam profile is pictured, and the resonator of interest, in this case a spherical particle, is placed at the focus of the beam. The dimensions of the simulation are shown. (b) Schematic of local field simulation: The incident beam properties are recreated by a series of dipole sources at six points along the x-, y-, and z-axes, along with additional dipoles at $(\pm x, \pm y, 0)$, $(\pm x, 0, \pm z)$, and $(0, \pm y, \pm z)$, not pictured here. The resonator of interest is placed at the center of the exciting dipoles, and the dimensions of the simulation are a cube measuring $0.5\mu m$ on each side. The exact dipoles needed at each point in space varies according to the type of illumination, and the configuration pictured here is for radially polarized illumination.

5.3 Results for dielectric antennas

From the full beam simulation, we extract the fraction of power scattered by the sphere normalized by the power incident in the beam, and plot this as a function of a normalized frequency parameter, which is the radius of the sphere divided by the wavelength of the incident light. The spectra obtained from the analytical local field theory are shown in Fig. 5.2 in the dashed lines. Note that the ratio of scattered to incident power sometimes exceeds 1 due to the normalization used, the reason for which is discussed in section 3.2. To compare the analytical local field results with the full beam results, we extract the electric and magnetic field magnitudes and gradients of the RP and AP beams and insert these into Eq. (5.1-5.2) to determine the scattered power. The resulting spectra are shown in Fig. 5.2 in the colored shapes. The analytical local field model and the full beam simulation show excellent quantitative agreement.

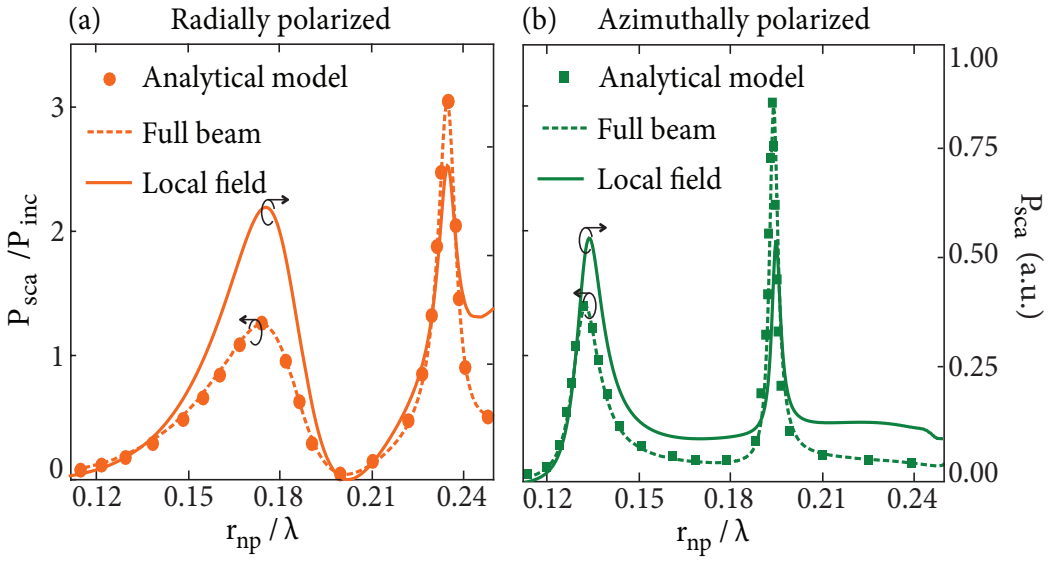

Figure 5.2: Scattering response of spherical nanoparticle under tightly focused (a) radially polarized and (b) azimuthally polarized illumination, as a function of normalized frequency (radius of sphere divided by wavelength of incident light). Results from analytical local field results are shown in colored shapes, FDTD full beam simulation results are shown in dashed lines, and FDTD local field simulation results are shown in solid lines.

The analytical theory simplifies the scattering interaction by connecting specific properties of the illuminating beam to individual multipolar modes. This concept suggests that the same multipolar modes should be excited in a spherical particle if the appropriate illuminating beam field properties are reproduced, without constructing the entire illumination beam. Based on this concept, we developed a new simulation technique to model structured light that uses a small number of dipole sources to recreate the field properties that drive multipolar modes in our resonator of interest. A schematic of the local field simulation is given in Fig. 1(b), and a full description of the files used to implement the local field simulations is given in Appendix C. Using the relevant equations for the illumination in question, we extract the amplitude and phase of the electric or magnetic field at eighteen points: two points along each of the x-, y-, and z-axes, and at $(\pm x, \pm y, 0)$, $(\pm x, 0, \pm z)$, and $(0, \pm y, \pm z)$. We place broadband dipole sources at each of these points and tune the amplitudes and phases to reflect those present in the incident illumination beam at a single wavelength (see Appendix C for more details). The scattering spectra obtained by the local field simulation for a spherical particle under RP and AP illumination is given in Fig. 5.2, shown in the solid lines. The local field FDTD simulation demonstrates excellent qualitative agreement with the full beam FDTD simulation in predicting the locations of multipolar mode resonances for a spherical particle.

The local field simulation confers a variety of advantages over the full beam simulation. First, the simulation region for the local field method can be made extremely small and is limited only by the size of the resonator in question, as the dipole sources can be placed within a few nanometers of the resonator. This results in a 2000x decrease in the required simulation volume. Additionally, the local field approach only requires knowledge of the excitation field at a few points in space, which is enough information to adequately reconstruct the field properties that drive the multipolar response of a resonator. This obviates the need to describe the illuminating beam in a full two-dimensional plane.

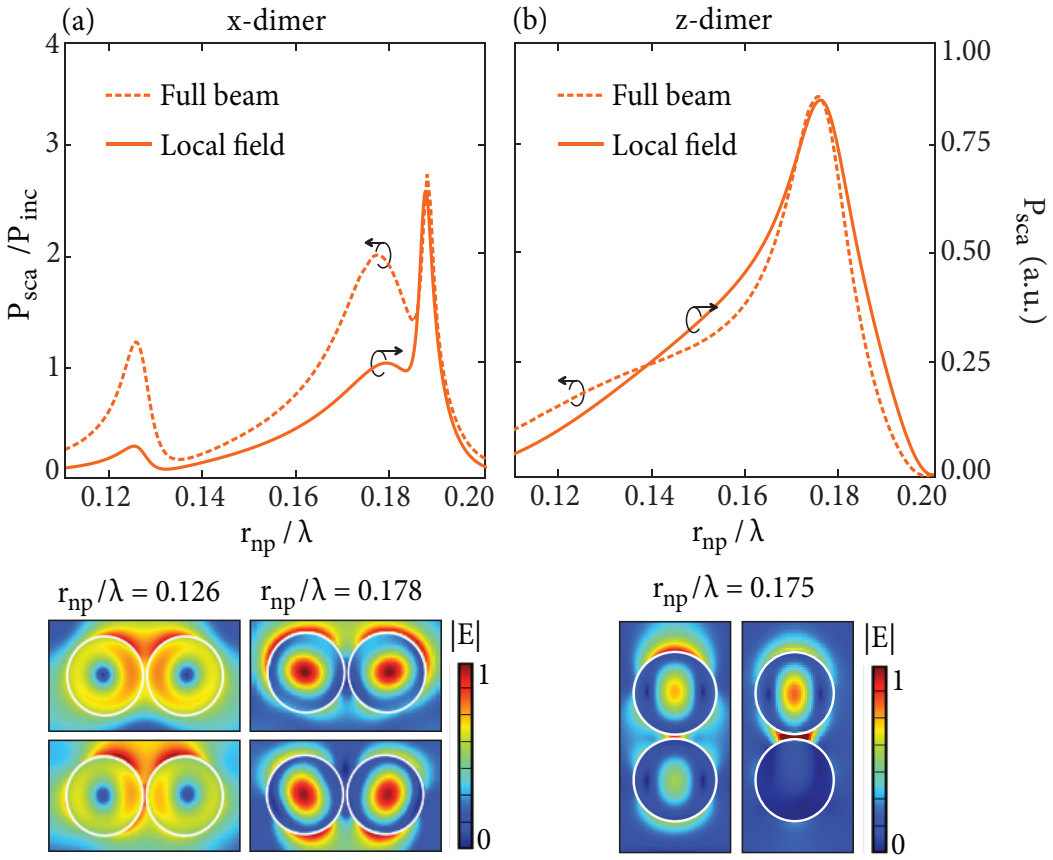

Figure 5.3: Scattering response of (a) x-dimer and (b) z-dimer antennas under tightly focused radially polarized illumination as a function of normalized frequency. FDTD results from full beam simulation are shown in dashed lines and FDTD local field simulation results are shown in solid lines. The two methods show excellent qualitative agreement in predicting the scattering response of the dimer antennas. Additionally, the field plots from the full beam simulations (top row/left column) are also compared with the field plots obtained from the local field simulations (bottom row/right column), which show good qualitative agreement with each other.

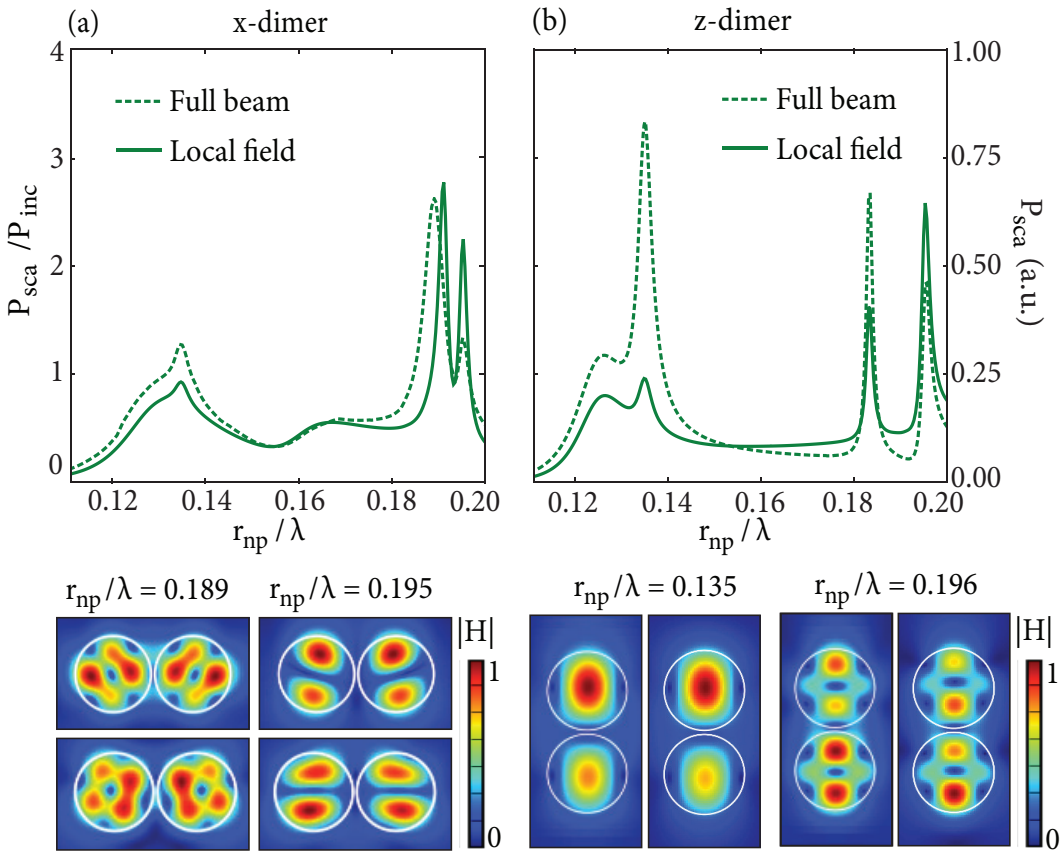

Figure 5.4: Scattering response of (a) x-dimer and (b) z-dimer antennas under tightly focused azimuthally polarized illumination as a function of normalized frequency. The field plots obtained from the full beam simulations (top row/left column) are compared with the field plots obtained from the local field simulations (bottom row/right column), which show good agreement with each other.

Combined, the advantages listed here result in a 60x speedup in the time required to obtain the scattering spectra. In addition to the time savings provided by this method, the local field simulation method is conceptually simpler and more intuitive than existing methods for modeling structured light interactions with nanoscale resonators.

The local field simulation effectively predicts the scattering response of spherical particles, and can also be used to predict the scattering response of arbitrary particles under illumination by any type of structured light. In this case, we use dimer antennas, an antenna system that has been explored extensively in chapter 4, as a stand-in for an

arbitrary resonator configuration. The dimer antenna considered here consists of two spherical particles with radius $r_{np} = 100nm$, index of refraction $n = 3.7$, and separation distance of $10nm$. Here we consider two types of antennas: 1) the x-dimer antenna, which is oriented along the x-axis, and 2) the z-dimer antenna, which is oriented along the z-axis. The vastly different symmetries of these antennas demonstrate the flexibility of the local field simulation method. We model the response of the dimer antennas under RP illumination using the local field simulation method, using the same setup that was used for the spherical particle. The resultant scattering response is compared with the response from the full beam simulation.

As seen in Fig. 5.3, the qualitative scattering response obtained by the local field simulation matches extremely well with the full beam simulation. The qualitative spectral response obtained from the local field simulation provides a wealth of information about the resonator response to RP illumination. We find that the x-dimer antenna couples to three modes in this wavelength regime, while the z-dimer antenna only couples to one. We can also extract the field plots of the excited modes from the local field simulation, which are compared with the field plots obtained from the full beam simulations, also pictured in Fig. 5.4. Using the information provided by the field plots, we can see, for example, that the x-dimer mode at $r_{np}/\lambda = 0.126$ provides better field electric enhancement in the dimer gap than the mode at $r_{np}/\lambda = 0.178$. We can also gain insight into the nature of the multipolar modes excited in the resonator from the field plots. For example, the null electric field in the center of the spheres that constitute the x-dimer mode at $r_{np}/\lambda = 0.126$ may be indicative of magnetic dipole-like modes, whereas the bright electric field in the spheres that constitute the x-dimer antenna in the mode at $r_{np}/\lambda = 0.178$ may be indicative of electric dipole-like modes. The real and imaginary parts of the electric and magnetic fields, which can also be obtained from the local field simulations, can provide additional insight about the nature of the dimer modes.

As another example, we model the interaction between the x- and z-dimer antennas and an AP beam. As seen in Fig. 5.4, we find excellent qualitative agreement between the spectral response and field plots obtained from the full beam simulation in comparison with the local field simulation. We see that the dimer antennas respond very differently to AP illumination as compared to RP illumination. The spectra obtained from the local field simulation show us that the dimers exhibit sharper resonances under AP illumination as compared with RP illumination. For example, we see that the z-dimer antenna couples to modes with a higher Q factor under AP illumination than the mode under RP illumination. Additionally, the local field method is able to accurately reproduce subtle nuances in the scattering spectra, such as the faint shoulder in the x-dimer response at $r_{np}/\lambda = 0.126$. The field plots also provide insight into the nature of the dimer modes. For example, the four-fold symmetry evident in the field plot of the x-dimer mode at $r_{np}/\lambda = 0.189$ suggests that the AP beam is exciting a higher order multipole mode at this wavelength.

As seen from Figs. 5.3 and 5.4, the local field simulation accurately predicts the coupling response for two completely different dimer geometries, quickly distinguishing between the scattering response under RP and AP illumination. The behavior of electric and magnetic fields within the resonators for both types of geometries is also easily extracted, even when the field patterns are complex. The wealth of information provided by the local field method, including the scattering response, approximate Q-factor of modes, and field plots, is essential information needed to evaluate resonator designs for specific metamaterial applications.

In conclusion, we presented a new method for modeling multipolar phenomena in arbitrary resonators under any type of illumination. We first validate the analytical local field theory for a sphere using numerical simulations. We then extend the concepts of the local field theory to implement a computationally efficient method for simulating

illumination of a sphere by structured light, deemed the local field simulation method. After demonstrating that this method works for a spherical particle, we extend our simulations to model the scattering response of dimer antennas under illumination by RP and AP beams, and show that the local field simulation accurately reproduces the fields in the resonators. This establishes the local field approach as a simple, intuitive, and efficient method for modeling the interaction of structured light with arbitrary particles for engineering novel metamaterials.

Chapter 6

Summary and future work

Metamaterials have proven to be a ground-breaking technology for achieving a wide variety of light control applications. However, conventional metamaterial design is limited to engineering particle properties and uses only linearly polarized plane wave illumination for manipulating light-matter interactions. This thesis shows that engineering the light source enables a new range of phenomena inaccessible by conventional metamaterial designs.

In chapter 2 we derived a new framework for determining the response of a spherical particle to any arbitrary type of illumination beam, known as the local field theory. We proved that individual multipolar resonances are driven by specific field properties of the illuminating beam. The local field theory drastically simplifies the steps required to determine the scattering response of a sphere to different types of illumination and provides an intuitive understanding of the origin of multipolar modes in sub-wavelength particles.

In chapter 3 we used the analytical local field equations to explore the response of a single dielectric sphere under illumination by cylindrical vector (CV) beams. We demonstrated that such beams are capable of coupling to dark modes and selectively

exciting individual multipolar modes, by engineering the relevant beam properties that drive dipolar and quadrupolar interactions. These beams significantly alter not just the scattering spectra of the spherical particle, but also the physical radiation of the excited multipolar modes.

In chapter 4 we investigated the response of dielectric dimer antennas to CV beams. We found that the beams induce hybridized electric and magnetic modes in the dimer antennas and that these hybridized modes provide excellent electric and magnetic field enhancements in the dimer gap. Horizontal dimers exhibited scattering responses with a mixture of electric and magnetic modes. Conversely, vertical dimers, in which the dimer axis coincides with the beam axis, exhibited selective excitation of electric or magnetic modes, similar to a sphere under CV beam illumination.

In chapter 5 we implemented a numerical simulation technique based on the analytical local field theory that drastically reduces the computation time required to determine the scattering response and radiation fields of an arbitrary particle under any type of illumination. This technique is very useful for qualitatively predicting a number of important features when screening particles for use in building metamaterials, including the frequency locations of multipolar resonances, Q-factors of resonances, and field profiles of excited modes.

This thesis focuses primarily on theories of multipolar scattering. Future work on theoretical formulations will be to improve on the numerical local field simulation to achieve quantitative agreement with the full beam simulation, to explore the response of dielectric particles to other types of illumination beams, and to explore optical forces that arise from multipolar modes [87, 88]. Experimentally, future work will include constructing an experimental setup to validate the theoretical phenomena proposed in this thesis, measuring the magnetic dipole enhancement in lanthanide ions using the structures proposed in this thesis [76], as well as extending the principles introduced

here to other material systems and geometries, particularly particle arrays. Based on the results presented in this thesis, beam engineering may prove to be an essential technique for designing metamaterials in the future.

Appendix A

Analytical theory: Mathematica code

A.1 Comparing Local field theory and Generalized Lorenz Mie Theory

User input: Input parameters and setup

```
SetDirectory[NotebookDirectory[]];

(* !!! INPUT !!! *)rnp=50*10^-9; (* radius of particle *)
(* !!! INPUT !!! *)\[Alpha]x=\[Pi]/2; (* half-angle of focus in radians *)
(* !!! INPUT !!! *)f=10.5rnp; (* fitting parameter *)
(* !!! INPUT !!! *)E0=1; (* fitting parameter *)
(* !!! INPUT !!! *)N1=1.3; (* refractive index of medium *)
(* !!! INPUT !!! *)\[Mu]1=1; (* permeability of medium *)

(* constants *)
\[Mu]0=4\[Pi]*10^\[Minus]7; (* permeability of free space *)
\[Epsilon]0=8.839388314328648`*^-12; (* permittivity of free space *)
```

```
(* properties of medium *)
\[Epsilon]1=N1^2; (* permittivity of medium *)
Z=Sqrt[(\[Mu]0*\[Mu]1)/(\[Epsilon]0*\[Epsilon]1)]; (* impedance of medium *)
k[\[Lambda]_]:=(2\[Pi])/\[Lambda]*N1; (* wavenumber in medium *)
c=299792458/N1; (* speed of light in medium *)
\[Omega][\[Lambda]_]=c*k[\[Lambda]]; (* frequency of light in medium *)

data1=Flatten[Import["J&C_Ag_n.xlsx"],1]; (* data on real part of index of Silver *)
data2=Flatten[Import["J&C_Ag_k.xlsx"],1]; (* data on imaginary part of index of Silver
    *)
nAg=Interpolation[data1];
\[Kappa]Ag=Interpolation[data2];

(* properties of particle *)
xm[\[Lambda]_]=k[\[Lambda]]*rnp; (* Mie parameter *)
Nr[\[Lambda]_]=nAg[\[Lambda]*1*^6]+I*\[Kappa]Ag[\[Lambda]*1*^6]; (* refractive index of
    particle *)
k1[\[Lambda]_]:=(2\[Pi])/\[Lambda]*Nr[\[Lambda]]; (* wavenumber in particle *)
m[\[Lambda]_]=k1[\[Lambda]]/k[\[Lambda]];
```

GLMT code

```
(* pi and tau functions *)
pi[n_,\[Theta]_]:=If[n==0,0,If[n==1,1,((2n-1)/(n-1)*Cos[\[Theta]]*pi[n-1,\[Theta]]-n/(n
    -1)*pi[n-2,\[Theta]])]];
tau[n_,\[Theta]_]:=n*Cos[\[Theta]]*pi[n,\[Theta]]-(n+1)*pi[n-1,\[Theta]]

(* beam coefficients *)
An[n_,\[Lambda]_,\[Alpha]_]:=(-I)^n*E0*k[\[Lambda]]*f*(2n+1)/(2n^2 (n+1)^2)*NIntegrate[
    Sqrt[Cos[\[Theta]]]*(pi[n,\[Theta]]+tau[n,\[Theta]])*Sin[\[Theta]],{\[Theta],0,\[
```

```
    Alpha]}];

(* Bessel functions *)
J[n_,\[Rho]_]:=J[n,\[Rho]]=SphericalBesselJ[n,\[Rho]];
\[Psi]n[n_,\[Rho]_]=\[Rho]*SphericalBesselJ[n,\[Rho]];
d\[Psi]n[n_,\[Rho]_]=SphericalBesselJ[n,\[Rho]]+\[Rho] (-(SphericalBesselJ[n,\[Rho]]/(2
    \[Rho]))+1/2 (SphericalBesselJ[-1+n,\[Rho]]-SphericalBesselJ[1+n,\[Rho]]));
\[Xi]n[n_,\[Rho]_]=\[Rho]*SphericalHankelH1[n,\[Rho]];
d\[Xi]n[n_,\[Rho]_]=SphericalHankelH1[n,\[Rho]]+\[Rho] (-(SphericalHankelH1[n,\[Rho]]/(2
     \[Rho]))+1/2 (SphericalHankelH1[-1+n,\[Rho]]-SphericalHankelH1[1+n,\[Rho]]));

(* Mie coefficients *)
an[n_,\[Lambda]_]:=(m[\[Lambda]]*\[Psi]n[n,m[\[Lambda]]*xm[\[Lambda]]]*d\[Psi]n[n,xm[\[
    Lambda]]]-\[Psi]n[n,xm[\[Lambda]]]*d\[Psi]n[n,m[\[Lambda]]*xm[\[Lambda]]])/(m[\[
    Lambda]]*\[Psi]n[n,m[\[Lambda]]*xm[\[Lambda]]]*d\[Xi]n[n,xm[\[Lambda]]]-\[Xi]n[n,xm
    [\[Lambda]]]*d\[Psi]n[n,m[\[Lambda]]*xm[\[Lambda]]]);

bn[n_,\[Lambda]_]:=(m[\[Lambda]]*\[Psi]n[n,xm[\[Lambda]]]*d\[Psi]n[n,m[\[Lambda]]*xm[\[
    Lambda]]]-\[Psi]n[n,m[\[Lambda]]*xm[\[Lambda]]]*d\[Psi]n[n,xm[\[Lambda]]])/(m[\[
    Lambda]]*\[Xi]n[n,xm[\[Lambda]]]*d\[Psi]n[n,m[\[Lambda]]*xm[\[Lambda]]]-\[Psi]n[n,m
    [\[Lambda]]*xm[\[Lambda]]]*d\[Xi]n[n,xm[\[Lambda]]]);

(* spherical vector harmonics for incoming fields *)
Mo1ni[n_,k_,r_,\[Theta]_,\[Phi]_]:={{0},{Cos[\[Phi]]*pi[n,\[Theta]]*J[n,k*r]},{-Sin[\[
    Phi]]*tau[n,\[Theta]]*J[n,k*r]}};
Ne1ni[n_,k_,r_,\[Theta]_,\[Phi]_]:={{Cos[\[Phi]]*n(n+1)*Sin[\[Theta]]*pi[n,\[Theta]]*J[
    n,k*r]/(k*r)},{Cos[\[Phi]]*tau[n,\[Theta]]*d\[Psi]n[n,k*r]/(k*r)},{-Sin[\[Phi]]*pi[n
    ,\[Theta]]*d\[Psi]n[n,k*r]/(k*r)}};
Me1ni[n_,k_,r_,\[Theta]_,\[Phi]_]:={{0},{-Sin[\[Phi]]*pi[n,\[Theta]]*J[n,k*r]},{-Cos[\[
    Phi]]*tau[n,\[Theta]]*J[n,k*r]}};
No1ni[n_,k_,r_,\[Theta]_,\[Phi]_]:={{Sin[\[Phi]]*n*(n+1)*Sin[\[Theta]]*pi[n,\[Theta]]*J
```

```
    [n,k*r]/(k*r)},{Sin[\[Phi]]*tau[n,\[Theta]]*d\[Psi]n[n,k*r]/(k*r)},{Cos[\[Phi]]*pi[n
    ,\[Theta]]*d\[Psi]n[n,k*r]/(k*r)}});

(* electric and magnetic fields of incident beam *)
EiFPWsph[\[Lambda]_,\[Alpha]_, nmax_, r_,\[Theta]_,\[Phi]_]:=Flatten[Total[Table[An[n,\[
    Lambda],\[Alpha]]*(Ne1ni[n, k[\[Lambda]], r,\[Theta],\[Phi]]-I*Mo1ni[n,  k[\[Lambda
    ]], r,\[Theta],\[Phi]]), {n, 1, nmax}]]];
HiFPWsph[\[Lambda]_,\[Alpha]_, nmax_,r_,\[Theta]_,\[Phi]_]:=Flatten[Total[Table[-(k[\[
    Lambda]]/(\[Omega][\[Lambda]]*\[Mu]0))An[n,\[Lambda],\[Alpha]]*(No1ni[n,  k[\[Lambda
    ]], r,\[Theta],\[Phi]]+I*Me1ni[n, k[\[Lambda]],  r,\[Theta],\[Phi]]), {n, 1, nmax
    }]]];

(* Poynting vector of incident beam *)
Si[\[Lambda]_,\[Alpha]_,nmax_,r_,\[Theta]_,\[Phi]_]:=1/2 Re[EiFPWsph[\[Lambda],\[Alpha],
    nmax,r,\[Theta],\[Phi]]\[Cross]Conjugate[HiFPWsph[\[Lambda],\[Alpha],nmax,r,\[Theta
    ],\[Phi]]]];

(* power of incident beam integrated over a circular area *)
Pinc[\[Lambda]_,\[Alpha]_,nmax_,r_]:=f^2*NIntegrate[Re[Si[\[Lambda],\[Alpha],nmax,r,\[
    Theta],\[Phi]]][[1]]*Sin[\[Theta]],{\[Theta],\[Pi]/2,\[Pi]},{\[Phi],0,2\[Pi]}];

(* power scattered by sphere from GLMT *)
Psca[\[Lambda]_,\[Alpha]_,nmax_]:=\[Pi]/(2Z*k[\[Lambda]]^2)*Total[Table[(2n^2 (n+1)^2)
    /(2n+1) Abs[An[n,\[Lambda],\[Alpha]]]^2+(Abs[an[n,\[Lambda]]]^2+Abs[bn[n,\[Lambda
    ]]]^2),{n,1,nmax}]];

(* fraction of power scattered by the sphere to incident power from GLMT *)
Ksca[\[Lambda]_,\[Alpha]_,nmax_,r_]:=Psca[\[Lambda],\[Alpha],nmax]/Pinc[\[Lambda],\[
    Alpha],nmax,r];
```

Local field code

```
(* conversion of spherical unit vectors to cartesian unit vectors *)
SphtoCarUV[\[Theta]_,\[Phi]_]:={{Sin[\[Theta]]*Cos[\[Phi]],Cos[\[Theta]]*Cos[\[Phi]],-
    Sin[\[Phi]]},{Sin[\[Theta]]*Sin[\[Phi]],Cos[\[Theta]]*Sin[\[Phi]],Cos[\[Phi]]},{Cos
    [\[Theta]],-Sin[\[Theta]],0}};

(* electric and magnetic fields of incident beam in spherical coordinates and unit
    vectors *)
EiFPW[\[Lambda]_,\[Alpha]_,n_,r_,\[Theta]_,\[Phi]_]:=An[n,\[Lambda],\[Alpha]]*(Ne1ni[n,
    k[\[Lambda]], r,\[Theta],\[Phi]]-I*Mo1ni[n,  k[\[Lambda]], r,\[Theta],\[Phi]]);
HiFPW[\[Lambda]_,\[Alpha]_,n_,r_,\[Theta]_,\[Phi]_]:=-(k[\[Lambda]]/(\[Omega][\[Lambda
    ]]*\[Mu]0))An[n,\[Lambda],\[Alpha]]*(No1ni[n,  k[\[Lambda]], r,\[Theta],\[Phi]]+I*
    Me1ni[n, k[\[Lambda]],  r,\[Theta],\[Phi]]);

(* electric and magnetic fields of incident beam in Cartesian coordinates and unit
    vectors *)
EiFPWcar[\[Lambda]_,\[Alpha]_,nmax_,x_,y_,z_]:=SphtoCarUV[ArcTan[z,Sqrt[x^2+y^2]],
    ArcTan[x, y]].EiFPW[\[Lambda],\[Alpha],nmax,Sqrt[x^2+y^2+z^2], ArcTan[z,Sqrt[x^2+y
    ^2]], ArcTan[x, y]];
HiFPWcar[\[Lambda]_,\[Alpha]_,nmax_,x_,y_,z_]:=SphtoCarUV[ArcTan[z,Sqrt[x^2+y^2]],
    ArcTan[x, y]].HiFPW[\[Lambda],\[Alpha],nmax,Sqrt[x^2+y^2+z^2], ArcTan[z,Sqrt[x^2+y
    ^2]], ArcTan[x, y]];

(* summation of electric field gradients for local field theory *)
delsumFPW[\[Lambda]_,nmax_,x_,y_,z_]:=
1/2*{{2*D[EiFPWcar[\[Lambda],\[Alpha]x,nmax,x,y,z][[1]],x],D[EiFPWcar[\[Lambda],\[Alpha]
    x,nmax,x,y,z][[1]],y]+D[EiFPWcar[\[Lambda],\[Alpha]x,nmax,x,y,z][[2]],x],D[EiFPWcar
    [\[Lambda],\[Alpha]x,nmax,x,y,z][[1]],z]+D[EiFPWcar[\[Lambda],\[Alpha]x,nmax,x,y,z
    ][[3]],x]},{D[EiFPWcar[\[Lambda],\[Alpha]x,nmax,x,y,z][[2]],x]+D[EiFPWcar[\[Lambda
    ],\[Alpha]x,nmax,x,y,z][[1]],y],2*D[EiFPWcar[\[Lambda],\[Alpha]x,nmax,x,y,z][[2]],y
    ],D[EiFPWcar[\[Lambda],\[Alpha]x,nmax,x,y,z][[2]],z]+D[EiFPWcar[\[Lambda],\[Alpha]x,
    nmax,x,y,z][[3]],y]},{D[EiFPWcar[\[Lambda],\[Alpha]x,nmax,x,y,z][[3]],x]+D[EiFPWcar
```

```
    [\[Lambda],\[Alpha]x,nmax,x,y,z][[1]],z],D[EiFPWcar[\[Lambda],\[Alpha]x,nmax,x,y,z
    ][[3]],y]+D[EiFPWcar[\[Lambda],\[Alpha]x,nmax,x,y,z][[2]],z],2*D[EiFPWcar[\[Lambda
    ],\[Alpha]x,nmax,x,y,z][[3]],z]}};
deltotFPW[\[Lambda]_,nmax_,x_,y_,z_]=delsumFPW[\[Lambda],2,x,y,z];
del[\[Lambda]_,nmax_,x_,y_,z_]:=Total[Flatten[Table[Norm[(deltotFPW[\[Lambda],nmax,x,y,z
    ]^2)[[i]]],{i,1,Length[deltotFPW[\[Lambda],nmax,x,y,z]]}]]];

(* summation of magnetic field gradients for local field theory *)
delsumFPWH[\[Lambda]_,nmax_,x_,y_,z_]:=
1/2*{{2*D[HiFPWcar[\[Lambda],\[Alpha]x,nmax,x,y,z][[1]],x],D[HiFPWcar[\[Lambda],\[Alpha]
    x,nmax,x,y,z][[1]],y]+D[HiFPWcar[\[Lambda],\[Alpha]x,nmax,x,y,z][[2]],x],D[HiFPWcar
    [\[Lambda],\[Alpha]x,nmax,x,y,z][[1]],z]+D[HiFPWcar[\[Lambda],\[Alpha]x,nmax,x,y,z
    ][[3]],x]},{D[HiFPWcar[\[Lambda],\[Alpha]x,nmax,x,y,z][[2]],x]+D[HiFPWcar[\[Lambda
    ],\[Alpha]x,nmax,x,y,z][[1]],y],2*D[HiFPWcar[\[Lambda],\[Alpha]x,nmax,x,y,z][[2]],y
    ],D[HiFPWcar[\[Lambda],\[Alpha]x,nmax,x,y,z][[2]],z]+D[HiFPWcar[\[Lambda],\[Alpha]x,
    nmax,x,y,z][[3]],y]},{D[HiFPWcar[\[Lambda],\[Alpha]x,nmax,x,y,z][[3]],x]+D[HiFPWcar
    [\[Lambda],\[Alpha]x,nmax,x,y,z][[1]],z],D[HiFPWcar[\[Lambda],\[Alpha]x,nmax,x,y,z
    ][[3]],y]+D[HiFPWcar[\[Lambda],\[Alpha]x,nmax,x,y,z][[2]],z],2*D[HiFPWcar[\[Lambda
    ],\[Alpha]x,nmax,x,y,z][[3]],z]}};
deltotFPWH[\[Lambda]_,nmax_,x_,y_,z_]=delsumFPWH[\[Lambda],2,x,y,z];
delFPWH[\[Lambda]_,nmax_,x_,y_,z_]:=Total[Flatten[Table[Norm[(deltotFPWH[\[Lambda],nmax,
    x,y,z]^2)[[i]]],{i,1,Length[deltotFPWH[\[Lambda],nmax,x,y,z]]}]]];

w=10^-30;

(* power scattered by sphere from local field theory *)
Ws2[e_,M_,\[Lambda]_,r_]:=e*Abs[an[1,\[Lambda]]]^2*(3\[Pi])/(k[\[Lambda]]*\[Omega][\[
    Lambda]]*\[Mu]0)*Norm[EiFPWsph[\[Lambda],\[Alpha]x,1,w,w,w]]^2+M*Abs[bn[1,\[Lambda
    ]]]^2*(3\[Pi])/(k[\[Lambda]]*\[Omega][\[Lambda]]*\[Mu]0)*Norm[HiFPWsph[\[Lambda],\[
    Alpha]x,1,w,w,w]]^2+e*Abs[an[2,\[Lambda]]]^2*(10\[Pi])/(k[\[Lambda]]^3*\[Omega][\[
    Lambda]]*\[Mu]0)*del[\[Lambda],2,w,w,w]+M*Abs[bn[2,\[Lambda]]]^2*(10\[Pi])/(k[\[
```

```
    Lambda]]^3*\[Omega][\[Lambda]]*\[Mu]0)*Z^2*delFPWH[\[Lambda],2,w,w,w];

(* fraction of power scattered by the sphere to incident power from local field theory
    *)
Ksca2[e_,M_,\[Lambda]_,\[Alpha]_,nmax_,r_]:=Ws2[e,M,\[Lambda],10^3]/Pinc[\[Lambda],\[
    Alpha],nmax,r];
```

Plots of spectral response

```
(* results from GLMT *)
data1=ParallelTable[{x,Abs[Re[Ksca[x,\[Alpha]x,3,10rnp]]]},{x,300*^-9,700*^-9,(700*^-9-
    300*^-9)/200}];
ListPlot[{data1},Joined->True,PlotRange->All]

(* results from local field theory *)
data2=ParallelTable[{x,Abs[Re[Ksca2[1,1,x,\[Alpha]x,3,10rnp]]]},{x
    ,300*^-9,700*^-9,(700*^-9- 300*^-9)/200}];
ListPlot[{data2},Joined->True,PlotRange->All]
```

A.2 Calculation of incident power for a focused beam

Setup

```
SetDirectory[NotebookDirectory[]];


(* constants -- assuming medium is vacuum *)
c=3*^8; (* speed of light in a vacuum *)
\[Mu]=1.257*^-6; (* permeability of free space *)
\[Epsilon]0=1/(c^2 \[Mu]);(* permittivity of free space *)
\[Omega][\[Lambda]_]=(2.\[Pi]*c)/(\[Lambda]*1.*^-9); (* angular frequency in terms of
    wavelength *)
Z=Sqrt[\[Mu]/\[Epsilon]0]; (* impedance of free space *)
```

User input: Properties of medium and particle

```
(* physical properties of medium *)
(* !!! INPUT !!! *) Nr[\[Lambda]_]=1;  (* refractive index of medium*)
(* !!! INPUT !!! *) N1[\[Lambda]_]=3.7; (* refractive index of particle *)
(* !!! INPUT !!! *) rNP=100; (* radius of particle *)


kw[\[Lambda]_]=(2\[Pi])/(\[Lambda]*1*^-9)*Nr[\[Lambda]]; (* wavenumber of light in
    medium *)
\[Epsilon]1[\[Lambda]_]=N1[\[Lambda]]^2;
d[rNP_]=2*rNP; (* diameter of particle *)
m[\[Lambda]_]=N1[\[Lambda]]/Nr[\[Lambda]]; (* relative refractive index of medium and
    particle *)
kp[\[Lambda]_]=kw[\[Lambda]]*m[\[Lambda]]; (* wavenumber of light in particle *)
xM[xm_]=2\[Pi]*Nr[\[Lambda]]*m; (* Mie parameter, as defined on pg. 100of B&H, where xm=
    rNP/lambda *)
```

Bessel functions

```
(* Bessel and Hankel functions *)
J[n_,\[Rho]_]=SphericalBesselJ[n,\[Rho]];
Y[n_,\[Rho]_]=SphericalBesselY[n,\[Rho]];
H[n_,\[Rho]_]=SphericalHankelH1[n,\[Rho]];

(* Ricatti-Bessel functions *)
\[Psi]n[n_,\[Rho]_]=\[Rho]*SphericalBesselJ[n,\[Rho]];
d\[Psi]n[n_,\[Rho]_]=SphericalBesselJ[n,\[Rho]]+\[Rho] (-(SphericalBesselJ[n,\[Rho]]/(2
    \[Rho]))+1/2 (SphericalBesselJ[-1+n,\[Rho]]-SphericalBesselJ[1+n,\[Rho]]));
\[Xi]n[n_,\[Rho]_]=\[Rho]*SphericalHankelH1[n,\[Rho]];
d\[Xi]n[n_,\[Rho]_]=SphericalHankelH1[n,\[Rho]]+\[Rho] (-(SphericalHankelH1[n,\[Rho]]/(2
     \[Rho]))+1/2 (SphericalHankelH1[-1+n,\[Rho]]-SphericalHankelH1[1+n,\[Rho]]));
```

Mie scattering coefficients and spherical vector harmonics

```
(* Mie coefficients *)
an[n_,\[Lambda]_,xm_]=(m[\[Lambda]]*\[Psi]n[n,m[\[Lambda]]*xM[xm]]*d\[Psi]n[n,xM[xm]]-\[
    Psi]n[n,xM[xm]]*d\[Psi]n[n,m[\[Lambda]]*xM[xm]])/(m[\[Lambda]]*\[Psi]n[n,m[\[Lambda
    ]]*xM[xm]]*d\[Xi]n[n,xM[xm]]-\[Xi]n[n,xM[xm]]*d\[Psi]n[n,m[\[Lambda]]*xM[xm]]);
bn[n_,\[Lambda]_,xm_]=(\[Psi]n[n,m[\[Lambda]]*xM[xm]]*d\[Psi]n[n,xM[xm]]-m[\[Lambda]]*\[
    Psi]n[n,xM[xm]]*d\[Psi]n[n,m[\[Lambda]]*xM[xm]])/(\[Psi]n[n,m[\[Lambda]]*xM[xm]]*d\[
    Xi]n[n,xM[xm]]-m[\[Lambda]]*\[Xi]n[n,xM[xm]]*d\[Psi]n[n,m[\[Lambda]]*xM[xm]]);
```

User input: Angular spectrum decomposition of incident beam

```
(* !!! INPUT !!! *) \[Alpha]t=\[Pi]/3; (* half-angle annular aperture of focusing lens
    *)
(* !!! INPUT !!! *) N\[Theta]t=10; (* number of plane waves in theta *)
(* !!! INPUT !!! *) N\[Phi]t=10; (* number of plane waves in phi *)

(* angular spectrum of incident wave in Cartesian unit vectors *)
(* linearly polarized *)
```

```
angspecLP[\[Theta]_,\[Phi]_]={(Cos[\[Theta]]Cos[\[Phi]]^2+Sin[\[Phi]]^2),(Cos[\[Theta]]
    Cos[\[Phi]]Sin[\[Phi]]-Cos[\[Phi]]Sin[\[Phi]]),-Sin[\[Theta]]Cos[\[Phi]]};
angspecMLP[\[Theta]_,\[Phi]_]=-{(1-Cos[\[Theta]])Cos[\[Phi]]Sin[\[Phi]],-(1-(1-Cos[\[
    Theta]])Sin[\[Phi]]^2),Sin[\[Theta]]Sin[\[Phi]]};

(* radially polarized *)
angspecRP[\[Theta]_,\[Phi]_]={Cos[\[Theta]]Cos[\[Phi]],Cos[\[Theta]]Sin[\[Phi]],Sin[\[
    Theta]]};
angspecMRP[\[Theta]_,\[Phi]_]={-Sin[\[Phi]],Cos[\[Phi]],0};

(* azimuthally polarized *)
angspecAP[\[Theta]_,\[Phi]_]={-Sin[\[Phi]],Cos[\[Phi]],0};
angspecMAP[\[Theta]_,\[Phi]_]={-Cos[\[Theta]]Cos[\[Phi]],-Cos[\[Theta]]Sin[\[Phi]],Sin
    [\[Theta]]};

\[Theta]ii=Table[((i-1)\[Alpha]t)/N\[Theta]t,{i,1,N\[Theta]t+1,1}]; (**)
\[Phi]jj=Table[((j-1) 2 \[Pi])/N\[Phi]t,{j,1,N\[Phi]t+1,1}];

(* incident electric and magnetic fields *)
ikr[\[Lambda]_,\[Theta]_,\[Phi]_,xp_,yp_,zp_]=I*kw[\[Lambda]]*(Sin[\[Theta]]*Cos[\[Phi
    ]]*(xp)+Sin[\[Theta]]*Sin[\[Phi]]*(yp)-Cos[\[Theta]]*(zp));
(* !!! INPUT !!! *)
(*-- choose desired angular spectrum*)Ei[\[Theta]_,\[Phi]_,\[Lambda]_,x_,y_,z_]=-I/\[
    Lambda]*angspecAP[\[Theta],\[Phi]]*Sqrt[Abs[Cos[\[Theta]]]]*Sin[\[Theta]]*Exp[ikr[\[
    Lambda],\[Theta],\[Phi],x,y,z]]*\[Alpha]t/N\[Theta]t*2\[Pi]/N\[Phi]t;
Einc[\[Lambda]_,xp_,yp_,zp_]=Flatten[Table[Table[Ei[\[Theta]ii[[i]],\[Phi]jj[[j]],\[
    Lambda],xp,yp,zp],{i,1.,N\[Theta]t+1,1.}],{j,1.,N\[Phi]t+1,1.}],1];
E0sum[\[Lambda]_,xp_,yp_,zp_]=Total[Einc[\[Lambda],xp,yp,zp]];

(* !!! INPUT !!! *)
(*-- choose desired angular spectrum*)Hi[\[Theta]_,\[Phi]_,\[Lambda]_,x_,y_,z_]=-I/\[
```

```
    Lambda]*1/Z*angspecMAP[\[Theta],\[Phi]]*Exp[I*\[Pi]]*Sqrt[Abs[Cos[\[Theta]]]]*Sin[\[
    Theta]]*Exp[ikr[\[Lambda],\[Theta],\[Phi],x,y,z]]*\[Alpha]t/N\[Theta]t*2\[Pi]/N\[Phi
    ]t;
Hinc[\[Lambda]_,xp_,yp_,zp_]=Flatten[Table[Table[Hi[\[Theta]ii[[i]],\[Phi]jj[[j]],\[
    Lambda],xp,yp,zp],{i,1.,N\[Theta]t+1,1.}],{j,1.,N\[Phi]t+1,1.}],1];
H0sum[\[Lambda]_,xp_,yp_,zp_]=Total[Hinc[\[Lambda],xp,yp,zp]];
```

Calculation of incident power

```
w=10^-30;

(* !!! INPUT !!! *) lb=0.05;  (* lower bound of rnp/lambda *)
(* !!! INPUT !!! *) ub=0.25; (* upper bound of rnp/lambda *)
(* !!! INPUT !!! *) numS=100; (* number of wavelength steps *)

r\[Lambda]=Table[x,{x,lb,ub,(ub-lb)/numS}];
(* table of normalized frequency points *)
\[Lambda]t=rNP/r\[Lambda];(* table of wavelength points *)

w=10^-30;

(* calculation of Poynting vector in Cartesian coordinate system *)
Sw[\[Lambda]t_,x_,y_,z_]:={1/2*Re[E0sum[\[Lambda]t,x,y,z][[2]]*Conjugate[H0sum[\[Lambda]
    t,x,y,z]][[3]]-E0sum[\[Lambda]t,x,y,z][[3]]*Conjugate[H0sum[\[Lambda]t,x,y,z
    ]][[2]]],1/2*Re[E0sum[\[Lambda]t,x,y,z][[3]]*Conjugate[H0sum[\[Lambda]t,x,y,z
    ]][[1]]-E0sum[\[Lambda]t,x,y,z][[1]]*Conjugate[H0sum[\[Lambda]t,x,y,z]][[3]]],1/2*Re
    [E0sum[\[Lambda]t,x,y,z][[1]]*Conjugate[H0sum[\[Lambda]t,x,y,z]][[2]]-E0sum[\[Lambda
    ]t,x,y,z][[2]]*Conjugate[H0sum[\[Lambda]t,x,y,z]][[1]]]};

(* calculation of Poynting vector in spherical coordinate system *)
Swsph[\[Lambda]t_,r_,\[Theta]_,\[Phi]_]:=1/2*Re[E0sum[\[Lambda]t,r Cos[\[Phi]] Sin[\[
```

```
    Theta]],r Sin[\[Theta]] Sin[\[Phi]],r Cos[\[Theta]]]\[Cross]Conjugate[H0sum[\[Lambda
    ]t,r Cos[\[Phi]] Sin[\[Theta]],r Sin[\[Theta]] Sin[\[Phi]],r Cos[\[Theta]]]]];

(* algorithm for finding width of main lobe of incident beam, stored in 'rrpp' *)
rrpp={};

(* !!! INPUT !!! *) ll=10^-8; (* lower bound for width of main lobe of incident beam in
    m *)
(* !!! INPUT !!! *) ul=10^-5; (* upper bound for width of main lobe of incident beam in
    m*)
(* !!! INPUT !!! *) numl=100; (* number of width steps *)

(* algorithm for finding minimum and maximum points in a list *)
findExtremaPos[list_List] :=
 Module[{signs, extremaPos, minPos, maxPos},
 signs = Sign[Differences[list]];
 signs = signs //. {a___, q_, 0, z__} -> {a, q, q, z};
 extremaPos = 1 + Accumulate@(Length /@ Split[signs]);
 If[First@signs == 1, minPos = extremaPos[[2 ;; -2 ;; 2]];
 maxPos = extremaPos[[1 ;; -2 ;; 2]],
 minPos = extremaPos[[1 ;; -2 ;; 2]];
 maxPos = extremaPos[[2 ;; -2 ;; 2]]];
 {minPos, maxPos}]

(* loop over all wavelengths of interest *)
Do[
S[x_]=Sw[\[Lambda]t[[i]],x,w,w];

ff =Table[Abs[S[x]][[3]],{x,ll,ul,(ul-ll)/numl}];

(* get extreme points *)
```

```
{min, max} = findExtremaPos[ff];

ListPlot[ff, Joined -> True,
 Epilog -> {PointSize[Large], Red, Point[{#, ff[[#]]} & /@ min],
 Blue, Point[{#, ff[[#]]} & /@ max]}, PlotRange -> All]

AppendTo[rrpp,min[[1]]*(ul-ll)/numl]
,{i,1,Length[\[Lambda]t]}]

(* incident power in a circular area *)
Pn[i_]:=NIntegrate[Norm[Swsph[\[Lambda]t[[1]],r,\[Pi]/2,\[Phi]][[3]]]*(r)*Sin[\[Pi]/2],{
    r,0,rrpp[[i]]},{\[Phi],0,2\[Pi]},Method->{"MonteCarloRule","SymbolicProcessing"->
    None},WorkingPrecision->5,PrecisionGoal->3];
```

Plot of incident power

```
(* plot of incident power over wavelength spectrum *)
power=ParallelTable[{\[Lambda]t[[x]],Re[Pn[x]]},{x,1,Length[rrpp],1}];
ListPlot[power,Joined->True,PlotRange->All]

rrpp={10^-7,10^-6,10^-5,10^-4};
(* plot of incident power over different radii of integration defined above in rrpp *)
power=ParallelTable[{rrpp[[x]],Re[Pn[x]]},{x,1,Length[rrpp],1}];
ListPlot[power,Joined->True,PlotRange->All]
```

A.3 Power scattered by a sphere under focused linearly, radially, and azimuthally polarized illumination

Setup

```
SetDirectory[NotebookDirectory[]];


(* constants -- assuming medium is vacuum *)
c=3*^8; (* speed of light in a vacuum *)
\[Mu]=1.257*^-6; (* permeability of free space *)
\[Epsilon]0=1/(c^2 \[Mu]);(* permittivity of free space *)
\[Omega][\[Lambda]_]=(2.\[Pi]*c)/(\[Lambda]*1.*^-9); (* angular frequency in terms of
    wavelength *)
Z=Sqrt[\[Mu]/\[Epsilon]0]; (* impedance of free space *)
```

User inputs: Properties of medium and particle

```
(* physical properties of medium *)
(* !!! INPUT !!! *) Nr[\[Lambda]_]=1;  (* refractive index of medium*)
(* !!! INPUT !!! *) N1[\[Lambda]_]=3.7; (* refractive index of particle *)
(* !!! INPUT !!! *) rnp=100; (* radius of particle *)


kw[\[Lambda]_]=(2\[Pi])/(\[Lambda]*1*^-9)*Nr[\[Lambda]]; (* wavenumber of light in
    medium *)
\[Epsilon]1[\[Lambda]_]=N1[\[Lambda]]^2;
d[rnp_]=2*rnp; (* diameter of particle *)
m[\[Lambda]_]=N1[\[Lambda]]/Nr[\[Lambda]]; (* relative refractive index of medium and
    particle *)
kp[\[Lambda]_]=kw[\[Lambda]]*m[\[Lambda]]; (* wavenumber of light in particle *)
```

```
xM[xm_]=2\[Pi]*Nr[\[Lambda]]*xm; (* Mie parameter, as defined on pg. 100of B&H, where xm
    =rNP/lambda *)
```

Bessel functions

```
(* Bessel and Hankel functions *)
J[n_,\[Rho]_]=SphericalBesselJ[n,\[Rho]];
Y[n_,\[Rho]_]=SphericalBesselY[n,\[Rho]];
H[n_,\[Rho]_]=SphericalHankelH1[n,\[Rho]];

(* Ricatti-Bessel functions *)
\[Psi]n[n_,\[Rho]_]=\[Rho]*SphericalBesselJ[n,\[Rho]];
d\[Psi]n[n_,\[Rho]_]=SphericalBesselJ[n,\[Rho]]+\[Rho] (-(SphericalBesselJ[n,\[Rho]]/(2
    \[Rho]))+1/2 (SphericalBesselJ[-1+n,\[Rho]]-SphericalBesselJ[1+n,\[Rho]]));
\[Xi]n[n_,\[Rho]_]=\[Rho]*SphericalHankelH1[n,\[Rho]];
d\[Xi]n[n_,\[Rho]_]=SphericalHankelH1[n,\[Rho]]+\[Rho] (-(SphericalHankelH1[n,\[Rho]]/(2
     \[Rho]))+1/2 (SphericalHankelH1[-1+n,\[Rho]]-SphericalHankelH1[1+n,\[Rho]]));
```

Mie scattering coefficients and spherical vector harmonics

```
(* Mie coefficients *)
an[n_,\[Lambda]_,xm_]=(m[\[Lambda]]*\[Psi]n[n,m[\[Lambda]]*xM[xm]]*d\[Psi]n[n,xM[xm]]-\[
    Psi]n[n,xM[xm]]*d\[Psi]n[n,m[\[Lambda]]*xM[xm]])/(m[\[Lambda]]*\[Psi]n[n,m[\[Lambda
    ]]*xM[xm]]*d\[Xi]n[n,xM[xm]]-\[Xi]n[n,xM[xm]]*d\[Psi]n[n,m[\[Lambda]]*xM[xm]]);
bn[n_,\[Lambda]_,xm_]=(\[Psi]n[n,m[\[Lambda]]*xM[xm]]*d\[Psi]n[n,xM[xm]]-m[\[Lambda]]*\[
    Psi]n[n,xM[xm]]*d\[Psi]n[n,m[\[Lambda]]*xM[xm]])/(\[Psi]n[n,m[\[Lambda]]*xM[xm]]*d\[
    Xi]n[n,xM[xm]]-m[\[Lambda]]*\[Xi]n[n,xM[xm]]*d\[Psi]n[n,m[\[Lambda]]*xM[xm]]);
```

User input: Angular spectrum decomposition of incident beam

```
(* !!! INPUT !!! *) \[Alpha]t=\[Pi]/3; (* half-angle annular aperture of focusing lens
    *)
(* !!! INPUT !!! *) N\[Theta]t=100; (* number of plane waves in theta *)
```

```
(* !!! INPUT !!! *) N\[Phi]t=100; (* number of plane waves in phi *)

(* angular spectrum of incident wave in Cartesian unit vectors *)
(* linearly polarized *)
angspecLP[\[Theta]_,\[Phi]_]={(Cos[\[Theta]]Cos[\[Phi]]^2+Sin[\[Phi]]^2),(Cos[\[Theta]]
    Cos[\[Phi]]Sin[\[Phi]]-Cos[\[Phi]]Sin[\[Phi]]),-Sin[\[Theta]]Cos[\[Phi]]};
angspecMLP[\[Theta]_,\[Phi]_]=-{(1-Cos[\[Theta]])Cos[\[Phi]]Sin[\[Phi]],-(1-(1-Cos[\[
    Theta]])Sin[\[Phi]]^2),Sin[\[Theta]]Sin[\[Phi]]};

(* radially polarized *)
angspecRP[\[Theta]_,\[Phi]_]={Cos[\[Theta]]Cos[\[Phi]],Cos[\[Theta]]Sin[\[Phi]],Sin[\[
    Theta]]};
angspecMRP[\[Theta]_,\[Phi]_]={-Sin[\[Phi]],Cos[\[Phi]],0};

(* azimuthally polarized *)
angspecAP[\[Theta]_,\[Phi]_]={-Sin[\[Phi]],Cos[\[Phi]],0};
angspecMAP[\[Theta]_,\[Phi]_]={-Cos[\[Theta]]Cos[\[Phi]],-Cos[\[Theta]]Sin[\[Phi]],Sin
    [\[Theta]]};

\[Theta]ii=Table[((i-1)\[Alpha]t)/N\[Theta]t,{i,1,N\[Theta]t+1,1}]; (**)
\[Phi]jj=Table[((j-1) 2 \[Pi])/N\[Phi]t,{j,1,N\[Phi]t+1,1}];

(* incident electric and magnetic fields *)
ikr[\[Lambda]_,\[Theta]_,\[Phi]_,xp_,yp_,zp_]=I*kw[\[Lambda]]*(Sin[\[Theta]]*Cos[\[Phi
    ]]*(xp)+Sin[\[Theta]]*Sin[\[Phi]]*(yp)-Cos[\[Theta]]*(zp));
(* !!! INPUT !!! *)
(*-- choose desired angular spectrum*)Ei[\[Theta]_,\[Phi]_,\[Lambda]_,x_,y_,z_]=-I/\[
    Lambda]*angspecAP[\[Theta],\[Phi]]*Sqrt[Abs[Cos[\[Theta]]]]*Sin[\[Theta]]*Exp[ikr[\[
    Lambda],\[Theta],\[Phi],x,y,z]]*\[Alpha]t/N\[Theta]t*2\[Pi]/N\[Phi]t;
Einc[\[Lambda]_,xp_,yp_,zp_]=Flatten[Table[Table[Ei[\[Theta]ii[[i]],\[Phi]jj[[j]],\[
    Lambda],xp,yp,zp],{i,1.,N\[Theta]t+1,1.}],{j,1.,N\[Phi]t+1,1.}],1];
```

```
E0sum[\[Lambda]_,xp_,yp_,zp_]=Total[Einc[\[Lambda],xp,yp,zp]];


(* !!! INPUT !!! *)
(*-- choose desired angular spectrum*)Hi[\[Theta]_,\[Phi]_,\[Lambda]_,x_,y_,z_]=-I/\[
    Lambda]*1/Z*angspecMAP[\[Theta],\[Phi]]*Exp[I*\[Pi]]*Sqrt[Abs[Cos[\[Theta]]]]*Sin[\[
    Theta]]*Exp[ikr[\[Lambda],\[Theta],\[Phi],x,y,z]]*\[Alpha]t/N\[Theta]t*2\[Pi]/N\[Phi
    ]t;
Hinc[\[Lambda]_,xp_,yp_,zp_]=Flatten[Table[Table[Hi[\[Theta]ii[[i]],\[Phi]jj[[j]],\[
    Lambda],xp,yp,zp],{i,1.,N\[Theta]t+1,1.}],{j,1.,N\[Phi]t+1,1.}],1];
H0sum[\[Lambda]_,xp_,yp_,zp_]=Total[Hinc[\[Lambda],xp,yp,zp]];
```

Gradient of incident beam at a point in space

```
(* gradient of incident electric field *)
delsum1[i_,j_,\[Lambda]_,x_,y_,z_]=
1/2*{{2D[Ei[\[Theta]ii[[i]],\[Phi]jj[[j]],\[Lambda],x,y,z][[1]],x],D[Ei[\[Theta]ii[[i
    ]],\[Phi]jj[[j]],\[Lambda],x,y,z][[1]],y]+D[Ei[\[Theta]ii[[i]],\[Phi]jj[[j]],\[
    Lambda],x,y,z][[2]],x],D[Ei[\[Theta]ii[[i]],\[Phi]jj[[j]],\[Lambda],x,y,z][[1]],z]+D
    [Ei[\[Theta]ii[[i]],\[Phi]jj[[j]],\[Lambda],x,y,z][[3]],x]},{D[Ei[\[Theta]ii[[i]],\[
    Phi]jj[[j]],\[Lambda],x,y,z][[2]],x]+D[Ei[\[Theta]ii[[i]],\[Phi]jj[[j]],\[Lambda],x,
    y,z][[1]],y],2D[Ei[\[Theta]ii[[i]],\[Phi]jj[[j]],\[Lambda],x,y,z][[2]],y],D[Ei[\[
    Theta]ii[[i]],\[Phi]jj[[j]],\[Lambda],x,y,z][[2]],z]+D[Ei[\[Theta]ii[[i]],\[Phi]jj[[
    j]],\[Lambda],x,y,z][[3]],y]},{D[Ei[\[Theta]ii[[i]],\[Phi]jj[[j]],\[Lambda],x,y,z
    ][[3]],x]+D[Ei[\[Theta]ii[[i]],\[Phi]jj[[j]],\[Lambda],x,y,z][[1]],z],D[Ei[\[Theta]
    ii[[i]],\[Phi]jj[[j]],\[Lambda],x,y,z][[3]],y]+D[Ei[\[Theta]ii[[i]],\[Phi]jj[[j]],\[
    Lambda],x,y,z][[2]],z],2D[Ei[\[Theta]ii[[i]],\[Phi]jj[[j]],\[Lambda],x,y,z][[3]],z
    ]}};
deltot[\[Lambda]_,x_,y_,z_]=Total[Flatten[Table[Table[delsum1[i,j,\[Lambda],x,y,z],{i,1,
    N\[Theta]t+1,1}],{j,1,N\[Phi]t+1}],1]];
del[\[Lambda]_,x_,y_,z_]:=Norm[Flatten[deltot[\[Lambda],x,y,z]]]^2;
```

```
(* gradient of incident magnetic field *)
delsumH1[i_,j_,\[Lambda]_,x_,y_,z_]=
1/2*{{2D[Hi[\[Theta]ii[[i]],\[Phi]jj[[j]],\[Lambda],x,y,z][[1]],x],D[Hi[\[Theta]ii[[i
    ]],\[Phi]jj[[j]],\[Lambda],x,y,z][[1]],y]+D[Hi[\[Theta]ii[[i]],\[Phi]jj[[j]],\[
    Lambda],x,y,z][[2]],x],D[Hi[\[Theta]ii[[i]],\[Phi]jj[[j]],\[Lambda],x,y,z][[1]],z]+D
    [Hi[\[Theta]ii[[i]],\[Phi]jj[[j]],\[Lambda],x,y,z][[3]],x]},{D[Hi[\[Theta]ii[[i]],\[
    Phi]jj[[j]],\[Lambda],x,y,z][[2]],x]+D[Hi[\[Theta]ii[[i]],\[Phi]jj[[j]],\[Lambda],x,
    y,z][[1]],y],2D[Hi[\[Theta]ii[[i]],\[Phi]jj[[j]],\[Lambda],x,y,z][[2]],y],D[Hi[\[
    Theta]ii[[i]],\[Phi]jj[[j]],\[Lambda],x,y,z][[2]],z]+D[Hi[\[Theta]ii[[i]],\[Phi]jj[[
    j]],\[Lambda],x,y,z][[3]],y]},{D[Hi[\[Theta]ii[[i]],\[Phi]jj[[j]],\[Lambda],x,y,z
    ][[3]],x]+D[Hi[\[Theta]ii[[i]],\[Phi]jj[[j]],\[Lambda],x,y,z][[1]],z],D[Hi[\[Theta]
    ii[[i]],\[Phi]jj[[j]],\[Lambda],x,y,z][[3]],y]+D[Hi[\[Theta]ii[[i]],\[Phi]jj[[j]],\[
    Lambda],x,y,z][[2]],z],2D[Hi[\[Theta]ii[[i]],\[Phi]jj[[j]],\[Lambda],x,y,z][[3]],z
    ]}};
deltotH[\[Lambda]_,x_,y_,z_]=Total[Flatten[Table[Table[delsumH1[i,j,\[Lambda],x,y,z],{i
    ,1,N\[Theta]t+1,1}],{j,1,N\[Phi]t+1}],1]];
delH[\[Lambda]_,x_,y_,z_]:=Norm[Flatten[deltotH[\[Lambda],x,y,z]]]^2;
```

User input: Calculation of scattered power

```
(* power scattered by spherical particle, local field expressions *)
Ws2[e_,M_,\[Lambda]_,xp_,yp_,zp_,xm_]:=e*Abs[an[1,\[Lambda],xm]]^2*(3\[Pi])/(kw[\[Lambda
    ]]*\[Omega][\[Lambda]]*\[Mu])*Norm[E0sum[\[Lambda],xp,yp,zp]]^2+e*Abs[an[2,\[Lambda
    ],xm]]^2*(10\[Pi])/(kw[\[Lambda]]^3*\[Omega][\[Lambda]]*\[Mu])*del[\[Lambda],xp,yp,
    zp]+M*Abs[bn[1,\[Lambda],xm]]^2*(3\[Pi])/(kw[\[Lambda]]*\[Omega][\[Lambda]]*\[Mu])*Z
    ^2*Norm[H0sum[\[Lambda],xp,yp,zp]]^2+M*Abs[bn[2,\[Lambda],xm]]^2*(10\[Pi])/(kw[\[
    Lambda]]^3*\[Omega][\[Lambda]]*\[Mu])*Z^2*delH[\[Lambda],xp,yp,zp];

w=10^-30;

(* !!! INPUT !!! ) lb=0.05;  (* lower bound of rnp/lambda *)
```

```
(* !!! INPUT !!! *) ub=0.25; (* upper bound of rnp/lambda *)
(* !!! INPUT !!! *) numS=20; (* number of wavelength steps *)

r\[Lambda]=Table[x,{x,lb,ub,(ub-lb)/numS}]; (* table of normalized frequency points *)
\[Lambda]t=rNP/r\[Lambda];
```

Plot of spectral response

```
(* plot of spectral response of scattered power *)
data=ParallelTable[{r\[Lambda][[x]],Re[(Ws2[1,1,\[Lambda]t[[x]],w,w,w,r\[Lambda][[x]]])
    ]},{x,1,Length[r\[Lambda]],1}];
ListPlot[data,Joined->True,PlotRange->All]
```

A.4 Radiation patterns of a sphere

Setup

```
SetDirectory[NotebookDirectory[]];


(* constants -- assuming medium is vacuum *)
c=3*^8; (* speed of light in a vacuum *)
\[Mu]=1.257*^-6; (* permeability of free space *)
\[Epsilon]0=1/(c^2 \[Mu]);(* permittivity of free space *)
\[Omega][\[Lambda]_]=(2.\[Pi]*c)/(\[Lambda]*1.*^-9); (* angular frequency in terms of
    wavelength *)
Z=Sqrt[\[Mu]/\[Epsilon]0]; (* impedance of free space *)
```

User input: Properties of medium and particle

```
(* physical properties of medium *)
(* !!! INPUT !!! *) Nr[\[Lambda]_]=1;  (* refractive index of medium*)
(* !!! INPUT !!! *) N1[\[Lambda]_]=3.7; (* refractive index of particle *)
(* !!! INPUT !!! *) rnp=100; (* radius of particle *)


kw[\[Lambda]_]=(2\[Pi])/(\[Lambda]*1*^-9)*Nr[\[Lambda]]; (* wavenumber of light in
    medium *)
\[Epsilon]1[\[Lambda]_]=N1[\[Lambda]]^2;
d[rnp_]=2*rnp; (* diameter of particle *)
m[\[Lambda]_]=N1[\[Lambda]]/Nr[\[Lambda]]; (* relative refractive index of medium and
    particle *)
kp[\[Lambda]_]=kw[\[Lambda]]*m[\[Lambda]]; (* wavenumber of light in particle *)
xM[xm_]=2\[Pi]*Nr[\[Lambda]]*m[\[Lambda]]; (* Mie parameter, as defined on pg. 100of B&H
    , where xm=rNP/lambda *)
```

Bessel functions and angle-dependent functions

```
(* Bessel and Hankel functions *)
J[n_,\[Rho]_]=SphericalBesselJ[n,\[Rho]];
Y[n_,\[Rho]_]=SphericalBesselY[n,\[Rho]];
H[n_,\[Rho]_]=SphericalHankelH1[n,\[Rho]];

(* Ricatti-Bessel functions *)
\[Psi]n[n_,\[Rho]_]=\[Rho]*SphericalBesselJ[n,\[Rho]];
d\[Psi]n[n_,\[Rho]_]=SphericalBesselJ[n,\[Rho]]+\[Rho] (-(SphericalBesselJ[n,\[Rho]]/(2
    \[Rho]))+1/2 (SphericalBesselJ[-1+n,\[Rho]]-SphericalBesselJ[1+n,\[Rho]]));
\[Xi]n[n_,\[Rho]_]=\[Rho]*SphericalHankelH1[n,\[Rho]];
d\[Xi]n[n_,\[Rho]_]=SphericalHankelH1[n,\[Rho]]+\[Rho] (-(SphericalHankelH1[n,\[Rho]]/(2
     \[Rho]))+1/2 (SphericalHankelH1[-1+n,\[Rho]]-SphericalHankelH1[1+n,\[Rho]]));

(* angle-dependent functions *)
pi[n_,\[Theta]_]=If[n==0,0,If[n==1,1,(2 n-1)/(n-1) Cos[\[Theta]] pi[n-1,\[Theta]]-n/(n
    -1) pi[n-2,\[Theta]]]];
tau[n_,\[Theta]_]=n Cos[\[Theta]] pi[n,\[Theta]]-(n+1) pi[n-1,\[Theta]];
p[n_,\[Theta]_]=If[\[Theta]==0,1,LegendreP[n, 0, Cos[\[Theta]]]];
t[n_,\[Theta]_]=If[\[Theta]==0,0,1/Sin[\[Theta]] ((-1-n) Cos[\[Theta]]p[n,\[Theta]]+(1+n
    ) p[n+1,\[Theta]]) ];
```

Mie scattering coefficients and spherical vector harmonics

```
(* Mie coefficients *)
an[n_,\[Lambda]_]=(m[\[Lambda]]*\[Psi]n[n,m[\[Lambda]]*xM[\[Lambda]]]*d\[Psi]n[n,xM[\[
    Lambda]]]-\[Psi]n[n,xM[\[Lambda]]]*d\[Psi]n[n,m[\[Lambda]]*xM[\[Lambda]]])/(m[\[
    Lambda]]*\[Psi]n[n,m[\[Lambda]]*xM[\[Lambda]]]*d\[Xi]n[n,xM[\[Lambda]]]-\[Xi]n[n,xM
    [\[Lambda]]]*d\[Psi]n[n,m[\[Lambda]]*xM[\[Lambda]]]);
bn[n_,\[Lambda]_]=(\[Psi]n[n,m[\[Lambda]]*xM[\[Lambda]]]*d\[Psi]n[n,xM[\[Lambda]]]-m[\[
    Lambda]]*\[Psi]n[n,xM[\[Lambda]]]*d\[Psi]n[n,m[\[Lambda]]*xM[\[Lambda]]])/(\[Psi]n[n
    ,m[\[Lambda]]*xM[\[Lambda]]]*d\[Xi]n[n,xM[\[Lambda]]]-m[\[Lambda]]*\[Xi]n[n,xM[\[
```

```
    Lambda]]]*d\[Psi]n[n,m[\[Lambda]]*xM[\[Lambda]]]);

(* spherical vector harmonics for incoming waves *)
Mo1ni[n_,k_,r_,\[Theta]_,\[Phi]_]={0,Cos[\[Phi]]*pi[n,\[Theta]]*J[n,k*r],-Sin[\[Phi]]*
    tau[n,\[Theta]]*J[n,k*r]};
Ne1ni[n_,k_,r_,\[Theta]_,\[Phi]_]={Cos[\[Phi]]*n(n+1)*Sin[\[Theta]]*pi[n,\[Theta]]*J[n,k
    *r]/(k*r),Cos[\[Phi]]*tau[n,\[Theta]]*d\[Psi]n[n,k*r]/(k*r),-Sin[\[Phi]]*pi[n,\[
    Theta]]*d\[Psi]n[n,k*r]/(k*r)};
Me1ni[n_,k_,r_,\[Theta]_,\[Phi]_]={0,-Sin[\[Phi]]*pi[n,\[Theta]]*J[n,k*r],-Cos[\[Phi]]*
    tau[n,\[Theta]]*J[n,k*r]};
No1ni[n_,k_,r_,\[Theta]_,\[Phi]_]={Sin[\[Phi]]*n*(n+1)*Sin[\[Theta]]*pi[n,\[Theta]]*J[n,
    k*r]/(k*r),Sin[\[Phi]]*tau[n,\[Theta]]*d\[Psi]n[n,k*r]/(k*r),Cos[\[Phi]]*pi[n,\[
    Theta]]*d\[Psi]n[n,k*r]/(k*r)};

(* spherical vector harmonics for outgoing waves, far field *)
Mo1n[n_,k_,r_,\[Theta]_,\[Phi]_]={0,Cos[\[Phi]]*pi[n,\[Theta]]*SphericalBesselJ[n,k*r],-
    Sin[\[Phi]]*tau[n,\[Theta]]*SphericalBesselJ[n,k*r]};
Me1n[n_,k_,r_,\[Theta]_,\[Phi]_]={0,-Sin[\[Phi]]*pi[n,\[Theta]]*SphericalBesselJ[n,k*r
    ],-Cos[\[Phi]]*tau[n,\[Theta]]*SphericalBesselJ[n,k*r]};
No1n[n_,k_,r_,\[Theta]_,\[Phi]_]={Sin[\[Phi]]*n(n+1)*Sin[\[Theta]]*pi[n,\[Theta]]*
    SphericalBesselJ[n,k*r]/(k*r),Sin[\[Phi]]*tau[n,\[Theta]]*d\[Psi]n[n,k*r]/(k*r),Cos
    [\[Phi]]*pi[n,\[Theta]]*d\[Psi]n[n,k*r]/(k*r)};
Ne1n[n_,k_,r_,\[Theta]_,\[Phi]_]={Cos[\[Phi]]*n(n+1)*Sin[\[Theta]]*pi[n,\[Theta]]*
    SphericalBesselJ[n,k*r]/(k*r),Cos[\[Phi]]*tau[n,\[Theta]]*d\[Psi]n[n,k*r]/(k*r),-Sin
    [\[Phi]]*pi[n,\[Theta]]*d\[Psi]n[n,k*r]/(k*r)};

Ne0ni[n_, k_, r_, \[Theta]_, \[Phi]_]={n*(n + 1)*p[n,\[Theta]]*(J[n, k*r]/(k*r)), t[n,\[
    Theta]]*d\[Psi]n[n, k*r]/(k*r), 0};
Me0ni[n_,k_,r_,\[Theta]_,\[Phi]_]={0,0,-t[n,\[Theta]]*J[n,k*r]};

Ne0n[n_, k_, r_, \[Theta]_, \[Phi]_]={{n*(n + 1)*p[n,\[Theta]]*(H[n, k*r]/(k*r))}, {t[n
```

```
    ,\[Theta]]*d\[Xi]n[n, k*r]/(k*r)}, {0}};
Me0n[n_,k_,r_,\[Theta]_,\[Phi]_]=({{0},{0},{-t[n,\[Theta]]*H[n,k*r]}});
```

Coordinate system transformations

```
(* conversion from Cartesian coordinates to spherical coordinates *)
CartoSphCS[x_,y_,z_]:=CoordinateTransform[{"Cartesian"->"Spherical"},{x,y,z}];
rp[x_,y_,z_]:=CartoSphCS[x,y,z][[1]];
\[Theta]p[x_,y_,z_]:=CartoSphCS[x,y,z][[2]];
\[Phi]p[x_,y_,z_]:=CartoSphCS[x,y,z][[3]];

(* conversion from spherical unit vectors to Cartesian unit vectors *)SphtoCarUV[\[Theta
    ]_,\[Phi]_]:={{Sin[\[Theta]]*Cos[\[Phi]],Cos[\[Theta]]*Cos[\[Phi]],-Sin[\[Phi]]},{
    Sin[\[Theta]]*Sin[\[Phi]],Cos[\[Theta]]*Sin[\[Phi]],Cos[\[Phi]]},{Cos[\[Theta]],-Sin
    [\[Theta]],0}};
```

User input: Scattered electric fields

```
(* Specify the scattered electric fields by the particle in this section. Expressions
    here are taken from 1) plane wave illumination: C.F.Bohren and D.R.Huffman,
    Absorption and scattering of light by small particles, John Wiley & Sons, 2008. and
    2) focused radially polarized illumination: N.M.Mojarad and M.Agio,Tailoring the
    excitation of localized surface plasmon-polariton resonances by focusing radially-
    polarized beams, Optics Express 17 (1), 117\[Dash]122, 2009. *)

(*
n = mode order;
e = electric modes;
M = magnetic modes;
\[Lambda] = wavelength of light;
r, \[Theta], \[Phi] = spherical coordinates
*)
```

```
(* scattered electric field under plane wave illumination *)
EsSphPW[n_,e_,M_,\[Lambda]_,r_,\[Theta]_,\[Phi]_]:=I^n*(2n+1)/(n(n+1))*(e*I*an[n,\[
    Lambda]]*Ne1n[n,kw[\[Lambda]],r,\[Theta],\[Phi]]-M*bn[n,\[Lambda]]*Mo1n[n,kw[\[
    Lambda]],r,\[Theta],\[Phi]]);
(* conversion to spherical unit vectors *)
EsSphPWCarUV[n_,e_,M_,\[Lambda]_,r_,\[Theta]_,\[Phi]_]:=SphtoCarUV[\[Theta],\[Phi]].
    EsSphPW[n,e,M,\[Lambda],r,\[Theta],\[Phi]];

(* scattered electric field under focsued radially polarized illumination *)
(* !!! INPUT !!! *)\[Alpha]=\[Pi]/3; (* half-angle of focusing aperture *)
(* beam coefficient *)
Bn[n_]:=I^n (2n + 1)/(2n(n+1)) NIntegrate[Sqrt[Cos[\[Theta]]]*t[n,\[Theta]]*Sin[\[Theta
    ]]^2, {\[Theta], 0,\[Alpha]}, PrecisionGoal->2, MaxRecursion->5,Method->{"
    NewtonCotesRule", "SymbolicProcessing"->0}];
EsSphFRPW[n_,e_,M_,\[Lambda]_,r_,\[Theta]_,\[Phi]_]:=Bn[n]*e*an[n,\[Lambda]]*Ne0n[n,kw
    [\[Lambda]],r,\[Theta],\[Phi]];
(* conversion to spherical unit vectors *)
EsSphFRPWCarUV[n_,e_,M_,\[Lambda]_,r_,\[Theta]_,\[Phi]_]:=SphtoCarUV[\[Theta],\[Phi]].
    EsSphFRPW[n,e,M,\[Lambda],r,\[Theta],\[Phi]];
```

User input: Plot of radiation patterns

```
(* !!! INPUT !!! *)
(* Replace  "EsSphFRPWCarUV[n,e,M,\[Lambda],r,\[Theta],\[Phi]]" in the following plot
    expression with desired expression from previous section above. \[Lambda] choice
    should not matter. For example, to plot radiation pattern of electric dipole under
    focused radially-polarized illumination, choose n=1 to select the dipole modes, e =
    1 to select electric modes, M = 0 to suppress magnetic modes, \[Lambda] = anything,
    r = 1 for far-field plots, and leave \[Theta] and \[Phi] as symbols *)
```

```
plt=SphericalPlot3D[Norm[EsSphFRPWCarUV[2,1,0,420,1,\[Theta],\[Phi]]],{\[Theta],0,\[Pi
    ]},{\[Phi],0,2\[Pi]},Boxed->False,Axes->False,PlotStyle->Directive[Opacity[1]],
    Lighting->Automatic,ViewVertical->{0,0,1},Mesh->None,ColorFunction->Function[{x,y,z,
    r,\[Theta],\[Phi]},Darker[Hue[-\[Phi]]]],ColorFunctionScaling->True,PerformanceGoal
    ->"Quality",PlotPoints->10]

(* Inreacing "PlotPoints" gives a finer mesh for the radiation pattern plot. 200 should
    be sufficient for high-quality plot but takes more time to compute *)
```

A.5 Fraction of power scattered by quadrupole:dipole modes

Setup

```
SetDirectory[NotebookDirectory[]];


(* constants -- assuming medium is vacuum *)
c=3*^8; (* speed of light in a vacuum *)
\[Mu]=1.257*^-6; (* permeability of free space *)
\[Epsilon]0=1/(c^2 \[Mu]);(* permittivity of free space *)
\[Omega][\[Lambda]_]=(2.\[Pi]*c)/(\[Lambda]*1.*^-9); (* angular frequency in terms of
    wavelength *)
Z=Sqrt[\[Mu]/\[Epsilon]0]; (* impedance of free space *)
```

User input: Properties of medium and particle

```
(* physical properties of medium *)
(* !!! INPUT !!! *) Nr[\[Lambda]_]=1;  (* refractive index of medium*)
(* !!! INPUT !!! *) N1[\[Lambda]_]=3.7; (* refractive index of particle *)
(* !!! INPUT !!! *) rnp=100; (* radius of particle *)


kw[\[Lambda]_]=(2\[Pi])/(\[Lambda]*1*^-9)*Nr[\[Lambda]]; (* wavenumber of light in
    medium *)
\[Epsilon]1[\[Lambda]_]=N1[\[Lambda]]^2;
d[rnp_]=2*rnp; (* diameter of particle *)
m[\[Lambda]_]=N1[\[Lambda]]/Nr[\[Lambda]]; (* relative refractive index of medium and
    particle *)
kp[\[Lambda]_]=kw[\[Lambda]]*m[\[Lambda]]; (* wavenumber of light in particle *)
xM[xm_]=2\[Pi]*N1[\[Lambda]]*xm; (* Mie parameter *)(* Mie parameter, as defined on pg.
    100 of B&H, where xm=rNP/lambda *)
```

Bessel functions and angle-dependent functions

```
(* Bessel and Hankel functions *)
J[n_,\[Rho]_]=SphericalBesselJ[n,\[Rho]];
Y[n_,\[Rho]_]=SphericalBesselY[n,\[Rho]];
H[n_,\[Rho]_]=SphericalHankelH1[n,\[Rho]];

(* Ricatti-Bessel functions *)
\[Psi]n[n_,\[Rho]_]=\[Rho]*SphericalBesselJ[n,\[Rho]];
d\[Psi]n[n_,\[Rho]_]=SphericalBesselJ[n,\[Rho]]+\[Rho] (-(SphericalBesselJ[n,\[Rho]]/(2
    \[Rho]))+1/2 (SphericalBesselJ[-1+n,\[Rho]]-SphericalBesselJ[1+n,\[Rho]]));
\[Xi]n[n_,\[Rho]_]=\[Rho]*SphericalHankelH1[n,\[Rho]];
d\[Xi]n[n_,\[Rho]_]=SphericalHankelH1[n,\[Rho]]+\[Rho] (-(SphericalHankelH1[n,\[Rho]]/(2
     \[Rho]))+1/2 (SphericalHankelH1[-1+n,\[Rho]]-SphericalHankelH1[1+n,\[Rho]]));

(* angle-dependent functions *)
pi[n_,\[Theta]_]=If[n==0,0,If[n==1,1,(2 n-1)/(n-1) Cos[\[Theta]] pi[n-1,\[Theta]]-n/(n
    -1) pi[n-2,\[Theta]]]];
tau[n_,\[Theta]_]=n Cos[\[Theta]] pi[n,\[Theta]]-(n+1) pi[n-1,\[Theta]];
p[n_,\[Theta]_]=If[\[Theta]==0,1,LegendreP[n, 0, Cos[\[Theta]]]];
t[n_,\[Theta]_]=If[\[Theta]==0,0,1/Sin[\[Theta]] ((-1-n) Cos[\[Theta]]p[n,\[Theta]]+(1+n
    ) p[n+1,\[Theta]]) ];
```

Mie scattering coefficients and spherical vector harmonics

```
(* Mie coefficients *)
an[n_,\[Lambda]_,xm_]=(m[\[Lambda]]*\[Psi]n[n,m[\[Lambda]]*xM[xm]]*d\[Psi]n[n,xM[xm]]-\[
    Psi]n[n,xM[xm]]*d\[Psi]n[n,m[\[Lambda]]*xM[xm]])/(m[\[Lambda]]*\[Psi]n[n,m[\[Lambda
    ]]*xM[xm]]*d\[Xi]n[n,xM[xm]]-\[Xi]n[n,xM[xm]]*d\[Psi]n[n,m[\[Lambda]]*xM[xm]]);
bn[n_,\[Lambda]_,xm_]=(\[Psi]n[n,m[\[Lambda]]*xM[xm]]*d\[Psi]n[n,xM[xm]]-m[\[Lambda]]*\[
    Psi]n[n,xM[xm]]*d\[Psi]n[n,m[\[Lambda]]*xM[xm]])/(\[Psi]n[n,m[\[Lambda]]*xM[xm]]*d\[
    Xi]n[n,xM[xm]]-m[\[Lambda]]*\[Xi]n[n,xM[xm]]*d\[Psi]n[n,m[\[Lambda]]*xM[xm]]);
```

```
(* spherical vector harmonics for incoming waves *)
Mo1ni[n_,k_,r_,\[Theta]_,\[Phi]_]={0,Cos[\[Phi]]*pi[n,\[Theta]]*J[n,k*r],-Sin[\[Phi]]*
    tau[n,\[Theta]]*J[n,k*r]};
Ne1ni[n_,k_,r_,\[Theta]_,\[Phi]_]={Cos[\[Phi]]*n(n+1)*Sin[\[Theta]]*pi[n,\[Theta]]*J[n,k
    *r]/(k*r),Cos[\[Phi]]*tau[n,\[Theta]]*d\[Psi]n[n,k*r]/(k*r),-Sin[\[Phi]]*pi[n,\[
    Theta]]*d\[Psi]n[n,k*r]/(k*r)};
Me1ni[n_,k_,r_,\[Theta]_,\[Phi]_]={0,-Sin[\[Phi]]*pi[n,\[Theta]]*J[n,k*r],-Cos[\[Phi]]*
    tau[n,\[Theta]]*J[n,k*r]};
No1ni[n_,k_,r_,\[Theta]_,\[Phi]_]={Sin[\[Phi]]*n*(n+1)*Sin[\[Theta]]*pi[n,\[Theta]]*J[n,
    k*r]/(k*r),Sin[\[Phi]]*tau[n,\[Theta]]*d\[Psi]n[n,k*r]/(k*r),Cos[\[Phi]]*pi[n,\[
    Theta]]*d\[Psi]n[n,k*r]/(k*r)};

(* spherical vector harmonics for outgoing waves, far field *)
Mo1n[n_,k_,r_,\[Theta]_,\[Phi]_]={0,Cos[\[Phi]]*pi[n,\[Theta]]*SphericalBesselJ[n,k*r],-
    Sin[\[Phi]]*tau[n,\[Theta]]*SphericalBesselJ[n,k*r]};
Me1n[n_,k_,r_,\[Theta]_,\[Phi]_]={0,-Sin[\[Phi]]*pi[n,\[Theta]]*SphericalBesselJ[n,k*r
    ],-Cos[\[Phi]]*tau[n,\[Theta]]*SphericalBesselJ[n,k*r]};
No1n[n_,k_,r_,\[Theta]_,\[Phi]_]={Sin[\[Phi]]*n(n+1)*Sin[\[Theta]]*pi[n,\[Theta]]*
    SphericalBesselJ[n,k*r]/(k*r),Sin[\[Phi]]*tau[n,\[Theta]]*d\[Psi]n[n,k*r]/(k*r),Cos
    [\[Phi]]*pi[n,\[Theta]]*d\[Psi]n[n,k*r]/(k*r)};
Ne1n[n_,k_,r_,\[Theta]_,\[Phi]_]={Cos[\[Phi]]*n(n+1)*Sin[\[Theta]]*pi[n,\[Theta]]*
    SphericalBesselJ[n,k*r]/(k*r),Cos[\[Phi]]*tau[n,\[Theta]]*d\[Psi]n[n,k*r]/(k*r),-Sin
    [\[Phi]]*pi[n,\[Theta]]*d\[Psi]n[n,k*r]/(k*r)};

Ne0ni[n_, k_, r_, \[Theta]_, \[Phi]_]={n*(n + 1)*p[n,\[Theta]]*(J[n, k*r]/(k*r)), t[n,\[
    Theta]]*d\[Psi]n[n, k*r]/(k*r), 0};
Me0ni[n_,k_,r_,\[Theta]_,\[Phi]_]={0,0,-t[n,\[Theta]]*J[n,k*r]};

Ne0n[n_, k_, r_, \[Theta]_, \[Phi]_]={{n*(n + 1)*p[n,\[Theta]]*(H[n, k*r]/(k*r))}, {t[n
    ,\[Theta]]*d\[Xi]n[n, k*r]/(k*r)}, {0}};
```

```
Me0n[n_,k_,r_,\[Theta]_,\[Phi]_]=({{0},{0},{-t[n,\[Theta]]*H[n,k*r]}});
```

Rotations and coordinate transformations

```
RzCCW[\[Phi]r_]={{Cos[\[Phi]r],Sin[\[Phi]r],0},{-Sin[\[Phi]r],Cos[\[Phi]r],0},{0,0,1}};
RxCCW[\[Theta]r_]={{1,0,0},{0,Cos[\[Theta]r],Sin[\[Theta]r]},{0,-Sin[\[Theta]r],Cos[\[
    Theta]r]}};
RyCCW[\[Theta]r_]={{Cos[\[Theta]r],0,-Sin[\[Theta]r]},{0,1,0},{Sin[\[Theta]r],0,Cos[\[
    Theta]r]}};

(* conversion from MCS (Cartesian) to RCS (Cartesian) by rotation angles \[Theta]xr, \[
    Theta]yr, and \[Phi]r *)
R[\[Theta]xr_,\[Theta]yr_,\[Phi]r_]=RxCCW[\[Theta]xr].RyCCW[\[Theta]yr].RzCCW[\[Phi]r];

Rinv[\[Theta]xr_,\[Theta]yr_,\[Phi]r_]=Inverse[R[\[Theta]xr,\[Theta]yr,\[Phi]r]];

SphtoCarp[\[Theta]_,\[Phi]_]={{Sin[\[Theta]]*Cos[\[Phi]],Cos[\[Theta]]*Cos[\[Phi]],-Sin
    [\[Phi]]},{Sin[\[Theta]]*Sin[\[Phi]],Cos[\[Theta]]*Sin[\[Phi]],Cos[\[Phi]]},{Cos[\[
    Theta]],-Sin[\[Theta]],0}};

SphtoCarCS[r_,\[Theta]_,\[Phi]_]=CoordinateTransform[{"Spherical"->"Cartesian"},{r,\[
    Theta],\[Phi]}];
CartoSphCS[x_,y_,z_]=CoordinateTransform[{"Cartesian"->"Spherical"},{x,y,z}];
```

User input: Angular spectrum decomposition of incident beam

```
(* !!! INPUT !!! *) N\[Theta]t=100; (* number of plane waves in theta *)
(* !!! INPUT !!! *) N\[Phi]t=100; (* number of plane waves in phi *)

(* angular spectrum of incident wave in Cartesian unit vectors *)
(* linearly polarized *)
angspecLP[\[Theta]_,\[Phi]_]={(Cos[\[Theta]]Cos[\[Phi]]^2+Sin[\[Phi]]^2),(Cos[\[Theta]]
```

```
    Cos[\[Phi]]Sin[\[Phi]]-Cos[\[Phi]]Sin[\[Phi]]),-Sin[\[Theta]]Cos[\[Phi]]};
angspecMLP[\[Theta]_,\[Phi]_]=-{(1-Cos[\[Theta]])Cos[\[Phi]]Sin[\[Phi]],-(1-(1-Cos[\[
    Theta]])Sin[\[Phi]]^2),Sin[\[Theta]]Sin[\[Phi]]};

(* radially polarized *)
angspecRP[\[Theta]_,\[Phi]_]={Cos[\[Theta]]Cos[\[Phi]],Cos[\[Theta]]Sin[\[Phi]],Sin[\[
    Theta]]};
angspecMRP[\[Theta]_,\[Phi]_]={-Sin[\[Phi]],Cos[\[Phi]],0};

(* azimuthally polarized *)
angspecAP[\[Theta]_,\[Phi]_]={-Sin[\[Phi]],Cos[\[Phi]],0};
angspecMAP[\[Theta]_,\[Phi]_]={-Cos[\[Theta]]Cos[\[Phi]],-Cos[\[Theta]]Sin[\[Phi]],Sin
    [\[Theta]]};

\[Theta]ii[\[Alpha]t_]=Table[((i-1)\[Alpha]t)/N\[Theta]t,{i,1,N\[Theta]t+1,1}];
\[Phi]jj=Table[((j-1) 2 \[Pi])/N\[Phi]t,{j,1,N\[Phi]t+1,1}];

(* incident electric and magnetic fields *)
ikr[\[Lambda]_,\[Theta]_,\[Phi]_,xp_,yp_,zp_]=I*kw[\[Lambda]]*(Sin[\[Theta]]*Cos[\[Phi
    ]]*(xp)+Sin[\[Theta]]*Sin[\[Phi]]*(yp)-Cos[\[Theta]]*(zp));

(* !!! INPUT !!! *)
(*-- choose desired angular spectrum*)
Ei[\[Alpha]t_,\[Theta]_,\[Phi]_,\[Lambda]_,x_,y_,z_]=-I/\[Lambda]*angspecRP[\[Theta],\[
    Phi]]*Sqrt[Abs[Cos[\[Theta]]]]*Sin[\[Theta]]*Exp[ikr[\[Lambda],\[Theta],\[Phi],x,y,z
    ]]*\[Alpha]t/N\[Theta]t*2\[Pi]/N\[Phi]t;
Einc[\[Lambda]_,\[Alpha]t_,xp_,yp_,zp_]=Flatten[Table[Table[Ei[\[Alpha]t,\[Theta]ii[\[
    Alpha]t][[i]],\[Phi]jj[[j]],\[Lambda],xp,yp,zp],{i,1.,N\[Theta]t+1,1.}],{j,1.,N\[Phi
    ]t+1,1.}],1];
E0sum[\[Lambda]_,\[Alpha]t_,xp_,yp_,zp_]=Total[Einc[\[Lambda],\[Alpha]t,xp,yp,zp]];
```

```
(* !!! INPUT !!! *)
(*-- choose desired angular spectrum*)
Hi[\[Alpha]t_,\[Theta]_,\[Phi]_,\[Lambda]_,x_,y_,z_]=-kw[\[Lambda]]/(\[Omega][\[Lambda
    ]]*\[Mu])*I*angspecMRP[\[Theta],\[Phi]]*Sqrt[Abs[Cos[\[Theta]]]]*Sin[\[Theta]]*Exp[
    ikr[\[Lambda],\[Theta],\[Phi],x,y,z]]*\[Alpha]t/N\[Theta]t*2\[Pi]/N\[Phi]t;
Hinc[\[Lambda]_,\[Alpha]t_,xp_,yp_,zp_]=Flatten[Table[Table[Hi[\[Alpha]t,\[Theta]ii[\[
    Alpha]t][[i]],\[Phi]jj[[j]],\[Lambda],xp,yp,zp],{i,1.,N\[Theta]t+1,1.}],{j,1.,N\[Phi
    ]t+1,1.}],1];
H0sum[\[Lambda]_,\[Alpha]t_,xp_,yp_,zp_]=Total[Hinc[\[Lambda],\[Alpha]t,xp,yp,zp]];
```

Gradient of incident beam at a point in space

```
delsum1[\[Alpha]t_,i_,j_,\[Lambda]_,x_,y_,z_]=
1/2*{{2D[Ei[\[Alpha]t,\[Theta]ii[\[Alpha]t][[i]],\[Phi]jj[[j]],\[Lambda],x,y,z][[1]],x],
    D[Ei[\[Alpha]t,\[Theta]ii[\[Alpha]t][[i]],\[Phi]jj[[j]],\[Lambda],x,y,z][[1]],y]+D[
    Ei[\[Alpha]t,\[Theta]ii[\[Alpha]t][[i]],\[Phi]jj[[j]],\[Lambda],x,y,z][[2]],x],D[Ei
    [\[Alpha]t,\[Theta]ii[\[Alpha]t][[i]],\[Phi]jj[[j]],\[Lambda],x,y,z][[1]],z]+D[Ei[\[
    Alpha]t,\[Theta]ii[\[Alpha]t][[i]],\[Phi]jj[[j]],\[Lambda],x,y,z][[3]],x]},{D[Ei[\[
    Alpha]t,\[Theta]ii[\[Alpha]t][[i]],\[Phi]jj[[j]],\[Lambda],x,y,z][[2]],x]+D[Ei[\[
    Alpha]t,\[Theta]ii[\[Alpha]t][[i]],\[Phi]jj[[j]],\[Lambda],x,y,z][[1]],y],2D[Ei[\[
    Alpha]t,\[Theta]ii[\[Alpha]t][[i]],\[Phi]jj[[j]],\[Lambda],x,y,z][[2]],y],D[Ei[\[
    Alpha]t,\[Theta]ii[\[Alpha]t][[i]],\[Phi]jj[[j]],\[Lambda],x,y,z][[2]],z]+D[Ei[\[
    Alpha]t,\[Theta]ii[\[Alpha]t][[i]],\[Phi]jj[[j]],\[Lambda],x,y,z][[3]],y]},{D[Ei[\[
    Alpha]t,\[Theta]ii[\[Alpha]t][[i]],\[Phi]jj[[j]],\[Lambda],x,y,z][[3]],x]+D[Ei[\[
    Alpha]t,\[Theta]ii[\[Alpha]t][[i]],\[Phi]jj[[j]],\[Lambda],x,y,z][[1]],z],D[Ei[\[
    Alpha]t,\[Theta]ii[\[Alpha]t][[i]],\[Phi]jj[[j]],\[Lambda],x,y,z][[3]],y]+D[Ei[\[
    Alpha]t,\[Theta]ii[\[Alpha]t][[i]],\[Phi]jj[[j]],\[Lambda],x,y,z][[2]],z],2D[Ei[\[
    Alpha]t,\[Theta]ii[\[Alpha]t][[i]],\[Phi]jj[[j]],\[Lambda],x,y,z][[3]],z]}};
deltot[\[Alpha]t_,\[Lambda]_,x_,y_,z_]=Total[Flatten[Table[Table[delsum1[\[Alpha]t,i,j
    ,\[Lambda],x,y,z],{i,1,N\[Theta]t+1,1}],{j,1,N\[Phi]t+1}],1]];
del[\[Alpha]t_,\[Lambda]_,x_,y_,z_]:=Norm[Flatten[deltot[\[Alpha]t,\[Lambda],x,y,z]]]^2;
```

```
delsumH1[\[Alpha]t_,i_,j_,\[Lambda]_,x_,y_,z_]=
1/2*{{2D[Hi[\[Alpha]t,\[Theta]ii[\[Alpha]t][[i]],\[Phi]jj[[j]],\[Lambda],x,y,z][[1]],x],
    D[Hi[\[Alpha]t,\[Theta]ii[\[Alpha]t][[i]],\[Phi]jj[[j]],\[Lambda],x,y,z][[1]],y]+D[
    Hi[\[Alpha]t,\[Theta]ii[\[Alpha]t][[i]],\[Phi]jj[[j]],\[Lambda],x,y,z][[2]],x],D[Hi
    [\[Alpha]t,\[Theta]ii[\[Alpha]t][[i]],\[Phi]jj[[j]],\[Lambda],x,y,z][[1]],z]+D[Hi[\[
    Alpha]t,\[Theta]ii[\[Alpha]t][[i]],\[Phi]jj[[j]],\[Lambda],x,y,z][[3]],x]},{D[Hi[\[
    Alpha]t,\[Theta]ii[\[Alpha]t][[i]],\[Phi]jj[[j]],\[Lambda],x,y,z][[2]],x]+D[Hi[\[
    Alpha]t,\[Theta]ii[\[Alpha]t][[i]],\[Phi]jj[[j]],\[Lambda],x,y,z][[1]],y],2D[Hi[\[
    Alpha]t,\[Theta]ii[\[Alpha]t][[i]],\[Phi]jj[[j]],\[Lambda],x,y,z][[2]],y],D[Hi[\[
    Alpha]t,\[Theta]ii[\[Alpha]t][[i]],\[Phi]jj[[j]],\[Lambda],x,y,z][[2]],z]+D[Hi[\[
    Alpha]t,\[Theta]ii[\[Alpha]t][[i]],\[Phi]jj[[j]],\[Lambda],x,y,z][[3]],y]},{D[Hi[\[
    Alpha]t,\[Theta]ii[\[Alpha]t][[i]],\[Phi]jj[[j]],\[Lambda],x,y,z][[3]],x]+D[Hi[\[
    Alpha]t,\[Theta]ii[\[Alpha]t][[i]],\[Phi]jj[[j]],\[Lambda],x,y,z][[1]],z],D[Hi[\[
    Alpha]t,\[Theta]ii[\[Alpha]t][[i]],\[Phi]jj[[j]],\[Lambda],x,y,z][[3]],y]+D[Hi[\[
    Alpha]t,\[Theta]ii[\[Alpha]t][[i]],\[Phi]jj[[j]],\[Lambda],x,y,z][[2]],z],2D[Hi[\[
    Alpha]t,\[Theta]ii[\[Alpha]t][[i]],\[Phi]jj[[j]],\[Lambda],x,y,z][[3]],z]}};
deltotH[\[Alpha]t_,\[Lambda]_,x_,y_,z_]=Total[Flatten[Table[Table[delsumH1[\[Alpha]t,i,j
    ,\[Lambda],x,y,z],{i,1,N\[Theta]t+1,1}],{j,1,N\[Phi]t+1}],1]];
delH[\[Alpha]t_,\[Lambda]_,x_,y_,z_]:=Norm[Flatten[deltotH[\[Alpha]t,\[Lambda],x,y,z
    ]]]^2;
```

Power scattered by spherical particle

```
Ws2[\[Alpha]t_,e_,M_,\[Lambda]_,xp_,yp_,zp_,xm_]:=e*Abs[an[1,\[Lambda],xm]]^2*(3\[Pi])/(
    kw[\[Lambda]]*\[Omega][\[Lambda]]*\[Mu])*Norm[E0sum[\[Lambda],\[Alpha]t,xp,yp,zp
    ]]^2+e*Abs[an[2,\[Lambda],xm]]^2*(10\[Pi])/(kw[\[Lambda]]^3*\[Omega][\[Lambda]]*\[Mu
    ])*del[\[Alpha]t,\[Lambda],xp,yp,zp]+M*Abs[bn[1,\[Lambda],xm]]^2*(3\[Pi])/(kw[\[
    Lambda]]*\[Omega][\[Lambda]]*\[Mu])*Z^2*Norm[H0sum[\[Lambda],\[Alpha]t,xp,yp,zp]]^2+
    M*Abs[bn[2,\[Lambda],xm]]^2*(10\[Pi])/(kw[\[Lambda]]^3*\[Omega][\[Lambda]]*\[Mu])*Z
    ^2*delH[\[Alpha]t,\[Lambda],xp,yp,zp];
```

```
(* power scattered by individual multipolar modes *)
WsED[\[Alpha]t_,\[Lambda]_,xp_,yp_,zp_,xm_]:=Abs[an[1,\[Lambda],xm]]^2*(3\[Pi])/(kw[\[
    Lambda]]*\[Omega][\[Lambda]]*\[Mu])*Norm[E0sum[\[Lambda],\[Alpha]t,xp,yp,zp]]^2;
WsEQ[\[Alpha]t_,\[Lambda]_,xp_,yp_,zp_,xm_]:=Abs[an[2,\[Lambda],xm]]^2*(10\[Pi])/(kw[\[
    Lambda]]^3*\[Omega][\[Lambda]]*\[Mu])*del[\[Alpha]t,\[Lambda],xp,yp,zp];
WsMD[\[Alpha]t_,\[Lambda]_,xp_,yp_,zp_,xm_]:=Abs[bn[1,\[Lambda],xm]]^2*(3\[Pi])/(kw[\[
    Lambda]]*\[Omega][\[Lambda]]*\[Mu])*Z^2*Norm[H0sum[\[Lambda],\[Alpha]t,xp,yp,zp]]^2;
WsMQ[\[Alpha]t_,\[Lambda]_,xp_,yp_,zp_,xm_]:=Abs[bn[2,\[Lambda],xm]]^2*(10\[Pi])/(kw[\[
    Lambda]]^3*\[Omega][\[Lambda]]*\[Mu])*Z^2*delH[\[Alpha]t,\[Lambda],xp,yp,zp];
```

Plot of ratio of power scattered by one mode to another

```
(* !!! INPUT !!! *)
(* Enter wavelengths of modes of interest on resonance. In this example the EQ mode
    resonance is at r/\[Lambda] = 0.234 and the ED resonance is at r/\[Lambda] = 0.174
    *)
w=10^-30;
data=ParallelTable[{x,WsEQ[x,rnp/0.234,w,w,w,0.234]/WsED[x,rnp/0.174,w,w,w,0.174]},{x
    ,0.1,\[Pi]/2,(\[Pi]/2-0.1)/40}];
ListPlot[data,Joined->True,PlotRange->All]
```

A.6 Standing wave illumination for selective excitation of multipolar modes

Setup

```
SetDirectory[NotebookDirectory[]];


(* constants -- assuming medium is vacuum *)
c=3*^8; (* speed of light in a vacuum *)
\[Mu]=1.257*^-6; (* permeability of free space *)
\[Epsilon]0=1/(c^2 \[Mu]);(* permittivity of free space *)
\[Omega][\[Lambda]_]=(2.\[Pi]*c)/(\[Lambda]*1.*^-9); (* angular frequency in terms of
    wavelength *)
Z=Sqrt[\[Mu]/\[Epsilon]0]; (* impedance of free space *)
```

User input: Properties of medium and particle

```
(* physical properties of medium *)
(* !!! INPUT !!! *) Nr[\[Lambda]_]=1;  (* refractive index of medium*)
(* !!! INPUT !!! *) N1[\[Lambda]_]=3.7; (* refractive index of particle *)
(* !!! INPUT !!! *) rNP=100; (* radius of particle *)


kw[\[Lambda]_]=(2\[Pi])/(\[Lambda]*1*^-9)*Nr[\[Lambda]]; (* wavenumber of light in
    medium *)
\[Epsilon]1[\[Lambda]_]=N1[\[Lambda]]^2;
d[rnp_]=2*rNP; (* diameter of particle *)
m[\[Lambda]_]=N1[\[Lambda]]/Nr[\[Lambda]]; (* relative refractive index of medium and
    particle *)
kp[\[Lambda]_]=kw[\[Lambda]]*m[\[Lambda]]; (* wavenumber of light in particle *)
xM[xm_]=2\[Pi]*N1[\[Lambda]]*xm; (* Mie parameter *)(* Mie parameter, as defined on pg.
    100 of B&H, where xm=rNP/lambda *)
```

Bessel functions

```
(* ALL THINGS BESSEL *)
(* Bessel and Hankel functions *)
J[n_,\[Rho]_]=SphericalBesselJ[n,\[Rho]];
Y[n_,\[Rho]_]=SphericalBesselY[n,\[Rho]];
H[n_,\[Rho]_]=SphericalHankelH1[n,\[Rho]];

(* Ricatti-Bessel functions *)
\[Psi]n[n_,\[Rho]_]=\[Rho]*SphericalBesselJ[n,\[Rho]];
d\[Psi]n[n_,\[Rho]_]=SphericalBesselJ[n,\[Rho]]+\[Rho] (-(SphericalBesselJ[n,\[Rho]]/(2
    \[Rho]))+1/2 (SphericalBesselJ[-1+n,\[Rho]]-SphericalBesselJ[1+n,\[Rho]]));
\[Xi]n[n_,\[Rho]_]=\[Rho]*SphericalHankelH1[n,\[Rho]];
d\[Xi]n[n_,\[Rho]_]=SphericalHankelH1[n,\[Rho]]+\[Rho] (-(SphericalHankelH1[n,\[Rho]]/(2
     \[Rho]))+1/2 (SphericalHankelH1[-1+n,\[Rho]]-SphericalHankelH1[1+n,\[Rho]]));
```

Mie scattering coefficients and vector spherical harmonics

```
(* ALL THINGS MIE *)
(* Mie coefficients *)
an[n_,\[Lambda]_]=(m[\[Lambda]]*\[Psi]n[n,m[\[Lambda]]*xM[\[Lambda]]]*d\[Psi]n[n,xM[\[
    Lambda]]]-\[Psi]n[n,xM[\[Lambda]]]*d\[Psi]n[n,m[\[Lambda]]*xM[\[Lambda]]])/(m[\[
    Lambda]]*\[Psi]n[n,m[\[Lambda]]*xM[\[Lambda]]]*d\[Xi]n[n,xM[\[Lambda]]]-\[Xi]n[n,xM
    [\[Lambda]]]*d\[Psi]n[n,m[\[Lambda]]*xM[\[Lambda]]]);
bn[n_,\[Lambda]_]=(\[Psi]n[n,m[\[Lambda]]*xM[\[Lambda]]]*d\[Psi]n[n,xM[\[Lambda]]]-m[\[
    Lambda]]*\[Psi]n[n,xM[\[Lambda]]]*d\[Psi]n[n,m[\[Lambda]]*xM[\[Lambda]]])/(\[Psi]n[n
    ,m[\[Lambda]]*xM[\[Lambda]]]*d\[Xi]n[n,xM[\[Lambda]]]-m[\[Lambda]]*\[Xi]n[n,xM[\[
    Lambda]]]*d\[Psi]n[n,m[\[Lambda]]*xM[\[Lambda]]]);
```

User input: Angular spectrum decomposition of incident beam

```
(* !!! INPUT !!! *) \[Alpha]t=\[Pi]/3; (* half-angle annular aperture of focusing lens
    *)
```

```
(* !!! INPUT !!! *) N\[Theta]t=100; (* number of plane waves in theta *)
(* !!! INPUT !!! *) N\[Phi]t=100; (* number of plane waves in phi *)

\[Theta]ii=Table[((i-1)\[Alpha]t)/N\[Theta]t,{i,1,N\[Theta]t+1,1}];
\[Phi]jj=Table[((j-1) 2 \[Pi])/N\[Phi]t,{j,1,N\[Phi]t+1,1}];

(* angular spectrum of incident wave in Cartesian unit vectors *)
(* Standing wave illumination of radially polarized beam *)
angspecRP1[\[Theta]_,\[Phi]_]={-Cos[\[Theta]]Cos[\[Phi]],-Cos[\[Theta]]Sin[\[Phi]],Sin
    [\[Theta]]};
angspecMRP1[\[Theta]_,\[Phi]_]={Sin[\[Phi]],-Cos[\[Phi]],0};

angspecRP2[\[Theta]_,\[Phi]_]={-Cos[\[Theta]]Cos[\[Phi]],-Cos[\[Theta]]Sin[\[Phi]],-Sin
    [\[Theta]]};
angspecMRP2[\[Theta]_,\[Phi]_]={-Sin[\[Phi]],Cos[\[Phi]],0};

ikrRP1[\[Lambda]_,\[Theta]_,\[Phi]_,xp_,yp_,zp_]=I*kw[\[Lambda]]*(Sin[\[Theta]]*Cos[\[
    Phi]]*(xp)+Sin[\[Theta]]*Sin[\[Phi]]*(yp)+Cos[\[Theta]]*(zp));
ikrRP2[\[Lambda]_,\[Theta]_,\[Phi]_,xp_,yp_,zp_]=I*kw[\[Lambda]]*(Sin[\[Theta]]*Cos[\[
    Phi]]*(xp)+Sin[\[Theta]]*Sin[\[Phi]]*(yp)-Cos[\[Theta]]*(zp));

(* Standing wave illumination of radially polarized beam with pi phase shift in one beam
     *)
angspecRPpi1[\[Theta]_,\[Phi]_]={-Cos[\[Theta]]Cos[\[Phi]],-Cos[\[Theta]]Sin[\[Phi]],Sin
    [\[Theta]]};
angspecMRPpi1[\[Theta]_,\[Phi]_]={Sin[\[Phi]],-Cos[\[Phi]],0};

angspecRPpi2[\[Theta]_,\[Phi]_]={-Cos[\[Theta]]Cos[\[Phi]],-Cos[\[Theta]]Sin[\[Phi]],-
    Sin[\[Theta]]};
angspecMRPpi2[\[Theta]_,\[Phi]_]={-Sin[\[Phi]],Cos[\[Phi]],0};
```

```
ikrRPpi1[\[Lambda]_,\[Theta]_,\[Phi]_,xp_,yp_,zp_]=I*kw[\[Lambda]]*(Sin[\[Theta]]*Cos[\[
    Phi]]*(xp)+Sin[\[Theta]]*Sin[\[Phi]]*(yp)+Cos[\[Theta]]*(zp));
ikrRPpi2[\[Lambda]_,\[Theta]_,\[Phi]_,xp_,yp_,zp_]=I*\[Pi]+I*kw[\[Lambda]]*(Sin[\[Theta
    ]]*Cos[\[Phi]]*(xp)+Sin[\[Theta]]*Sin[\[Phi]]*(yp)-Cos[\[Theta]]*(zp));

(* Standing wave illumination of azimuthally polarized beam *)
angspecAP1[\[Theta]_,\[Phi]_]={-Sin[\[Phi]],Cos[\[Phi]],0};
angspecMAP1[\[Theta]_,\[Phi]_]={-Cos[\[Theta]]Cos[\[Phi]],-Cos[\[Theta]]Sin[\[Phi]],Sin
    [\[Theta]]};

angspecAP2[\[Theta]_,\[Phi]_]={Sin[\[Phi]],-Cos[\[Phi]],0};
angspecMAP2[\[Theta]_,\[Phi]_]={-Cos[\[Theta]]Cos[\[Phi]],-Cos[\[Theta]]Sin[\[Phi]],-Sin
    [\[Theta]]};

ikrAP1[\[Lambda]_,\[Theta]_,\[Phi]_,xp_,yp_,zp_]=I*kw[\[Lambda]]*(Sin[\[Theta]]*Cos[\[
    Phi]]*(xp)+Sin[\[Theta]]*Sin[\[Phi]]*(yp)+Cos[\[Theta]]*(zp));
ikrAP2[\[Lambda]_,\[Theta]_,\[Phi]_,xp_,yp_,zp_]=I*kw[\[Lambda]]*(Sin[\[Theta]]*Cos[\[
    Phi]]*(xp)+Sin[\[Theta]]*Sin[\[Phi]]*(yp)-Cos[\[Theta]]*(zp));

(* Standing wave illumination of azimuthally polarized beam with pi phase shift in one
    beam *)
angspecAPpi1[\[Theta]_,\[Phi]_]={-Sin[\[Phi]],Cos[\[Phi]],0};
angspecMAPpi1[\[Theta]_,\[Phi]_]={-Cos[\[Theta]]Cos[\[Phi]],-Cos[\[Theta]]Sin[\[Phi]],
    Sin[\[Theta]]};

angspecAPpi2[\[Theta]_,\[Phi]_]={Sin[\[Phi]],-Cos[\[Phi]],0};
angspecMAPpi2[\[Theta]_,\[Phi]_]={-Cos[\[Theta]]Cos[\[Phi]],-Cos[\[Theta]]Sin[\[Phi]],-
    Sin[\[Theta]]};

ikrAPpi1[\[Lambda]_,\[Theta]_,\[Phi]_,xp_,yp_,zp_]=I*kw[\[Lambda]]*(Sin[\[Theta]]*Cos[\[
    Phi]]*(xp)+Sin[\[Theta]]*Sin[\[Phi]]*(yp)+Cos[\[Theta]]*(zp));
```

```
ikrAPpi2[\[Lambda]_,\[Theta]_,\[Phi]_,xp_,yp_,zp_]=I*\[Pi]+I*kw[\[Lambda]]*(Sin[\[Theta
    ]]*Cos[\[Phi]]*(xp)+Sin[\[Theta]]*Sin[\[Phi]]*(yp)-Cos[\[Theta]]*(zp));

(* electric field of incident beam *)
(* !!! INPUT !!! *)
(*-- choose desired angular spectrum*)
Ei1[\[Theta]_,\[Phi]_,\[Lambda]_,x_,y_,z_]=-I/\[Lambda]*\[Alpha]t/N\[Theta]t*2\[Pi]/N\[
    Phi]t*angspecAPpi1[\[Theta],\[Phi]]*Sqrt[Cos[\[Theta]]]*Sin[\[Theta]]*Exp[ikrAPpi1
    [\[Lambda],\[Theta],\[Phi],x,y,z]];
Einc1[\[Lambda]_,xp_,yp_,zp_]=Flatten[Table[Table[Ei1[\[Theta]ii[[i]],\[Phi]jj[[j]],\[
    Lambda],xp,yp,zp],{i,1.,N\[Theta]t+1,1.}],{j,1.,N\[Phi]t+1,1.}],1];
Ei2[\[Theta]_,\[Phi]_,\[Lambda]_,x_,y_,z_]=-I/\[Lambda]*\[Alpha]t/N\[Theta]t*2\[Pi]/N\[
    Phi]t*angspecAPpi2[\[Theta],\[Phi]]*Sqrt[Cos[\[Theta]]]*Sin[\[Theta]]*Exp[ikrAPpi2
    [\[Lambda],\[Theta],\[Phi],x,y,z]];
Einc2[\[Lambda]_,xp_,yp_,zp_]=Flatten[Table[Table[Ei2[\[Theta]ii[[i]],\[Phi]jj[[j]],\[
    Lambda],xp,yp,zp],{i,1.,N\[Theta]t+1,1.}],{j,1.,N\[Phi]t+1,1.}],1];
Einc[\[Lambda]_,xp_,yp_,zp_]=Join[Einc1[\[Lambda],xp,yp,zp],Einc2[\[Lambda],xp,yp,zp]];
E0sum[\[Lambda]_,xp_,yp_,zp_]=Total[Einc[\[Lambda],xp,yp,zp]];
a=Length[Einc[\[Lambda],xp,yp,zp]];

(* magnetic field of incident beam *)
(* !!! INPUT !!! *)
(*-- choose desired angular spectrum*)
Hi1[\[Theta]_,\[Phi]_,\[Lambda]_,x_,y_,z_]=-I/\[Lambda]*1/Z*\[Alpha]t/N\[Theta]t*2\[Pi]/
    N\[Phi]t*angspecMAPpi1[\[Theta],\[Phi]]*Sqrt[Cos[\[Theta]]]*Sin[\[Theta]]*Exp[
    ikrAPpi1[\[Lambda],\[Theta],\[Phi],x,y,z]];
Hinc1[\[Lambda]_,xp_,yp_,zp_]=Flatten[Table[Table[Hi1[\[Theta]ii[[i]],\[Phi]jj[[j]],\[
    Lambda],xp,yp,zp],{i,1.,N\[Theta]t+1,1.}],{j,1.,N\[Phi]t+1,1.}],1];
Hi2[\[Theta]_,\[Phi]_,\[Lambda]_,x_,y_,z_]=-I/\[Lambda]*1/Z*\[Alpha]t/N\[Theta]t*2\[Pi]/
    N\[Phi]t*angspecMAPpi2[\[Theta],\[Phi]]*Sqrt[Cos[\[Theta]]]*Sin[\[Theta]]*Exp[
    ikrAPpi2[\[Lambda],\[Theta],\[Phi],x,y,z]];
```

```
Hinc2[\[Lambda]_,xp_,yp_,zp_]=Flatten[Table[Table[Hi2[\[Theta]ii[[i]],\[Phi]jj[[j]],\[
    Lambda],xp,yp,zp],{i,1.,N\[Theta]t+1,1.}],{j,1.,N\[Phi]t+1,1.}],1];
Hinc[\[Lambda]_,xp_,yp_,zp_]=Join[Hinc1[\[Lambda],xp,yp,zp],Hinc2[\[Lambda],xp,yp,zp]];
H0sum[\[Lambda]_,xp_,yp_,zp_]=Total[Hinc[\[Lambda],xp,yp,zp]];

w=10^-30;
```

Gradient of incident beam at a point in space

```
delsum1[i_,j_,\[Lambda]_,x_,y_,z_]=
1/2*{{2D[Ei1[\[Theta]ii[[i]],\[Phi]jj[[j]],\[Lambda],x,y,z][[1]],x],D[Ei1[\[Theta]ii[[i
    ]],\[Phi]jj[[j]],\[Lambda],x,y,z][[1]],y]+D[Ei1[\[Theta]ii[[i]],\[Phi]jj[[j]],\[
    Lambda],x,y,z][[2]],x],D[Ei1[\[Theta]ii[[i]],\[Phi]jj[[j]],\[Lambda],x,y,z][[1]],z]+
    D[Ei1[\[Theta]ii[[i]],\[Phi]jj[[j]],\[Lambda],x,y,z][[3]],x]},{D[Ei1[\[Theta]ii[[i
    ]],\[Phi]jj[[j]],\[Lambda],x,y,z][[2]],x]+D[Ei1[\[Theta]ii[[i]],\[Phi]jj[[j]],\[
    Lambda],x,y,z][[1]],y],2D[Ei1[\[Theta]ii[[i]],\[Phi]jj[[j]],\[Lambda],x,y,z][[2]],y
    ],D[Ei1[\[Theta]ii[[i]],\[Phi]jj[[j]],\[Lambda],x,y,z][[2]],z]+D[Ei1[\[Theta]ii[[i
    ]],\[Phi]jj[[j]],\[Lambda],x,y,z][[3]],y]},{D[Ei1[\[Theta]ii[[i]],\[Phi]jj[[j]],\[
    Lambda],x,y,z][[3]],x]+D[Ei1[\[Theta]ii[[i]],\[Phi]jj[[j]],\[Lambda],x,y,z][[1]],z],
    D[Ei1[\[Theta]ii[[i]],\[Phi]jj[[j]],\[Lambda],x,y,z][[3]],y]+D[Ei1[\[Theta]ii[[i
    ]],\[Phi]jj[[j]],\[Lambda],x,y,z][[2]],z],2D[Ei1[\[Theta]ii[[i]],\[Phi]jj[[j]],\[
    Lambda],x,y,z][[3]],z]}};
delsum2[i_,j_,\[Lambda]_,x_,y_,z_]=
1/2*{{2D[Ei2[\[Theta]ii[[i]],\[Phi]jj[[j]],\[Lambda],x,y,z][[1]],x],D[Ei2[\[Theta]ii[[i
    ]],\[Phi]jj[[j]],\[Lambda],x,y,z][[1]],y]+D[Ei2[\[Theta]ii[[i]],\[Phi]jj[[j]],\[
    Lambda],x,y,z][[2]],x],D[Ei2[\[Theta]ii[[i]],\[Phi]jj[[j]],\[Lambda],x,y,z][[1]],z]+
    D[Ei2[\[Theta]ii[[i]],\[Phi]jj[[j]],\[Lambda],x,y,z][[3]],x]},{D[Ei2[\[Theta]ii[[i
    ]],\[Phi]jj[[j]],\[Lambda],x,y,z][[2]],x]+D[Ei2[\[Theta]ii[[i]],\[Phi]jj[[j]],\[
    Lambda],x,y,z][[1]],y],2D[Ei2[\[Theta]ii[[i]],\[Phi]jj[[j]],\[Lambda],x,y,z][[2]],y
    ],D[Ei2[\[Theta]ii[[i]],\[Phi]jj[[j]],\[Lambda],x,y,z][[2]],z]+D[Ei2[\[Theta]ii[[i
    ]],\[Phi]jj[[j]],\[Lambda],x,y,z][[3]],y]},{D[Ei2[\[Theta]ii[[i]],\[Phi]jj[[j]],\[
```

```
    Lambda],x,y,z][[3]],x]+D[Ei2[\[Theta]ii[[i]],\[Phi]jj[[j]],\[Lambda],x,y,z][[1]],z],
    D[Ei2[\[Theta]ii[[i]],\[Phi]jj[[j]],\[Lambda],x,y,z][[3]],y]+D[Ei2[\[Theta]ii[[i
    ]],\[Phi]jj[[j]],\[Lambda],x,y,z][[2]],z],2D[Ei2[\[Theta]ii[[i]],\[Phi]jj[[j]],\[
    Lambda],x,y,z][[3]],z]}};
deltot[\[Lambda]_,x_,y_,z_]=Total[Flatten[Table[Table[delsum1[i,j,\[Lambda],x,y,z]+
    delsum2[i,j,\[Lambda],x,y,z],{i,1,N\[Theta]t+1,1}],{j,1,N\[Phi]t+1}],1]];
del[\[Lambda]_,x_,y_,z_]:=Norm[Flatten[deltot[\[Lambda],x,y,z]]]^2;

delsumH1[i_,j_,\[Lambda]_,x_,y_,z_]=
1/2*{{2D[Hi1[\[Theta]ii[[i]],\[Phi]jj[[j]],\[Lambda],x,y,z][[1]],x],D[Hi1[\[Theta]ii[[i
    ]],\[Phi]jj[[j]],\[Lambda],x,y,z][[1]],y]+D[Hi1[\[Theta]ii[[i]],\[Phi]jj[[j]],\[
    Lambda],x,y,z][[2]],x],D[Hi1[\[Theta]ii[[i]],\[Phi]jj[[j]],\[Lambda],x,y,z][[1]],z]+
    D[Hi1[\[Theta]ii[[i]],\[Phi]jj[[j]],\[Lambda],x,y,z][[3]],x]},{D[Hi1[\[Theta]ii[[i
    ]],\[Phi]jj[[j]],\[Lambda],x,y,z][[2]],x]+D[Hi1[\[Theta]ii[[i]],\[Phi]jj[[j]],\[
    Lambda],x,y,z][[1]],y],2D[Hi1[\[Theta]ii[[i]],\[Phi]jj[[j]],\[Lambda],x,y,z][[2]],y
    ],D[Hi1[\[Theta]ii[[i]],\[Phi]jj[[j]],\[Lambda],x,y,z][[2]],z]+D[Hi1[\[Theta]ii[[i
    ]],\[Phi]jj[[j]],\[Lambda],x,y,z][[3]],y]},{D[Hi1[\[Theta]ii[[i]],\[Phi]jj[[j]],\[
    Lambda],x,y,z][[3]],x]+D[Hi1[\[Theta]ii[[i]],\[Phi]jj[[j]],\[Lambda],x,y,z][[1]],z],
    D[Hi1[\[Theta]ii[[i]],\[Phi]jj[[j]],\[Lambda],x,y,z][[3]],y]+D[Hi1[\[Theta]ii[[i
    ]],\[Phi]jj[[j]],\[Lambda],x,y,z][[2]],z],2D[Hi1[\[Theta]ii[[i]],\[Phi]jj[[j]],\[
    Lambda],x,y,z][[3]],z]}};
delsumH2[i_,j_,\[Lambda]_,x_,y_,z_]=
1/2*{{2D[Hi2[\[Theta]ii[[i]],\[Phi]jj[[j]],\[Lambda],x,y,z][[1]],x],D[Hi2[\[Theta]ii[[i
    ]],\[Phi]jj[[j]],\[Lambda],x,y,z][[1]],y]+D[Hi2[\[Theta]ii[[i]],\[Phi]jj[[j]],\[
    Lambda],x,y,z][[2]],x],D[Hi2[\[Theta]ii[[i]],\[Phi]jj[[j]],\[Lambda],x,y,z][[1]],z]+
    D[Hi2[\[Theta]ii[[i]],\[Phi]jj[[j]],\[Lambda],x,y,z][[3]],x]},{D[Hi2[\[Theta]ii[[i
    ]],\[Phi]jj[[j]],\[Lambda],x,y,z][[2]],x]+D[Hi2[\[Theta]ii[[i]],\[Phi]jj[[j]],\[
    Lambda],x,y,z][[1]],y],2D[Hi2[\[Theta]ii[[i]],\[Phi]jj[[j]],\[Lambda],x,y,z][[2]],y
    ],D[Hi2[\[Theta]ii[[i]],\[Phi]jj[[j]],\[Lambda],x,y,z][[2]],z]+D[Hi2[\[Theta]ii[[i
    ]],\[Phi]jj[[j]],\[Lambda],x,y,z][[3]],y]},{D[Hi2[\[Theta]ii[[i]],\[Phi]jj[[j]],\[
    Lambda],x,y,z][[3]],x]+D[Hi2[\[Theta]ii[[i]],\[Phi]jj[[j]],\[Lambda],x,y,z][[1]],z],
```

```
    D[Hi2[\[Theta]ii[[i]],\[Phi]jj[[j]],\[Lambda],x,y,z][[3]],y]+D[Hi2[\[Theta]ii[[i
    ]],\[Phi]jj[[j]],\[Lambda],x,y,z][[2]],z],2D[Hi2[\[Theta]ii[[i]],\[Phi]jj[[j]],\[
    Lambda],x,y,z][[3]],z]}};
deltotH[\[Lambda]_,x_,y_,z_]=Total[Flatten[Table[Table[delsumH1[i,j,\[Lambda],x,y,z]+
    delsumH2[i,j,\[Lambda],x,y,z],{i,1,N\[Theta]t+1,1}],{j,1,N\[Phi]t+1}],1]];
delH[\[Lambda]_,x_,y_,z_]:=Norm[Flatten[deltotH[\[Lambda],x,y,z]]]^2;

w=10^-30;

deltot1[\[Lambda]_,x_,y_,z_]=Total[Flatten[Table[Table[delsum1[i,j,\[Lambda],x,y,z],{i
    ,1,N\[Theta]t+1,1}],{j,1,N\[Phi]t+1}],1]];
deltot2[\[Lambda]_,x_,y_,z_]=Total[Flatten[Table[Table[delsum2[i,j,\[Lambda],x,y,z],{i
    ,1,N\[Theta]t+1,1}],{j,1,N\[Phi]t+1}],1]];

deltotH1[\[Lambda]_,x_,y_,z_]=Total[Flatten[Table[Table[delsumH1[i,j,\[Lambda],x,y,z],{i
    ,1,N\[Theta]t+1,1}],{j,1,N\[Phi]t+1}],1]];
deltotH2[\[Lambda]_,x_,y_,z_]=Total[Flatten[Table[Table[delsumH2[i,j,\[Lambda],x,y,z],{i
    ,1,N\[Theta]t+1,1}],{j,1,N\[Phi]t+1}],1]];
```

User input: Calculation of scattered cross section

```
(* !!! INPUT !!! *) lb=0.05;  (* lower bound of rnp/lambda *)
(* !!! INPUT !!! *) ub=0.25; (* upper bound of rnp/lambda *)
(* !!! INPUT !!! *) numS=20; (* number of wavelength steps *)

r\[Lambda]=Table[x,{x,lb,ub,(ub-lb)/numS}];
\[Lambda]t=rNP/r\[Lambda];

(* Local field expression for power scattered by spherical particle *)
Ws2[e_,M_,\[Lambda]_,x_,y_,z_]:=Abs[e*an[1,\[Lambda]]]^2*(3\[Pi])/(kw[\[Lambda]]*\[Omega
    ][\[Lambda]]*\[Mu])*Norm[E0sum[\[Lambda],w,w,w]]^2+M*Abs[bn[1,\[Lambda]]]^2*(3\[Pi])
```

```
    /(kw[\[Lambda]]*\[Omega][\[Lambda]]*\[Mu])*Z^2*Norm[H0sum[\[Lambda],w,w,w]]^2+e*Abs[
    an[2,\[Lambda]]]^2*(10\[Pi])/(kw[\[Lambda]]^3*\[Omega][\[Lambda]]*\[Mu])*del[\[
    Lambda],w,w,w]+M*Abs[bn[2,\[Lambda]]]^2*(10\[Pi])/(kw[\[Lambda]]^3*\[Omega][\[Lambda
    ]]*\[Mu])*Z^2*delH[\[Lambda],w,w,w];

(* Calculation of power scattered by sphere over a range of rnp/lambda *)
data=Table[{x,Re[Ws2[1,1,\[Lambda]t[[x]],w,w,w]]},{x,1,Length[\[Lambda]t],1}];

(* Calculation of incident intensity over a range of rnp/lambda *)
rrpp={};

Do[
S[x_]=Ec[\[Lambda]t[[i]],x,w,w];
ff =Table[S[x],{x,ll,ul,(ul-ll)/num}];

(* Evaluate extreme points *)
{min, max} = findExtremaPos[ff];

ListPlot[ff, Joined -> True,
 Epilog -> {PointSize[Large], Red, Point[{#, ff[[#]]} & /@ min],
 Blue, Point[{#, ff[[#]]} & /@ max]}, PlotRange -> All]

AppendTo[rrpp,min[[1]]*(ul-ll)/num]

,{i,1,Length[\[Lambda]t]}]

EcSphint[i_]:=1/(\[Pi]*rrpp[[i]]^2)*NIntegrate[EcSph[\[Lambda]t[[i]],r,\[Pi]/2,\[Phi]]*r
    ,{r,0,rrpp[[i]]},{\[Phi],0,2\[Pi]}];
eng=Table[{r\[Lambda][[x]],Re[EcSphint[x]]},{x,1,Length[r\[Lambda]],1}];
f=Interpolation[eng];
engsmart=Table[f[j],{j,0.05,0.25,(0.25-0.05)/500}];
```

```
(* Calculation of scattering cross-section over a range of rnp/lambda *)
data2=data1[[All,2]]/engsmart;
ListPlot[data2]
```

Appendix B

Numerical full beam simulations using Lumerical FDTD

This section contains instructions on using Lumerical FDTD to obtain the scattering response of spherical and dimer antennas under focused beam illumination using the full beam technique. The steps required are as follows:

1. Generate simulation files of the incident illumination beam, without the resonator of interest in place (referred to as "source" files), using the script file given in B.1 and run these files

2. Generate simulation files of the incident illumination beam, with the resonator of interest in place (referred to as "scatt" files), using the script file given in B.2 and run these files

3. Run the appropriate post-processing scripts, given in sections B.3 - B.7, to calculate: incident power, scattered power, field enhancement, radiation patterns, and field plots.

All simulation files and script files used to generate the figures in chapter 4 are available for download online through Google Drive. We implemented a three dimensional simulation in which the resonator of interest was placed at the focus of the beam under consideration. The electric and magnetic fields for focused radially (RP) and azimuthally polarized (AP) beams were calculated in a 2D plane using expressions from previous studies [34, 33]. These beams were injected into the simulation in a plane 1 μm away from the focus by using the Lumerical FDTD "Import Source" feature. The illumination beam was incident along the z-axis. We used symmetric boundary conditions along x and y for the RP beam and anti-symmetric boundary conditions for the AP beam, and perfectly matched layer (PML) boundary conditions for the remaining boundaries. A non-uniform mesh was used with a minimum element size of 5nm in the region of the scatterer. In all cases the simulations were run until the fields decayed to less than one millionth of the incident field strength. To construct the spectral response, the simulations were run at single wavelengths with and without the scatterer in place, and the scattered fields were obtained by subtracting the incident fields from the scattered plus incident fields.

B.1 Script file for generating source files

```
#####
# This script file is used to generate files that can be run in Lumerical FDTD
# The generated files simulate propagation of a focused linearly polarized beam in space
#####


# --- INPUT --- #
# load source file template
load("6282016-flpw-pws-dimer-inactive");
```

```
# --- INPUT --- #
lambda0 = floor(linspace(400,900,500)); # wavelengths to simulate at in units of nm

for(i=1:length(lambda0)) {
  # --- INPUT --- #
  NA = sin(pi/3);   # numerical aperture of focusing lens

  f = c/(lambda0(i)*10^-9); # frequency
  w = 2*pi*f;
  k = 2*pi/(lambda0(i)*10^-9); # wavenumber
  knum=100; # number of k-vectors in discretizations
  xynum=knum*2+1; # number of position vectors in discretization
  simsize=5e-6; # size of x- and y- dimensions of input plane in units of m

  # define position vectors
  x = linspace(-simsize,simsize,xynum); # array of position vectors in x
  y = linspace(-simsize,simsize,xynum); # array of position vectors in y
  z = 0; # this is z z-normal source

  # --- INPUT --- #
  z0=1e-6;   # distance of injection plane from focal plane in units of m

  X = meshgridx(x,y); # create a 2D grid of points in x
  Y = meshgridy(x,y); # create a 2D grid of points in y

  # define array of k-vectors
  kx = linspace(-k,k,knum);
  ky = linspace(-k,k,knum);
  Kx = meshgridx(kx,ky);
  Ky = meshgridy(kx,ky);
```

```
Kz = k*sqrt(1-Kx^2/k^2-Ky^2/k^2);
phi = atan2(Ky,Kx);
theta = real(acos(sqrt(1-Kx^2/k^2-Ky^2/k^2)));
envelope = exp(-0.5*(Kx^2 + Ky^2)/(NA*k)^2); # envelope function to for chosen NA;
    defined from M. Mansuripur, J. Opt. Soc. Am. A., 3(12), 2086 (1986)

# define filter to remove evanescent non-propagating plane waves
ux=kx/k;
uy=ky/k;
Ux = meshgridx(ux,uy);
Uy = meshgridy(ux,uy);
Uxy = sqrt(Ux^2+Uy^2)+1e-5; # add 1e-5 to avoid divide by zero problems
Uz  = sqrt(1-Uxy^2);
filter = (Ux^2+Uy^2 < 1);

# --- INPUT --- #
# define angular spectrum of incident beam
# example here is for focused linearly polarized beam
Exk = (cos(theta)*cos(phi)*cos(phi)+sin(phi)*sin(phi))*envelope;
Eyk = (cos(theta)*cos(phi)*sin(phi)-cos(phi)*sin(phi))*envelope;
Ezk = sin(theta)*cos(phi)*envelope;
Ex = czt(Exk*exp(-1i*Kz*z0)*filter,kx,ky,x,y);
Ey = czt(Eyk*exp(-1i*Kz*z0)*filter,kx,ky,x,y);
Ez = czt(Ezk*exp(-1i*Kz*z0)*filter,kx,ky,x,y);

Hxk = sqrt(eps0/mu0)*((1-cos(theta))*cos(phi)*sin(phi))*envelope;
Hyk = sqrt(eps0/mu0)*-(1-(1-cos(theta))*sin(phi)*sin(phi))*envelope;
Hzk = sqrt(eps0/mu0)*(sin(theta)*sin(phi))*envelope;
Hx = czt(Hxk*exp(-1i*Kz*z0)*filter,kx,ky,x,y);
Hy = czt(Hyk*exp(-1i*Kz*z0)*filter,kx,ky,x,y);
Hz = czt(Hzk*exp(-1i*Kz*z0)*filter,kx,ky,x,y);
```

```
# scale field so |E|^2=1
E2 = abs(Ex)^2+abs(Ey)^2+abs(Ez)^2;
scaleFactor = sqrt(max(E2));
Ex = Ex/scaleFactor;
Ey = Ey/scaleFactor;
Ez = Ez/scaleFactor;
Hx = Hx/scaleFactor;
Hy = Hy/scaleFactor;
Hz = Hz/scaleFactor;

# package field data into the EM fields dataset that can be loaded into the Import
    source
EM = rectilineardataset("EM fields",x,y,z);
EM.addparameter("lambda",c/f,"f",f);
EM.addattribute("E",Ex,Ey,Ez);
EM.addattribute("H",Hx,Hy,Hz);

# directly load dataset into source
select("import_beam");
importdataset(EM);
set("z",z0);
set("center wavelength",lambda0(i)*10^-9);
set("wavelength span",0);

select("Psource");
set("lda",lambda0(i)*10^-9);

# output which simulation is being saved
?"saving simulation " + num2str(i) + " of " + num2str(length(lambda0));
```

```
  # save the simulation at every wavelength
  f_name="4212017-frpw-pws-wl"+num2str(lambda0(i))+"nm-source";
  save(f_name);
}
```

B.2 Script file for generating scatt files

```
#####
# This script file is used to generate files that can be run in Lumerical FDTD
# The generated files simulate propagation of a focused linearly polarized beam in space
     with a resonator at the focus
#####

# --- INPUT --- #
# load source file template
load("6282016-flpw-pws-dimer-active");

# --- INPUT --- #
lambda0 = floor(linspace(400,900,500)); # wavelengths to simulate at in units of nm

for(i=1:length(lambda0)) {
  # --- INPUT --- #
  NA = sin(pi/3);   # numerical aperture of focusing lens

  f = c/(lambda0(i)*10^-9); # frequency
  w = 2*pi*f;
  k = 2*pi/(lambda0(i)*10^-9); # wavenumber
  knum=100; # number of k-vectors in discretizations
  xynum=knum*2+1; # number of position vectors in discretization
  simsize=5e-6; # size of x- and y- dimensions of input plane in units of m
```

```
# define position vectors
x = linspace(-simsize,simsize,xynum); # array of position vectors in x
y = linspace(-simsize,simsize,xynum); # array of position vectors in y
z = 0; # this is a z-normal source

# --- INPUT --- #
z0=1e-6;   # distance of injection plane from focal plane in units of m

X = meshgridx(x,y); # create a 2D grid of points in x
Y = meshgridy(x,y); # create a 2D grid of points in y

# define array of k-vectors
kx = linspace(-k,k,knum);
ky = linspace(-k,k,knum);
Kx = meshgridx(kx,ky);
Ky = meshgridy(kx,ky);
Kz = k*sqrt(1-Kx^2/k^2-Ky^2/k^2);
phi = atan2(Ky,Kx);
theta = real(acos(sqrt(1-Kx^2/k^2-Ky^2/k^2)));
envelope = exp(-0.5*(Kx^2 + Ky^2)/(NA*k)^2); # envelope function to for chosen NA;
    defined from M. Mansuripur, J. Opt. Soc. Am. A., 3(12), 2086 (1986)

# define filter to remove evanescent non-propagating plane waves
ux=kx/k;
uy=ky/k;
Ux = meshgridx(ux,uy);
Uy = meshgridy(ux,uy);
Uxy = sqrt(Ux^2+Uy^2)+1e-5; # add 1e-5 to avoid divide by zero problems
Uz  = sqrt(1-Uxy^2);
filter = (Ux^2+Uy^2 < 1);
```

```
# --- INPUT --- #
# define angular spectrum of incident beam
# example here is for focused linearly polarized beam
Exk = (cos(theta)*cos(phi)*cos(phi)+sin(phi)*sin(phi))*envelope;
Eyk = (cos(theta)*cos(phi)*sin(phi)-cos(phi)*sin(phi))*envelope;
Ezk = sin(theta)*cos(phi)*envelope;
Ex = czt(Exk*exp(-1i*Kz*z0)*filter,kx,ky,x,y);
Ey = czt(Eyk*exp(-1i*Kz*z0)*filter,kx,ky,x,y);
Ez = czt(Ezk*exp(-1i*Kz*z0)*filter,kx,ky,x,y);

Hxk = sqrt(eps0/mu0)*((1-cos(theta))*cos(phi)*sin(phi))*envelope;
Hyk = sqrt(eps0/mu0)*-(1-(1-cos(theta))*sin(phi)*sin(phi))*envelope;
Hzk = sqrt(eps0/mu0)*(sin(theta)*sin(phi))*envelope;
Hx = czt(Hxk*exp(-1i*Kz*z0)*filter,kx,ky,x,y);
Hy = czt(Hyk*exp(-1i*Kz*z0)*filter,kx,ky,x,y);
Hz = czt(Hzk*exp(-1i*Kz*z0)*filter,kx,ky,x,y);

# scale field so |E|^2=1
E2 = abs(Ex)^2+abs(Ey)^2+abs(Ez)^2;
scaleFactor = sqrt(max(E2));
Ex = Ex/scaleFactor;
Ey = Ey/scaleFactor;
Ez = Ez/scaleFactor;
Hx = Hx/scaleFactor;
Hy = Hy/scaleFactor;
Hz = Hz/scaleFactor;

# package field data into the EM fields dataset that can be loaded into the Import
    source
EM = rectilineardataset("EM fields",x,y,z);
EM.addparameter("lambda",c/f,"f",f);
```

```
  EM.addattribute("E",Ex,Ey,Ez);
  EM.addattribute("H",Hx,Hy,Hz);

  # directly load dataset into source
  select("import_beam");
  importdataset(EM);
  set("z",z0);
  set("center wavelength",lambda0(i)*10^-9);
  set("wavelength span",0);

  select("Psource");
  set("lda",lambda0(i)*10^-9);

  # output which simulation is being saved
  ?"saving simulation " + num2str(i) + " of " + num2str(length(lambda0));

  # save the simulation at every wavelength
  f_name="4212017-frpw-pws-wl"+num2str(lambda0(i))+"nm-scatt";
  save(f_name);
}
```

B.3 Script file for calculating incident power of focused beam

```
#####
# This script file is used to calculate the incident power of a focused beam
# This script should be run after the "source" simulations are complete
#####

# preliminary setup
```

```
clear;
lda=0;
I_inc=0;
P_inc=0;

# --- INPUT --- #
lambda0 = floor(linspace(400,900,500)); # wavelengths in units of nm must be the same as
     wavelengths of "source" and "scatt" files

# at each wavelength, run the "Psource" analysis, which extracts the electric and
    magnetic fields on a cubic surface centered around the origin
for(i=1:length(lambda0)) {
  ?k=lambda0(i);

  load("4212017-frpw-pws-wl"+num2str(lambda0(i))+"nm-source");
  runanalysis("Psource");

  load("4212017-frpw-pws-wl"+num2str(lambda0(i))+"nm-scatt");
  runanalysis("Psource");
}

# at each wavelength, calculate the incident power
for(i=1:length(lambda0)) {
  ?k=lambda0(i);

  # load the source file at each wavelength
  load("4212017-frpw-pws-wl"+num2str(lambda0(i))+"nm-source");
  loaddata("fields_source_"+num2str(k));

  # get electric and magnetic fields
  e_ref_z2Ex=getdata("z normal monitor","Ex");
```

```
  e_ref_z2Ey=getdata("z normal monitor","Ey");
  h_ref_z2Hx=getdata("z normal monitor","Hx");
  h_ref_z2Hy=getdata("z normal monitor","Hy");

  # calculate area of the z monitor
  z2x=getdata("z normal monitor","x");
  z2y=getdata("z normal monitor","y");
  areaz=(max(z2x)-min(z2x)) *(max(z2y)-min(z2y));

  # calculate the z-oriented Poynting vector
  temp =real(pinch(e_ref_z2Ex*conj(h_ref_z2Hy)-e_ref_z2Ey*conj(h_ref_z2Hx)));

  # calculate the scattered power
  ps=0.5*integrate(temp,1:2,z2x,z2y);

  # calculate the average intensity over a 2D plane
  ave_intensity=ps/areaz;

  # save data to an array
  lambda=c/f;
  lda=[lda,lambda];
  I_inc=[I_inc,ave_intensity];
  P_inc=[P_inc,ps];

  # write data (wavelength and incident power) to file
  write("4232017-fapw-pws-Pinc.txt",num2str([lambda,ps]));
}
```

B.4 Script file for calculating power scattered by resonator

```
#####
# This script file is used to calculate the power scattered by a resonator under
    illumination by a focused beam
# This script should be run after the "source" and "scatt" simulations are complete
#####

# preliminary setup
clear;
lda=0;
I_inc=0;
P_inc=0;

# --- INPUT --- #
lambda0 = floor(linspace(400,900,500)); # wavelengths in units of nm must be the same as
     wavelengths of "source" and "scatt" files

# at each wavelegnth, run the "Psource" analysis, which extracts the electric and
    magnetic fields on a cubic surface centered around the origin
for(i=1:length(lambda0)) {
  ?k=lambda0(i);

  # --- INPUT --- #
  load("4212017-frpw-pws-wl"+num2str(lambda0(i))+"nm-source"); # load source files
  runanalysis("Psource");

  # --- INPUT --- #
  load("4212017-frpw-pws-wl"+num2str(lambda0(i))+"nm-scatt"); # load scatt files
```

```
  runanalysis("Psource");
}

# at each wavelength, calculate the scattered power
for(i=1:length(lambda0)) {
  ?k=lambda0(i);

  # load the "source" (incident) and "scatt" (incident+scattered) electric and magnetic
      fields on a cubic surface around the origin
  loaddata("fields_source_"+num2str(k));
  loaddata("fields_scattered_"+num2str(k));

  # calculate scattered fields at a single wavelength by subtracting the incident fields
       from the incident+scattered fields
  ey_x2=e_scatter_x2.Ey-e_ref_x2.Ey;
  ez_x2=e_scatter_x2.Ez-e_ref_x2.Ez;
  hy_x2=h_scatter_x2.Hy-h_ref_x2.Hy;
  hz_x2=h_scatter_x2.Hz-h_ref_x2.Hz;

  ex_y2=e_scatter_y2.Ex-e_ref_y2.Ex;
  ez_y2=e_scatter_y2.Ez-e_ref_y2.Ez;
  hx_y2=h_scatter_y2.Hx-h_ref_y2.Hx;
  hz_y2=h_scatter_y2.Hz-h_ref_y2.Hz;

  ex_z1=e_scatter_z1.Ex-e_ref_z1.Ex;
  ey_z1=e_scatter_z1.Ey-e_ref_z1.Ey;
  hx_z1=h_scatter_z1.Hx-h_ref_z1.Hx;
  hy_z1=h_scatter_z1.Hy-h_ref_z1.Hy;

  ex_z2=e_scatter_z2.Ex-e_ref_z2.Ex;
  ey_z2=e_scatter_z2.Ey-e_ref_z2.Ey;
```

```
hx_z2=h_scatter_z2.Hx-h_ref_z2.Hx;
hy_z2=h_scatter_z2.Hy-h_ref_z2.Hy;

# calculate the Poynting vector in the x normal direction
temp =real(pinch(ey_x2*conj(hz_x2)-ez_x2*conj(hy_x2)));
# calculate the scattered power in the x normal direction
px2=integrate(temp,1:2,x2y,x2z);

# calculate the Poynting vector in the y normal direction
temp =real(pinch(ez_y2*conj(hx_y2)-ex_y2*conj(hz_y2)));
# calculate the scattered power in the x normal direction
py2=integrate(temp,1:2,y2x,y2z);

# calculate the Poynting vector in the z normal direction for the bottom z monitor
temp =real(pinch(ex_z1*conj(hy_z1)-ey_z1*conj(hx_z1)));
# calculate the scattered power in the z normal direction for the bottom z monitor
pz1=integrate(temp,1:2,z2x,z2y);

# calculate the Poynting vector in the z normal direction for the top z monitor
temp =real(pinch(ex_z2*conj(hy_z2)-ey_z2*conj(hx_z2)));
# calculate the scattered power in the z normal direction for the top z monitor
pz2=integrate(temp,1:2,z2x,z2y);

# add up all the scattered power
P_scat= px2+px2+py2+py2+-pz1+pz2;

# calculate the size parameter
r=100*10^(-9);
lambda=c/f;
size_parameter = r/(lambda);
```

```
  # save data to an array
  sp=[sp,size_parameter];
  lda=[lda,lambda];
  P_sca=[P_sca,P_scat];

  # write data (wavelength and scattered power) to file
  write("4232017-flpw-dimer-pws-Pscat.txt",num2str([lambda,P_scat]));
}
```

B.5 Script file for calculating electric and magnetic intensity enhancement

```
#####
# This script file is used to calculate the electric and magnetic field enhancement at
    the origin
# This script should be run after the "source" and "scatt" simulations are complete
#####


# preliminary setup
clear;
sp=0;
lda=0;
E_mag=0;
H_mag=0;

# --- INPUT --- #
lambda0 = floor(linspace(400,900,500)); # wavelengths in units of nm must be the same as
     wavelengths of "source" and "scatt" files
```

```
for(j=1:length(lambda0)) { # iterate over all wavelengths

    ?lambda0(j); # display the current simulation wavelength

    ?"Importing source data";

    # --- INPUT --- #
    # load source file at each wavelength
    load("4212017-frpw-pws-wl"+num2str(lambda0(j))+"nm-source");

    # load the electric and magnetic fields in the xz-plane from the relevant field
        monitor
    Es = getresult("y normal monitor","E");
    Hs = getresult("y normal monitor","H");

    # extract the wavelength, x, and z coordinates from the field monitor
    lambda = Es.lambda;
    x = Es.x;
    z = Es.z;

    # remove irrelevant information from electric and magnetic field data
    Es = pinch(Es.E);
    Hs = pinch(Hs.H);

    Exs = pinch(Es(1:length(x),1:length(z),1));
    Eys = pinch(Es(1:length(x),1:length(z),2));
    Ezs = pinch(Es(1:length(x),1:length(z),3));

    Hxs = pinch(Hs(1:length(x),1:length(z),1));
    Hys = pinch(Hs(1:length(x),1:length(z),2));
    Hzs = pinch(Hs(1:length(x),1:length(z),3));
```

```
?"Importing scatt data";

# --- INPUT --- #
# load scatt file at each wavelength
load("4212017-frpw-pws-wl"+num2str(lambda0(j))+"nm-scatt");

# load the electric and magnetic fields in the xz-plane from the relevant field
    monitor
Esc = getresult("y normal monitor","E");
Hsc = getresult("y normal monitor","H");

# extract the wavelength, x, and z coordinates from the field monitor
lambda = Esc.lambda;
x = Esc.x;
z = Esc.z;

# remove irrelevant information from electric and magnetic field data
Esc = pinch(Esc.E);
Hsc = pinch(Hsc.H);

Exsc = pinch(Esc(1:length(x),1:length(z),1));
Eysc = pinch(Esc(1:length(x),1:length(z),2));
Ezsc = pinch(Esc(1:length(x),1:length(z),3));

Hxsc = pinch(Hsc(1:length(x),1:length(z),1));
Hysc = pinch(Hsc(1:length(x),1:length(z),2));
Hzsc = pinch(Hsc(1:length(x),1:length(z),3));
```

```
?"Pre-processing";

Exfinal=Exsc;
Eyfinal=Eysc;
Ezfinal=Ezsc;

Hxfinal=Hxsc;
Hyfinal=Hysc;
Hzfinal=Hzsc;

# calculate the norm of the scattered electric and magnetic fields
EfinalN = sqrt((abs(Exfinal)^2)+(abs(Eyfinal)^2)+(abs(Ezfinal)^2));
HfinalN = sqrt((abs(Hxfinal)^2)+(abs(Hyfinal)^2)+(abs(Hzfinal)^2));

# calculate the norm of the incident electric and magnetic fields
EsN = sqrt((abs(Exs)^2)+(abs(Eys)^2)+(abs(Ezs)^2));
HsN = sqrt((abs(Hxs)^2)+(abs(Hys)^2)+(abs(Hzs)^2));

# calculate the electric and magnetic intensity enhancement at all points in the xz-
    plane
EFH=(EfinalN/EsN)^2;
HFH=(HfinalN/HsN)^2;

?"Quantifying enhancement";
indexx=find(x,0); indexz=find(z,0); # find the correct x- and z-indices that
    descirbe the origin

?EF=EFH(indexx,indexz); # extract the electric intensity enhancement at the origin
?HF=HFH(indexx,indexz); # extract the magnetic intensity enhancement at the origin
```

```
    # save enhancement data to file
    f=getdata("import_beam","f");
    lambda=c/f;
    size_parameter=100e-9/lambda;

    lda=[lda,lambda];
    sp=[sp,size_parameter];
    E_mag=[E_mag,EF];
    H_mag=[H_mag,HF];

    # write data to file
    write("4232017-xpol-dimerx-EFH.txt",num2str([size_parameter,EF])); # electric
        intensity enhancement
    write("4232017-xpol-dimerx-HFH.txt",num2str([size_parameter,HF])); # magnetic
        intensity enhancement
}

?"Done";
```

B.6 Script file for plotting radiation patterns

```
#####
# This script file is used to plot the radiation pattern of a resonator at a single
    wavelength
# This script should be run after the "scatt" simulations are complete
#####

# --- INPUT --- #
twl=531e-9; # define wavelengths to simulate at in units of nm
ppres=100; # number of data points of radiation pattern
```

```
# --- INPUT --- #
# load scatt file at chosen wavelength
load("4212017-frpw-pws-wl"+num2str(twl*10^9)+"nm-scatt");

###############################################
# automatically unfold field data if symmetry BC is applied
if (havedata("Psource::x1", "f")) {
  symm_x = 0;
} else {
  xtemp = getdata("Psource::y2", "x");
  ztemp = getdata("Psource::y2", "z");
  Eztemp = pinch(getdata("Psource::y2", "Ez"));

  Ez2mid = sum(Eztemp(round(length(xtemp)/2), 1:length(ztemp))^2);
  if (Ez2mid != 0) {
    symm_x = 1;
  } else {
    symm_x = -1;
  }
}

if (havedata("Psource::y1", "f")) {
  symm_y = 0;
} else {
  ytemp = getdata("Psource::x2", "y");
  ztemp = getdata("Psource::x2", "z");
  Eztemp = pinch(getdata("Psource::x2", "Ez"));

  Ez2mid = sum(Eztemp(round(length(ytemp)/2), 1:length(ztemp))^2);
  if (Ez2mid != 0) {
    symm_y = 1;
```

```
  } else {
    symm_y = -1;
  }
}

if (havedata("Psource::z1", "f")) {
  symm_z = 0;
} else {
  xtemp = getdata("Psource::y2", "x");
  ztemp = getdata("Psource::y2", "z");
  Eytemp = pinch(getdata("Psource::y2", "Ey"));

  Ey2mid = sum(Eytemp(1:length(xtemp), round(length(ztemp)/2))^2);
  if (Ey2mid != 0) {
    symm_z = 1;
  } else {
    symm_z = -1;
  }
}

f = getdata("Psource::x2","f");   # get freqency data

#if (havedata("Psource::index","index_x")) {  # get refractive index.  Required to
    calcualte H2 from E2
#  n_index = getdata("Psource::index","index_x");
#} else {
#  n_index = getdata("scatt_ff::index","index_z");
#}

n=1;
```

```
##############################################
# define the angular resolution
phi = linspace(0,360,ppres);
npts = length(phi);

# define the field data matrices for angular distribution
E_xy = matrix(npts, 3, length(f)); # 3 for x, y, z component
E_yz = matrix(npts, 3, length(f)); # 3 for x, y, z component
E_xz = matrix(npts, 3, length(f)); # 3 for x, y, z component
E2_xy = matrix(npts,length(f));
E2_yz = matrix(npts,length(f));
E2_xz = matrix(npts,length(f));
H2_xy = matrix(npts,length(f));
H2_yz = matrix(npts,length(f));
H2_xz = matrix(npts,length(f));

# Identify the closest wavelength to target:
target_wavelength = twl;
i_target = find(f,c/target_wavelength);
?"Target wavelength = " + num2str(target_wavelength);
?"Wavelength used = " + num2str(c/f(i_target));

if (havedata("Psource::z2","Ex")) { # have z data, 3D simulation
##############################################
# Angular distribution calculation for a 3D simulation begins

 for (i = 1:length(f)){ # loop for all frequencies

 # print the frequency point number running in the loop
 ?"Angular distribution i="+num2str(i)+", "+num2str(c/f(i)*1e6)+"um";
```

```
#n = n_index(i);   # select the frequency point for the index

######## x-y plane (phi=0 corresponds to the direction (0,1,0))
?"    Projecting in x-y plane";
x = -sin(phi*pi/180); y = cos(phi*pi/180); z = 0;

# Calculate far field by summing contribution from each monitor
temp = farfieldexact("Psource::x2",x,y,z,i) + farfieldexact("Psource::y2",x,y,z,i) +
     farfieldexact("Psource::z2",x,y,z,i);
if(havedata("Psource::x1")){
  temp = temp - farfieldexact("Psource::x1",x,y,z,i);
}else{
  temp2 = farfieldexact("Psource::x2",-x,y,z,i);
  s = symm_x*[1,-1,-1];
  temp2(1:npts,1) = s(1)*temp2(1:npts,1);
  temp2(1:npts,2) = s(2)*temp2(1:npts,2);
  temp2(1:npts,3) = s(3)*temp2(1:npts,3);
  temp = temp - temp2;
}
if(havedata("Psource::y1")){
  temp = temp - farfieldexact("Psource::y1",x,y,z,i);
}else{
  temp2 = farfieldexact("Psource::y2",x,-y,z,i);
  s = symm_y*[-1,1,-1];
  temp2(1:npts,1) = s(1)*temp2(1:npts,1);
  temp2(1:npts,2) = s(2)*temp2(1:npts,2);
  temp2(1:npts,3) = s(3)*temp2(1:npts,3);
  temp = temp - temp2;
}
if(havedata("Psource::z1")){
  temp = temp - farfieldexact("Psource::z1",x,y,z,i);
```

```
}else{
  temp2 = farfieldexact("Psource::z2",x,y,-z,i);
  s = symm_z*[-1,-1,1];
  temp2(1:npts,1) = s(1)*temp2(1:npts,1);
  temp2(1:npts,2) = s(2)*temp2(1:npts,2);
  temp2(1:npts,3) = s(3)*temp2(1:npts,3);
  temp = temp - temp2;
}
E_xy (1:length(phi), 1:3, i) = temp;
E2_xy (1:length(phi), i) = sum(abs(temp)^2,2); # E2 = |Ex|^2 + |Ey|^2 + |Ez|^2
H2_xy (1:length(phi), i) = E2_xy (1:length(phi), i) * n^2 * eps0/mu0; # for a plane
    wave, E^2 and H^2 only differ by a factor of n^2*eps0/mu0

######## y-z plane (phi=0 corresponds to the direction (0,1,0))
?"    Projecting in y-z plane";
x = 0; y = cos(phi*pi/180);  z = sin(phi*pi/180);

# Calculate far field by summing contribution from each monitor
temp = farfieldexact("Psource::x2",x,y,z,i) + farfieldexact("Psource::y2",x,y,z,i) +
     farfieldexact("Psource::z2",x,y,z,i);
if(havedata("Psource::x1")){
  temp = temp - farfieldexact("Psource::x1",x,y,z,i);
}else{
  temp2 = farfieldexact("Psource::x2",-x,y,z,i);
  s = symm_x*[1,-1,-1];
  temp2(1:npts,1) = s(1)*temp2(1:npts,1);
  temp2(1:npts,2) = s(2)*temp2(1:npts,2);
  temp2(1:npts,3) = s(3)*temp2(1:npts,3);
  temp = temp - temp2;
}
if(havedata("Psource::y1")){
```

```
  temp = temp - farfieldexact("Psource::y1",x,y,z,i);
}else{
  temp2 = farfieldexact("Psource::y2",x,-y,z,i);
  s = symm_y*[-1,1,-1];
  temp2(1:npts,1) = s(1)*temp2(1:npts,1);
  temp2(1:npts,2) = s(2)*temp2(1:npts,2);
  temp2(1:npts,3) = s(3)*temp2(1:npts,3);
  temp = temp - temp2;
}
if(havedata("Psource::z1")){
  temp = temp - farfieldexact("Psource::z1",x,y,z,i);
}else{
  temp2 = farfieldexact("Psource::z2",x,y,-z,i);
  s = symm_z*[-1,-1,1];
  temp2(1:npts,1) = s(1)*temp2(1:npts,1);
  temp2(1:npts,2) = s(2)*temp2(1:npts,2);
  temp2(1:npts,3) = s(3)*temp2(1:npts,3);
  temp = temp - temp2;
}
E_yz (1:length(phi), 1:3, i) = temp;
E2_yz (1:length(phi), i) = sum(abs(temp)^2,2); # E2 = |Ex|^2 + |Ey|^2 + |Ez|^2
H2_yz (1:length(phi), i) = E2_yz (1:length(phi), i) * n^2 * eps0/mu0; # for a plane
    wave, E^2 and H^2 only differ by a factor of n^2*eps0/mu0

######### x-z plane (theta=0 corresponds to the direction (0,1,0))
?"    Projecting in x-z plane";
x = cos(phi*pi/180); y = 0; z = sin(phi*pi/180);

# Calculate far field by summing contribution from each monitor
temp = farfieldexact("Psource::x2",x,y,z,i) + farfieldexact("Psource::y2",x,y,z,i) +
     farfieldexact("Psource::z2",x,y,z,i);
```

```
if(havedata("Psource::x1")){
  temp = temp - farfieldexact("Psource::x1",x,y,z,i);
}else{
  temp2 = farfieldexact("Psource::x2",-x,y,z,i);
  s = symm_x*[1,-1,-1];
  temp2(1:npts,1) = s(1)*temp2(1:npts,1);
  temp2(1:npts,2) = s(2)*temp2(1:npts,2);
  temp2(1:npts,3) = s(3)*temp2(1:npts,3);
  temp = temp - temp2;
}
if(havedata("Psource::y1")){
  temp = temp - farfieldexact("Psource::y1",x,y,z,i);
}else{
  temp2 = farfieldexact("Psource::y2",x,-y,z,i);
  s = symm_y*[-1,1,-1];
  temp2(1:npts,1) = s(1)*temp2(1:npts,1);
  temp2(1:npts,2) = s(2)*temp2(1:npts,2);
  temp2(1:npts,3) = s(3)*temp2(1:npts,3);
  temp = temp - temp2;
}
if(havedata("Psource::z1")){
  temp = temp - farfieldexact("Psource::z1",x,y,z,i);
}else{
  temp2 = farfieldexact("Psource::z2",x,y,-z,i);
  s = symm_z*[-1,-1,1];
  temp2(1:npts,1) = s(1)*temp2(1:npts,1);
  temp2(1:npts,2) = s(2)*temp2(1:npts,2);
  temp2(1:npts,3) = s(3)*temp2(1:npts,3);
  temp = temp - temp2;
}
E_xz (1:length(phi), 1:3, i) = temp;
```

```
    E2_xz (1:length(phi), i) = sum(abs(temp)^2,2); # E2 = |Ex|^2 + |Ey|^2 + |Ez|^2
    H2_xz (1:length(phi), i) = E2_xz (1:length(phi), i) * n^2 * eps0/mu0; # for a plane
        wave, E^2 and H^2 only differ by a factor of n^2*eps0/mu0

} # end of the angular distribution for loop

 if (1) { # polar plot for target wavelength
     polar(phi*pi/180, E2_xy(1:length(phi), i_target), E2_yz(1:length(phi), i_target),
         E2_xz(1:length(phi), i_target),
     "angle (degrees)", "|E|^2", "|E|^2 vs angle @ "+num2str(c/f(i_target)*1e6)+"um");
     legend("xy plane","yz plane","xz plane");
 } # end of if polar plot

 if (1) { # polar plot for target wavelength
     polar(phi*pi/180,E2_yz(1:length(phi), i_target),
     "angle (degrees)", "|E|^2", "|E|^2 vs angle @ "+num2str(c/f(i_target)*1e6)+"um");
     legend("xy plane","yz plane","xz plane");
 } # end of if polar plot

 # create datasets for XY, YZ, XZ for angular distribution
 XY = matrixdataset("XY");
 XY.addparameter("phi",phi*pi/180.); #phi angle in radians
 XY.addparameter("lambda",c/f,"f",f);
 XY.addattribute("E",pinch(E_xy,2,1),pinch(E_xy,2,2),pinch(E_xy,2,3));  # Ex, Ey, Ez
 XY.addattribute("E2",E2_xy);
 XY.addattribute("H2",H2_xy);

 YZ = matrixdataset("YZ");
 YZ.addparameter("phi",phi*pi/180.); #phi angle in radians
 YZ.addparameter("lambda",c/f,"f",f);
 YZ.addattribute("E",pinch(E_yz,2,1),pinch(E_yz,2,2),pinch(E_yz,2,3));  # Ex, Ey, Ez
```

```
  YZ.addattribute("E2",E2_yz);
  YZ.addattribute("H2",H2_yz);

  XZ = matrixdataset("XZ");
  XZ.addparameter("phi",phi*pi/180.); #phi angle in radians
  XZ.addparameter("lambda",c/f,"f",f);
  XZ.addattribute("E",pinch(E_xz,2,1),pinch(E_xz,2,2),pinch(E_xz,2,3));  # Ex, Ey, Ez
  XZ.addattribute("E2",E2_xz);
  XZ.addattribute("H2",H2_xz);
# end of the angular distribution for a 3D simulation
###############################################
}
```

B.7 Script file for extracting field plots

```
#####
# This script file is used to extract data on the norm, absolute value, and phase of the
     electric and magnetic fields in the xy-, yz-, and xz-planes
# This script should be run after the "source" and "scatt" simulations are complete
#####

clear;

# --- INPUT --- #
lambda0 = 400; # define wavelengths to extract fields at in units of nm

# --- INPUT --- #
f_name = "10182016-flpw-long-dimer-xz"; # name of data files to save data to

# repeat for each wavelength of interest
for(i=1:length(lambda0)) {
```

```
?"Importing source data";

# --- INPUT --- #
load("6282016-frpw-pws-wl"+num2str(lambda0(i))+"nm-source"); # load electirc and
    magnetic fields from source files

# load the electric and magnetic fields in the xz-plane from the relevant field
    monitor
Es = getresult("y normal monitor","E");
Hs = getresult("y normal monitor","H");

# extract the wavelength, x, and z coordinates from the field monitor
lambda = Es.lambda;
x = Es.x;
z = Es.z;

# remove irrelevant information from electric and magnetic field data
Es = pinch(Es.E);
Hs = pinch(Hs.H);

Exs = pinch(Es(1:length(x),1:length(z),1));
Eys = pinch(Es(1:length(x),1:length(z),2));
Ezs = pinch(Es(1:length(x),1:length(z),3));

Hxs = pinch(Hs(1:length(x),1:length(z),1));
Hys = pinch(Hs(1:length(x),1:length(z),2));
Hzs = pinch(Hs(1:length(x),1:length(z),3));


?"Importing scatt data";
```

```
# --- INPUT --- #
load("6282016-frpw-pws-wl"+num2str(lambda0(i))+"nm-scatt"); # load electirc and
    magnetic fields from scatt files

# load the electric and magnetic fields in the xz-plane from the relevant field
    monitor
Esc = getresult("y normal monitor","E");
Hsc = getresult("y normal monitor","H");

# extract the wavelength, x, and z coordinates from the field monitor
lambda = Esc.lambda;
x = Esc.x;
z = Esc.z;

# remove irrelevant information from electric and magnetic field data
Esc = pinch(Esc.E);
Hsc = pinch(Hsc.H);

Exsc = pinch(Esc(1:length(x),1:length(z),1));
Eysc = pinch(Esc(1:length(x),1:length(z),2));
Ezsc = pinch(Esc(1:length(x),1:length(z),3));

Hxsc = pinch(Hsc(1:length(x),1:length(z),1));
Hysc = pinch(Hsc(1:length(x),1:length(z),2));
Hzsc = pinch(Hsc(1:length(x),1:length(z),3));


?"Pre-processing";

Exfinal=Exsc;
Eyfinal=Eysc;
```

```
Ezfinal=Ezsc;

Hxfinal=Hxsc;
Hyfinal=Hysc;
Hzfinal=Hzsc;

# calculate the norm of the scattered electric and magnetic fields
EfinalN = sqrt((abs(Exfinal)^2)+(abs(Eyfinal)^2)+(abs(Ezfinal)^2));
HfinalN = sqrt((abs(Hxfinal)^2)+(abs(Hyfinal)^2)+(abs(Hzfinal)^2));

# calculate the norm of the incident electric and magnetic fields
EsN = sqrt((abs(Exs)^2)+(abs(Eys)^2)+(abs(Ezs)^2));
HsN = sqrt((abs(Hxs)^2)+(abs(Hys)^2)+(abs(Hzs)^2));

# calculate the absolute value of the scattered electric and magnetic field
    components
EFxAbs = abs(Exfinal);
HFxAbs = abs(Hxfinal);
EFyAbs = abs(Eyfinal);
HFyAbs = abs(Hyfinal);
EFzAbs = abs(Ezfinal);
HFzAbs = abs(Hzfinal);

# calculate the phase of the scattered electric and magnetic field components
EFxArg = angle(Exfinal);
HFxArg = angle(Hxfinal);
EFyArg = angle(Eyfinal);
HFyArg = angle(Hyfinal);
EFzArg = angle(Ezfinal);
HFzArg = angle(Hzfinal);
```

```
# calculate the electric and magnetic field intensity enhancement
EFH = (EfinalN/EsN)^2;
HFH = (HfinalN/HsN)^2;

?"Data is pre-processed. Saving files";

# prepare data for saving
wl = num2str(lambda0(i));
ExAbs = pinch(EFxAbs(1:length(x),1:length(z)));
HxAbs = pinch(HFxAbs(1:length(x),1:length(z)));
EyAbs = pinch(EFyAbs(1:length(x),1:length(z)));
HyAbs = pinch(HFyAbs(1:length(x),1:length(z)));
EzAbs = pinch(EFzAbs(1:length(x),1:length(z)));
HzAbs = pinch(HFzAbs(1:length(x),1:length(z)));

ExArg = pinch(EFxArg(1:length(x),1:length(z)));
HxArg = pinch(HFxArg(1:length(x),1:length(z)));
EyArg = pinch(EFyArg(1:length(x),1:length(z)));
HyArg = pinch(HFyArg(1:length(x),1:length(z)));
EzArg = pinch(EFzArg(1:length(x),1:length(z)));
HzArg = pinch(HFzArg(1:length(x),1:length(z)));

Ei = pinch(EFH(1:length(x),1:length(z)));
Hi = pinch(HFH(1:length(x),1:length(z)));

# clear data files
rm(f_name + "-wl" + wl + "-AbsEx.txt");
rm(f_name + "-wl" + wl + "-AbsHx.txt");
rm(f_name + "-wl" + wl + "-AbsEy.txt");
rm(f_name + "-wl" + wl + "-AbsHy.txt");
rm(f_name + "-wl" + wl + "-AbsEz.txt");
```

```
rm(f_name + "-wl" + wl + "-AbsHz.txt");

rm(f_name + "-wl" + wl + "-ArgEx.txt");
rm(f_name + "-wl" + wl + "-ArgHx.txt");
rm(f_name + "-wl" + wl + "-ArgEy.txt");
rm(f_name + "-wl" + wl + "-ArgHy.txt");
rm(f_name + "-wl" + wl + "-ArgEz.txt");
rm(f_name + "-wl" + wl + "-ArgHz.txt");

rm(f_name + "-wl" + wl + "-EFH.txt");
rm(f_name + "-wl" + wl + "-HFH.txt");

# save data to files
write(f_name + "-wl" + wl + "-AbsEx.txt", num2str([0, transpose(x); z, transpose(
    ExAbs)]));
write(f_name + "-wl" + wl + "-AbsHx.txt", num2str([0, transpose(x); z, transpose(
    HxAbs)]));
write(f_name + "-wl" + wl + "-AbsEy.txt", num2str([0, transpose(x); z, transpose(
    EyAbs)]));
write(f_name + "-wl" + wl + "-AbsHy.txt", num2str([0, transpose(x); z, transpose(
    HyAbs)]));
write(f_name + "-wl" + wl + "-AbsEz.txt", num2str([0, transpose(x); z, transpose(
    EzAbs)]));
write(f_name + "-wl" + wl + "-AbsHz.txt", num2str([0, transpose(x); z, transpose(
    HzAbs)]));

write(f_name + "-wl" + wl + "-ArgEx.txt", num2str([0, transpose(x); z, transpose(
    ExArg)]));
write(f_name + "-wl" + wl + "-ArgHx.txt", num2str([0, transpose(x); z, transpose(
    HxArg)]));
write(f_name + "-wl" + wl + "-ArgEy.txt", num2str([0, transpose(x); z, transpose(
```

```
        EyArg)]));
    write(f_name + "-wl" + wl + "-ArgHy.txt", num2str([0, transpose(x); z, transpose(
        HyArg)]));
    write(f_name + "-wl" + wl + "-ArgEz.txt", num2str([0, transpose(x); z, transpose(
        EzArg)]));
    write(f_name + "-wl" + wl + "-ArgHz.txt", num2str([0, transpose(x); z, transpose(
        HzArg)]));

    write(f_name + "-wl" + wl + "-EFH.txt", num2str([0, transpose(x); z, transpose(Ei)])
        );
    write(f_name + "-wl" + wl + "-HFH.txt", num2str([0, transpose(x); z, transpose(Hi)])
        );
}

?"Done";
```

Appendix C

Numerical local field simulations using Lumerical FDTD

This section contains instructions on using Lumerical FDTD to obtain the scattering response of spherical and dimer antennas under focused beam illumination using the local field technique. The steps required are as follows:

1. Determine the amplitude and phase of the incident beam at the selected points in space, using the MATLAB script file given in C.1

2. Input the amplitude and phase of the incident beam obtained in step 1 into the dipole sources, without and without the resonator in place (referred to as the "source" and "scatt" files, respectively), using the script file given in C.2 and run these files

3. Run post-processing scripts to extract the scattering response, given in C.3, and the field plots, given in C.4

All simulation files and script files used to generate the figures in chapter 5 are available for download online through Google Drive. The field plots should be extracted using the

"field" *.fsp files, where the dipole sources are placed further away from the scatterer. We implemented a three dimensional simulation in which the resonator of interest was placed at the origin. The electric and magnetic fields for RP and AP beams were calculated at eighteen points in space: $(\pm x, 0, 0)$, $(0, \pm y, 0)$; $(0, 0, \pm z)$; $(\pm x, \pm y, 0)$; $(\pm x, 0, \pm z)$; and $(0, \pm y, \pm z)$. Dipole sources were placed at each of these points and were oriented along the x-, y-, and z-directions, and the amplitudes were taken to match those of the incident beam at the points mentioned previously. The phases were tuned relative to the points in the third and fourth quadrants in the Cartesian plane. We used perfectly matched layer (PML) boundary conditions for the all boundaries. A non-uniform mesh was used with a minimum element size of 5nm in the region of the scatterer. In all cases the simulations were run until the fields decayed to less than one millionth of the incident field strength. To construct the spectral response, the simulations were run at single wavelengths with and without the scatterer in place, and the scattered fields were obtained by subtracting the incident fields from the scattered plus incident fields.

C.1 MATLAB script for determining the amplitude and phase of incident beam

```
%%%%
% This script file is used to determine the amplitude and phase of the incident beam at
    chosen points in space
% In this example, the beam is a focused azimuthally polarized beam
%%%%

% preliminary setup
clear;
c=3*10^8;
```

```
mu=1.257*10^(-6);
eps0=1/(c^2*mu);
Z=(mu/eps0)^0.5;

% numerical integral of angular spectrum of incident beam
Hfieldx = @(x,y,z,alpha,lambda) integral2(@(th,phi) -1i/lambda*(-cos(th).*cos(phi)).*
    sqrt(cos(th)).*sin(th).*exp(1i*2*pi/lambda*(sin(th).*cos(phi).*x+sin(th).*sin(phi).*
    y-cos(th).*z)),0,alpha,0,2*pi);
Hfieldy = @(x,y,z,alpha,lambda) integral2(@(th,phi) -1i/lambda*(-cos(th).*sin(phi)).*
    sqrt(cos(th)).*sin(th).*exp(1i*2*pi/lambda*(sin(th).*cos(phi).*x+sin(th).*sin(phi).*
    y-cos(th).*z)),0,alpha,0,2*pi);
Hfieldz = @(x,y,z,alpha,lambda) integral2(@(th,phi) -1i/lambda*(sin(th)).*sqrt(cos(th))
    .*sin(th).*exp(1i*2*pi/lambda*(sin(th).*cos(phi).*x+sin(th).*sin(phi).*y-cos(th).*z)
    ),0,alpha,0,2*pi);

Efieldx = @(x,y,z,alpha,lambda) integral2(@(th,phi) -1i/lambda*(-sin(phi)).*sqrt(cos(th)
    ).*sin(th).*exp(1i*2*pi/lambda*(sin(th).*cos(phi).*x+sin(th).*sin(phi).*y-cos(th).*z
    )),0,alpha,0,2*pi);
Efieldy = @(x,y,z,alpha,lambda) integral2(@(th,phi) -1i/lambda*(cos(phi)).*sqrt(cos(th))
    .*sin(th).*exp(1i*2*pi/lambda*(sin(th).*cos(phi).*x+sin(th).*sin(phi).*y-cos(th).*z)
    ),0,alpha,0,2*pi);

wavelength=1116; % wavelength to extract field properties in units of um -- chosen to be
     longer wavelength so amplitude and phase are relatively stable
alphaA=pi/3; % half-angle annular aperture of focusing lens

wl=wavelength*10^-9;
lda=wl;
freq=c/wl;

coord=150*10^-9;
```

```
% extract field properties at (-coord, 0 , 0)
xx=-coord;
yy=0;
zz=0;

Hx_nx00=Hfieldx(xx,yy,zz,alphaA,wl);
Hx_nx00A=round(abs(Hx_nx00)*10^-6/(abs(Hx_nx00)*10^-6));
Hx_nx00P=atan2(imag(Hx_nx00),real(Hx_nx00))*180/pi-atan2(imag(Hx_nx00),real(Hx_nx00))
    *180/pi;

Hy_nx00=Hfieldy(xx,yy,zz,alphaA,wl);
Hy_nx00A=round(abs(Hy_nx00)*10^-6/(abs(Hx_nx00)*10^-6));
Hy_nx00P=atan2(imag(Hy_nx00),real(Hy_nx00))*180/pi-atan2(imag(Hx_nx00),real(Hx_nx00))
    *180/pi;

Hz_nx00=Hfieldz(xx,yy,zz,alphaA,wl);
Hz_nx00A=round(abs(Hz_nx00)*10^-6/(abs(Hx_nx00)*10^-6));
Hz_nx00P=atan2(imag(Hz_nx00),real(Hz_nx00))*180/pi-atan2(imag(Hx_nx00),real(Hx_nx00))
    *180/pi;

% extract field properties at other points relative to (-coord, 0, 0) -- input these
    properties into dipole sources
% change values of xx, yy, and zz to obtain field properties at all points of interest
xx=0;
yy=-coord;
zz=-coord;

Hx_=Hfieldx(xx,yy,zz,alphaA,wl);
Hx_Amplitude=round(abs(Hx_)*10^-6/(abs(Hx_nx00)*10^-6))
Hx_Phase=atan2(imag(Hx_),real(Hx_))*180/pi-atan2(imag(Hx_nx00),real(Hx_nx00))*180/pi
```

```
Hy_=Hfieldy(xx,yy,zz,alphaA,wl);
Hy_A=round(abs(Hy_)*10^-6/(abs(Hx_nx00)*10^-6))
Hy_P=atan2(imag(Hy_),real(Hy_))*180/pi-atan2(imag(Hx_nx00),real(Hx_nx00))*180/pi

Hz_=Hfieldz(xx,yy,zz,alphaA,wl);
Hz_Amplitude=round(abs(Hz_)*10^-6/(abs(Hx_nx00)*10^-6))
Hz_Phase=atan2(imag(Hz_),real(Hz_))*180/pi-atan2(imag(Hx_nx00),real(Hx_nx00))*180/pi
```

C.2 Script file for setting the dipole amplitude and phase

```
#####
# This script file is used to set the dipole amplitude and phase for the numerical local
     field simulation
#####

# (x,0,0)
select("NA source x_x00");
set("amplitude",1);
set("phase",0);
#set("x",0.22e-6);
#set("y",0);
#set("z",0);

select("NA source x_nx00");
set("amplitude",1);
set("phase",180);
#set("x",-0.22e-6);
#set("y",0);
#set("z",0);

select("NA source z_x00");
set("amplitude",3);
set("phase",-90);
#set("x",0.22e-6);
#set("y",0);
#set("z",0);
```

```
select("NA source z_nx00");
set("amplitude",3);
set("phase",-90);
#set("x",-0.22e-6);
#set("y",0);
#set("z",0);

# (0,y,0)
select("NA source y_0y0");
set("amplitude",1);
set("phase",180);
#set("x",0);
#set("y",0.22e-6);
#set("z",0);

select("NA source y_0ny0");
set("amplitude",1);
set("phase",0);
#set("x",0);
#set("y",-0.22e-6);
#set("z",0);

select("NA source z_0y0");
set("amplitude",3);
set("phase",-90);
#set("x",0);
#set("y",0.22e-6);
#set("z",0);

select("NA source z_0ny0");
set("amplitude",3);
```

```
set("phase",-90);
#set("x",0);
#set("y",-0.22e-6);
#set("z",0);

# (0,0,z)
select("NA source z_00z");
set("amplitude",3);
set("phase",-125);
#set("x",0);
#set("y",0);
#set("z",-0.22e-6);

select("NA source z_00nz");
set("amplitude",3);
set("phase",-55);
#set("x",0);
#set("y",0);
#set("z",-0.22e-6);

# (x,y,0)
select("NA source x_xy0");
set("amplitude",1);
set("phase",180);
#set("x",0.22e-6);
#set("y",0.22e-6);
#set("z",0);

select("NA source x_nxy0");
set("amplitude",1);
set("phase",0);
```

```
#set("x",-0.22e-6);
#set("y",0.22e-6);
#set("z",0);

select("NA source x_xny0");
set("amplitude",1);
set("phase",180);
#set("x",0.22e-6);
#set("y",-0.22e-6);
#set("z",0);

select("NA source x_nxny0");
set("amplitude",1);
set("phase",0);
#set("x",-0.22e-6);
#set("y",-0.22e-6);
#set("z",0);

select("NA source y_xy0");
set("amplitude",1);
set("phase",180);
#set("x",0.22e-6);
#set("y",0.22e-6);
#set("z",0);

select("NA source y_nxy0");
set("amplitude",1);
set("phase",180);
#set("x",-0.22e-6);
#set("y",0.22e-6);
#set("z",0);
```

```
select("NA source y_xny0");
set("amplitude",0.75);
#set("x",0.22e-6);
#set("y",-0.22e-6);
#set("z",0);

select("NA source y_nxny0");
set("amplitude",1);
set("phase",0);
#set("x",-0.22e-6);
#set("y",-0.22e-6);
#set("z",0);

select("NA source z_xy0");
set("amplitude",3);
set("phase",-90);
#set("x",0.22e-6);
#set("y",0.22e-6);
#set("z",0);

select("NA source z_nxy0");
set("amplitude",3);
set("phase",-90);
#set("x",-0.22e-6);
#set("y",0.22e-6);
#set("z",0);

select("NA source z_xny0");
set("amplitude",3);
set("phase",-90);
```

```
#set("x",0.22e-6);
#set("y",-0.22e-6);
#set("z",0);

select("NA source z_nxny0");
set("amplitude",3);
set("phase",-90);
#set("x",-0.22e-6);
#set("y",-0.22e-6);
#set("z",0);

# (x,0,z)
select("NA source x_x0z");
set("amplitude",1);
set("phase",144);
#set("x",0.22e-6);
#set("y",0);
#set("z",0.22e-6);

select("NA source x_nx0z");
set("amplitude",1);
set("phase",-36);
#set("x",-0.22e-6);
#set("y",0);
#set("z",0.22e-6);

select("NA source x_x0nz");
set("amplitude",1);
set("phase",-144);
#set("x",0.22e-6);
#set("y",0);
```

```
#set("z",-0.22e-6);

select("NA source x_nx0nz");
set("amplitude",1);
set("phase",36);
#set("x",-0.22e-6);
#set("y",0);
#set("z",-0.22e-6);

select("NA source z_x0z");
set("amplitude",3);
set("phase",-125);
#set("x",0.22e-6);
#set("y",0);
#set("z",0.22e-6);

select("NA source z_nx0z");
set("amplitude",3);
set("phase",-125);
#set("x",-0.22e-6);
#set("y",0);
#set("z",0.22e-6);

select("NA source z_x0nz");
set("amplitude",3);
set("phase",-55);
#set("x",0.22e-6);
#set("y",0);
#set("z",-0.22e-6);

select("NA source z_nx0nz");
```

```
set("amplitude",3);
set("phase",-55);
#set("x",-0.22e-6);
#set("y",0);
#set("z",-0.22e-6);

# (0,y,z)
select("NA source y_0yz");
set("amplitude",1);
set("phase",144);
#set("x",0);
#set("y",0.22e-6);
#set("z",0.22e-6);

select("NA source y_0nyz");
set("amplitude",1);
set("phase",-36);
#set("x",0);
#set("y",-0.22e-6);
#set("z",0.22e-6);

select("NA source y_0ynz");
set("amplitude",1);
set("phase",-144);
#set("x",0);
#set("y",0.22e-6);
#set("z",-0.22e-6);

select("NA source y_0nynz");
set("amplitude",1);
set("phase",36);
```

```
#set("x",0);
#set("y",-0.22e-6);
#set("z",-0.22e-6);

select("NA source z_0yz");
set("amplitude",3);
set("phase",-125);
#set("x",0);
#set("y",0.22e-6);
#set("z",0.22e-6);

select("NA source z_0nyz");
set("amplitude",3);
set("phase",-125);
#set("x",0);
#set("y",-0.22e-6);
#set("z",0.22e-6);

select("NA source z_0ynz");
set("amplitude",3);
set("phase",-55);
#set("x",0);
#set("y",0.22e-6);
#set("z",-0.22e-6);

select("NA source z_0nynz");
set("amplitude",3);
set("phase",-55);
#set("x",0);
#set("y",-0.22e-6);
#set("z",-0.22e-6);
```

C.3 Script file for extracting the scattering response

This script was adapted from the Lumerical Custom TFSF example.

```
#####
# This script file is used to extract the scattering response of an arbitrary resonator
# using the numerical local field simulation method
# This script should be run after the "source" and "scatt" simulations are complete
#####

# preliminary sertup
clear;
source_axis="z"; # the source is incident along the z-axis

# load data from monitors
y2x=getdata("scat::y2","x");
y2z=getdata("scat::y2","z");
aeray=(max(y2x)-min(y2x)) *(max(y2z)-min(y2z)); # area of the y monitor

z2x=getdata("scat::z2","x");
z2y=getdata("scat::z2","y");
areaz=(max(z2x)-min(z2x)) *(max(z2y)-min(z2y)); # area of the z monitor

# obtain electric and magnetic fields and power
if (havedata("scat::x1")) {
   mx=1;e_ref_x1=getresult("scat::x1","E");
   h_ref_x1=getresult("scat::x1","H");
}
e_ref_x2=getresult("scat::x2","E");
h_ref_x2=getresult("scat::x2","H");
if(source_axis=="x"){
   temp =real(pinch(e_ref_x2.Ey*conj(h_ref_x2.Hz)-e_ref_x2.Ez*conj(h_ref_x2.Hy)));
```

```
   ps=0.5*integrate(temp,1:2,x2y,x2z);
   area=areax;}

if (havedata("scat::y1")) {
   my=1;e_ref_y1=getresult("scat::y1","E");
   h_ref_y1=getresult("scat::y1","H");}
e_ref_y2=getresult("scat::y2","E");
h_ref_y2=getresult("scat::y2","H");
if(source_axis=="y"){
   temp =real(pinch(e_ref_y2.Ez*conj(h_ref_y2.Hx)-e_ref_y2.Ex*conj(h_ref_y2.Hz)));
   ps=0.5*integrate(temp,1:2,y2x,y2z);
   area=aeray;
}

if (havedata("scat::z1")) {
   mz=1;e_ref_z1=getresult("scat::z1","E");
   h_ref_z1=getresult("scat::z1","H");
}
e_ref_z2=getresult("scat::z2","E");
h_ref_z2=getresult("scat::z2","H");

if(source_axis=="z"){
   temp =real(pinch(e_ref_z2.Ex*conj(h_ref_z2.Hy)-e_ref_z2.Ey*conj(h_ref_z2.Hx)));
   ps=0.5*integrate(temp,1:2,z2x,z2y);
   area=areaz;
}

ave_intensity=ps/area; # calculate the average intensity

##################
# --- INPUT ---
```

```
# load simulation with the resonator
load("AP-Dimerz-Scatt");

#obtain E,H
if(mx==1){e_scatter_x1=getresult("scat::x1","E");h_scatter_x1=getresult("scat::x1","H")
    ;}
   e_scatter_x2=getresult("scat::x2","E");h_scatter_x2=getresult("scat::x2","H");
if(my==1){e_scatter_y1=getresult("scat::y1","E");h_scatter_y1=getresult("scat::y1","H")
    ;}
   e_scatter_y2=getresult("scat::y2","E");h_scatter_y2=getresult("scat::y2","H");
if(mz==1){e_scatter_z1=getresult("scat::z1","E");h_scatter_z1=getresult("scat::z1","H")
    ;}
   e_scatter_z2=getresult("scat::z2","E");h_scatter_z2=getresult("scat::z2","H");
# obtain the scattered field
## x1 x2
if(mx==1){
   ey_x1=e_scatter_x1.Ey-e_ref_x1.Ey;
   ez_x1=e_scatter_x1.Ez-e_ref_x1.Ez;
   hy_x1=h_scatter_x1.Hy-h_ref_x1.Hy;
   hz_x1=h_scatter_x1.Hz-h_ref_x1.Hz;}
ey_x2=e_scatter_x2.Ey-e_ref_x2.Ey;
ez_x2=e_scatter_x2.Ez-e_ref_x2.Ez;
hy_x2=h_scatter_x2.Hy-h_ref_x2.Hy;
hz_x2=h_scatter_x2.Hz-h_ref_x2.Hz;
## y1 y2
if(my==1){
   ex_y1=e_scatter_y1.Ex-e_ref_y1.Ex;
   ez_y1=e_scatter_y1.Ez-e_ref_y1.Ez;
   hx_y1=h_scatter_y1.Hx-h_ref_y1.Hx;
   hz_y1=h_scatter_y1.Hz-h_ref_y1.Hz;}
ex_y2=e_scatter_y2.Ex-e_ref_y2.Ex;
```

```
ez_y2=e_scatter_y2.Ez-e_ref_y2.Ez;
hx_y2=h_scatter_y2.Hx-h_ref_y2.Hx;
hz_y2=h_scatter_y2.Hz-h_ref_y2.Hz;
##z1 z2
if(mz==1){
   ex_z1=e_scatter_z1.Ex-e_ref_z1.Ex;
   ey_z1=e_scatter_z1.Ey-e_ref_z1.Ey;
   hx_z1=h_scatter_z1.Hx-h_ref_z1.Hx;
   hy_z1=h_scatter_z1.Hy-h_ref_z1.Hy;}
ex_z2=e_scatter_z2.Ex-e_ref_z2.Ex;
ey_z2=e_scatter_z2.Ey-e_ref_z2.Ey;
hx_z2=h_scatter_z2.Hx-h_ref_z2.Hx;
hy_z2=h_scatter_z2.Hy-h_ref_z2.Hy;
###### power
su=1;#used for calculating cross sections
##scattering
#x monitors
if(mx==1){
   temp =real(pinch(ey_x1*conj(hz_x1)-ez_x1*conj(hy_x1)));
   px1=su*integrate(temp,1:2,x2y,x2z);}
temp =real(pinch(ey_x2*conj(hz_x2)-ez_x2*conj(hy_x2)));
px2=su*integrate(temp,1:2,x2y,x2z);
#y monitors
if(my==1){
   temp =real(pinch(ez_y1*conj(hx_y1)-ex_y1*conj(hz_y1)));
   py1=su*integrate(temp,1:2,y2x,y2z);}
temp =real(pinch(ez_y2*conj(hx_y2)-ex_y2*conj(hz_y2)));
py2=su*integrate(temp,1:2,y2x,y2z);
#z monitors
if(mz==1){
   temp =real(pinch(ex_z1*conj(hy_z1)-ey_z1*conj(hx_z1)));
```

```
   pz1=su*integrate(temp,1:2,z2x,z2y);}
temp =real(pinch(ex_z2*conj(hy_z2)-ey_z2*conj(hx_z2)));
pz2=su*integrate(temp,1:2,z2x,z2y);

#totaling the power, for the case the source is along z axis
if( (mx==1) and (mz==1) ){
   P_scat=-px1+px2-py1+py2-pz1+pz2;
#   P_tot=px1_tot-px2_tot+py1_tot-py2_tot+pz1_tot-pz2_tot;
}
if( (mx==0) and (my==0) ){
   P_scat= px2+px2+py2+py2-pz1+pz2;
#   P_tot=     -2*px2_tot+py1_tot-py2_tot+pz1_tot-pz2_tot;
}
if( (mx==1) and (mz==0) ){
   P_scat=-px1+px2-py1+py2+pz2+pz2;
   P_tot=px1_tot-px2_tot+py1_tot-py2_tot      -2*pz2_tot;
}
if( (mx==0) and (mz==0) ){
   P_scat= px2+px2-py1+py2+pz2+pz2;
   P_tot=     -2*px2_tot+py1_tot-py2_tot      -2*pz2_tot;
}
scat_cross=P_scat;
f=getdata("scat::x1","f");

# write data (wavelength and qualitative scattered power) to file
write("Pscat_localfield_AP_dimerx.txt",num2str([(c/f*1e6),scat_cross]));
```

C.4 Script file for extracting field plots

```
# This file is used to save data of the electric
# and magentic field amplitude and phase
# This script should be run after the scatt file is complete

clear;

# --- INPUT --- #
# load scatt file
load("AP-dimerz-scatt");

# --- INPUT!!! ---
# name of file to save data to
f_name = "AP-Dimerz-LocalField";

?"Importing scatt data";

# load the electric and magnetic fields in the xz-plane from the relevant field monitor
Esc = getresult("y normal monitor","E");
Hsc = getresult("y normal monitor","H");

# extract the wavelength, x, and z coordinates from the field monitor
lambda = Hsc.lambda;
x = Hsc.x;
z = Hsc.z;

# --- INPUT!!! ---
# Choose the wavelength to extract data at
lambda0=512e-9;
```

```
wl = num2str(lambda0*10^9);

# Find the index of the correct wavelength since this is a broadband source
indexl = find(lambda, lambda0);

# remove irrelevant information from electric and magnetic field data
Esc = pinch(Esc.E);
Hsc = pinch(Hsc.H);

Exsc = pinch(Esc(1:length(x),1:length(z),indexl,1));
Eysc = pinch(Esc(1:length(x),1:length(z),indexl,2));
Ezsc = pinch(Esc(1:length(x),1:length(z),indexl,3));

Hxsc = pinch(Hsc(1:length(x),1:length(z),indexl,1));
Hysc = pinch(Hsc(1:length(x),1:length(z),indexl,2));
Hzsc = pinch(Hsc(1:length(x),1:length(z),indexl,3));

?"Pre-processing";

Exfinal=Exsc;
Eyfinal=Eysc;
Ezfinal=Ezsc;

Hxfinal=Hxsc;
Hyfinal=Hysc;
Hzfinal=Hzsc;

# calculate the norm of the scattered electric and magnetic fields
EfinalN = sqrt((abs(Exfinal)^2)+(abs(Eyfinal)^2)+(abs(Ezfinal)^2));
HfinalN = sqrt((abs(Hxfinal)^2)+(abs(Hyfinal)^2)+(abs(Hzfinal)^2));
```

```
# calculate the norm of the incident electric and magnetic fields
EsN = sqrt((abs(Exs)^2)+(abs(Eys)^2)+(abs(Ezs)^2));
HsN = sqrt((abs(Hxs)^2)+(abs(Hys)^2)+(abs(Hzs)^2));

# calculate the absolute value of the scattered electric and magnetic field components
EFxAbs = abs(Exfinal);
HFxAbs = abs(Hxfinal);
EFyAbs = abs(Eyfinal);
HFyAbs = abs(Hyfinal);
EFzAbs = abs(Ezfinal);
HFzAbs = abs(Hzfinal);

# calculate the phase of the scattered electric and magnetic field components
EFxArg = angle(Exfinal);
HFxArg = angle(Hxfinal);
EFyArg = angle(Eyfinal);
HFyArg = angle(Hyfinal);
EFzArg = angle(Ezfinal);
HFzArg = angle(Hzfinal);

# calculate the electric and magnetic field intensity enhancement
EFH = (EfinalN/EsN)^2;
HFH = (HfinalN/HsN)^2;

?"Data is pre-processed. Saving files";

# prepare data for saving
wl = num2str(lambda0(i));
ExAbs = pinch(EFxAbs(1:length(x),1:length(z)));
HxAbs = pinch(HFxAbs(1:length(x),1:length(z)));
EyAbs = pinch(EFyAbs(1:length(x),1:length(z)));
```

```
HyAbs = pinch(HFyAbs(1:length(x),1:length(z)));
EzAbs = pinch(EFzAbs(1:length(x),1:length(z)));
HzAbs = pinch(HFzAbs(1:length(x),1:length(z)));

ExArg = pinch(EFxArg(1:length(x),1:length(z)));
HxArg = pinch(HFxArg(1:length(x),1:length(z)));
EyArg = pinch(EFyArg(1:length(x),1:length(z)));
HyArg = pinch(HFyArg(1:length(x),1:length(z)));
EzArg = pinch(EFzArg(1:length(x),1:length(z)));
HzArg = pinch(HFzArg(1:length(x),1:length(z)));

Ei = pinch(EFH(1:length(x),1:length(z)));
Hi = pinch(HFH(1:length(x),1:length(z)));

# clear data files
rm(f_name + "-wl" + wl + "-AbsEx.txt");
rm(f_name + "-wl" + wl + "-AbsHx.txt");
rm(f_name + "-wl" + wl + "-AbsEy.txt");
rm(f_name + "-wl" + wl + "-AbsHy.txt");
rm(f_name + "-wl" + wl + "-AbsEz.txt");
rm(f_name + "-wl" + wl + "-AbsHz.txt");

rm(f_name + "-wl" + wl + "-ArgEx.txt");
rm(f_name + "-wl" + wl + "-ArgHx.txt");
rm(f_name + "-wl" + wl + "-ArgEy.txt");
rm(f_name + "-wl" + wl + "-ArgHy.txt");
rm(f_name + "-wl" + wl + "-ArgEz.txt");
rm(f_name + "-wl" + wl + "-ArgHz.txt");

rm(f_name + "-wl" + wl + "-EFH.txt");
rm(f_name + "-wl" + wl + "-HFH.txt");
```

```
# save data to files
write(f_name + "-wl" + wl + "-AbsEx.txt", num2str([0, transpose(x); z, transpose(ExAbs)
    ]));
write(f_name + "-wl" + wl + "-AbsHx.txt", num2str([0, transpose(x); z, transpose(HxAbs)
    ]));
write(f_name + "-wl" + wl + "-AbsEy.txt", num2str([0, transpose(x); z, transpose(EyAbs)
    ]));
write(f_name + "-wl" + wl + "-AbsHy.txt", num2str([0, transpose(x); z, transpose(HyAbs)
    ]));
write(f_name + "-wl" + wl + "-AbsEz.txt", num2str([0, transpose(x); z, transpose(EzAbs)
    ]));
write(f_name + "-wl" + wl + "-AbsHz.txt", num2str([0, transpose(x); z, transpose(HzAbs)
    ]));

write(f_name + "-wl" + wl + "-ArgEx.txt", num2str([0, transpose(x); z, transpose(ExArg)
    ]));
write(f_name + "-wl" + wl + "-ArgHx.txt", num2str([0, transpose(x); z, transpose(HxArg)
    ]));
write(f_name + "-wl" + wl + "-ArgEy.txt", num2str([0, transpose(x); z, transpose(EyArg)
    ]));
write(f_name + "-wl" + wl + "-ArgHy.txt", num2str([0, transpose(x); z, transpose(HyArg)
    ]));
write(f_name + "-wl" + wl + "-ArgEz.txt", num2str([0, transpose(x); z, transpose(EzArg)
    ]));
write(f_name + "-wl" + wl + "-ArgHz.txt", num2str([0, transpose(x); z, transpose(HzArg)
    ]));

write(f_name + "-wl" + wl + "-EFH.txt", num2str([0, transpose(x); z, transpose(Ei)]));
write(f_name + "-wl" + wl + "-HFH.txt", num2str([0, transpose(x); z, transpose(Hi)]));
```

```
?"Done";
```

Bibliography

[1] N. Mojarad, G. Zumofen, V. Sandoghdar, and M. Agio, *Metal nanoparticles in strongly confined beams: transmission, reflection and absorption*, *Journal European Optical Society-Rapid Publications* **4** (2009) 9014.

[2] P. Woźniak, P. Banzer, and G. Leuchs, *Selective switching of individual multipole resonances in single dielectric nanoparticles*, *Laser & Photonics Reviews* **9** (2015), no. 2 231–240.

[3] D. Schurig, J. Mock, B. Justice, S. A. Cummer, J. B. Pendry, A. Starr, and D. Smith, *Metamaterial electromagnetic cloak at microwave frequencies*, *Science* **314** (2006), no. 5801 977–980.

[4] J. Rowling, *Harry potter and the sorcerer's stone*, 1998.

[5] A. Alù and N. Engheta, *Cloaking and transparency for collections of particles with metamaterial and plasmonic covers*, *Optics Express* **15** (2007), no. 12 7578.

[6] T. Coenen, F. B. Arango, A. F. Koenderink, and A. Polman, *Directional emission from a single plasmonic scatterer*, *Nature Communications* **5** (2014) 3250.

[7] I. M. Hancu, A. G. Curto, M. Castro-Lopez, M. Kuttge, and N. F. van Hulst, *Multipolar Interference for Directed Light Emission*, *Nano Letters* **14** (Jan., 2014) 166–171.

[8] P. P. Iyer, N. A. Butakov, and J. A. Schuller, *Reconfigurable semiconductor phased-array metasurfaces*, *ACS Photonics* **2** (2015), no. 8 1077–1084.

[9] V. Veselago, L. Braginsky, V. Shklover, and C. Hafner, *Negative refractive index materials*, *Journal of Computational and Theoretical Nanoscience* **3** (2006), no. 2 189–218.

[10] X. Zhang and Z. Liu, *Superlenses to overcome the diffraction limit*, *Nature materials* **7** (2008), no. 6 435–441.

[11] P. Grahn, A. Shevchenko, and M. Kaivola, *Electric dipole-free interaction of visible light with pairs of subwavelength-size silver particles*, *Physical Review B* **86** (July, 2012) 035419.

[12] C. Menzel, E. Hebestreit, S. Mühlig, C. Rockstuhl, S. Burger, F. Lederer, and T. Pertsch, *The spectral shift between near- and far-field resonances of optical nano-antennas*, *Optics Express* **22** (Apr., 2014) 9971.

[13] D. Gómez, Z. Teo, M. Altissimo, T. Davis, S. Earl, and A. Roberts, *The dark side of plasmonics*, *Nano Letters* **13** (2013), no. 8 3722–3728.

[14] K. Sakai, K. Nomura, T. Yamamoto, and K. Sasaki, *Excitation of multipole plasmons by optical vortex beams*, *Scientific Reports* **5** (2015).

[15] A. Yanai, M. Grajower, G. M. Lerman, M. Hentschel, H. Giessen, and U. Levy, *Near-and far-field properties of plasmonic oligomers under radially and azimuthally polarized light excitation*, *ACS Nano* **8** (2014), no. 5 4969–4974.

[16] S. Orlov, U. Peschel, T. Bauer, and P. Banzer, *Analytical expansion of highly focused vector beams into vector spherical harmonics and its application to mie scattering*, *Physical Review A* **85** (2012), no. 6 063825.

[17] Z. Xi, L. Wei, A. Adam, and H. Urbach, *Broadband active tuning of unidirectional scattering from nanoantenna using combined radially and azimuthally polarized beams*, *Optics letters* **41** (2016), no. 1 33–36.

[18] M. Neugebauer, P. Woźniak, A. Bag, G. Leuchs, and P. Banzer, *Polarization-controlled directional scattering for nanoscopic position sensing*, *Nature communications* **7** (2016).

[19] G. Mie, *Beiträge zur optik trüber medien, speziell kolloidaler metallösungen*, *Annalen der physik* **330** (1908), no. 3 377–445.

[20] G. Gouesbet and G. Gréhan, *Generalized Lorenz-Mie Theories*. Springer Science & Business Media, 2011.

[21] S. Colak, C. Yeh, and L. W. Casperson, *Scattering of focused beams by tenuous particles*, *Applied optics* **18** (1979), no. 3 294–302.

[22] A. Alù and N. Engheta, *Guided propagation along quadrupolar chains of plasmonic nanoparticles*, *Physical Review B* **79** (June, 2009) 235412.

[23] A. Alù and N. Engheta, *Polarizabilities and effective parameters for collections of spherical nanoparticles formed by pairs of concentric double-negative, single-negative, and/or double-positive metamaterial layers*, *Journal of Applied Physics* **97** (May, 2005) 094310.

[24] I. Sersic, C. Tuambilangana, T. Kampfrath, and A. F. Koenderink, *Magnetoelectric point scattering theory for metamaterial scatterers*, *Physical Review B* **83** (June, 2011) 245102.

[25] F. Bernal Arango, T. Coenen, and A. F. Koenderink, *Underpinning Hybridization Intuition for Complex Nanoantennas by Magnetoelectric Quadrupolar Polarizability Retrieval*, *ACS Photonics* **1** (May, 2014) 444–453.

[26] S. Mühlig, C. Menzel, C. Rockstuhl, and F. Lederer, *Multipole analysis of meta-atoms*, *Metamaterials* **5** (2011), no. 2 64–73.

[27] L. Novotny and B. Hecht, *Principles of Nano-Optics*. Cambridge University Press, 2012.

[28] C. F. Bohren and D. R. Huffman, *Absorption and scattering of light by small particles*. John Wiley & Sons, 2008.

[29] J. A. Lock, *Partial-wave expansions of angular spectra of plane waves*, *JOSA A* **23** (2006), no. 11 2803–2809.

[30] J. Goodman, *Introduction to Fourier Optics, McGraw-Hill Physical and Quantum Electronics Series*. McGraw-Hill Book Co., New York, New York, 1968.

[31] D. Han, Y. Lai, K. H. Fung, Z.-Q. Zhang, and C. Chan, *Negative group velocity from quadrupole resonance of plasmonic spheres*, *Physical Review B* **79** (2009), no. 19 195444.

[32] N. A. Butakov and J. A. Schuller, *Designing multipolar resonances in dielectric metamaterials*, *Scientific Reports* **6** (2016).

[33] K. Sendur, W. Challener, and O. Mryasov, *Interaction of spherical nanoparticles with a highly focused beam of light*, *Optics express* **16** (2008), no. 5 2874–2886.

[34] N. M. Mojarad and M. Agio, *Tailoring the excitation of localized surface plasmon-polariton resonances by focusing radially-polarized beams*, *Optics Express* **17** (2009), no. 1 117–122.

[35] L. S. Slaughter, Y. Wu, B. A. Willingham, P. Nordlander, and S. Link, *Effects of symmetry breaking and conductive contact on the plasmon coupling in gold nanorod dimers*, *ACS Nano* **4** (2010), no. 8 4657–4666.

[36] S. Panaro, A. Nazir, C. Liberale, G. Das, H. Wang, F. De Angelis, R. Proietti Zaccaria, E. Di Fabrizio, and A. Toma, *Dark to bright mode conversion on dipolar nanoantennas: a symmetry-breaking approach*, *ACS Photonics* **1** (2014), no. 4 310–314.

[37] J. Sancho-Parramon and D. Jelovina, *Boosting fano resonances in single layered concentric core–shell particles*, *Nanoscale* **6** (2014), no. 22 13555–13564.

[38] T. H. Taminiau, S. Karaveli, N. F. Van Hulst, and R. Zia, *Quantifying the magnetic nature of light emission*, *Nature communications* **3** (2012) 979.

[39] A. G. Curto, T. H. Taminiau, G. Volpe, M. P. Kreuzer, R. Quidant, and N. F. van Hulst, *Multipolar radiation of quantum emitters with nanowire optical antennas*, *Nature Communications* **4** (Apr., 2013) 1750.

[40] E. Poutrina and A. Urbas, *Multipole analysis of unidirectional light scattering from plasmonic dimers*, *Journal of Optics* **16** (Nov., 2014) 114005.

[41] B. Rolly, J.-M. Geffrin, R. Abdeddaim, B. Stout, and N. Bonod, *Controllable emission of a dipolar source coupled with a magneto-dielectric resonant subwavelength scatterer*, *Scientific Reports* **3** (2013).

[42] C. Enkrich, M. Wegener, S. Linden, S. Burger, L. Zschiedrich, F. Schmidt, J. Zhou, T. Koschny, and C. Soukoulis, *Magnetic metamaterials at telecommunication and visible frequencies*, *Physical Review Letters* **95** (2005), no. 20 203901.

[43] C. Rockstuhl, F. Lederer, C. Etrich, T. Zentgraf, J. Kuhl, and H. Giessen, *On the reinterpretation of resonances in split-ring-resonators at normal incidence*, *Optics Express* **14** (2006), no. 19 8827–8836.

[44] N. Lindlein, R. Maiwald, H. Konermann, M. Sondermann, U. Peschel, and G. Leuchs, *A new 4π geometry optimized for focusing on an atom with a dipole-like radiation pattern*, *Laser Physics* **17** (2007), no. 7 927–934.

[45] N. J. Moore and M. A. Alonso, *Closed form formula for mie scattering of nonparaxial analogues of gaussian beams*, *Optics Express* **16** (2008), no. 8 5926–5933.

[46] P. Banzer, U. Peschel, S. Quabis, and G. Leuchs, *On the experimental investigation of the electric and magnetic response of a single nano-structure*, *Optics Express* **18** (2010), no. 10 10905–10923.

[47] J. Sancho-Parramon and S. Bosch, *Dark modes and fano resonances in plasmonic clusters excited by cylindrical vector beams*, *ACS Nano* **6** (2012), no. 9 8415–8423.

[48] X. Zambrana-Puyalto, X. Vidal, and G. Molina-Terriza, *Excitation of single multipolar modes with engineered cylindrically symmetric fields*, *Optics Express* **20** (2012), no. 22 24536–24544.

[49] X. Zambrana-Puyalto and G. Molina-Terriza, *The role of the angular momentum of light in mie scattering. excitation of dielectric spheres with laguerre–gaussian modes*, *Journal of Quantitative Spectroscopy and Radiative Transfer* **126** (2013) 50–55.

[50] M. Neugebauer, T. Bauer, P. Banzer, and G. Leuchs, *Polarization tailored light driven directional optical nanobeacon*, *Nano Letters* **14** (2014), no. 5 2546–2551.

[51] O. Demichel, M. Petit, G. Colas des Francs, A. Bouhelier, E. Hertz, F. Billard, F. de Fornel, and B. Cluzel, *Selective excitation of bright and dark plasmonic resonances of single gold nanorods*, *Optics Express* **22** (2014), no. 12 15088–15096.

[52] B. García-Cámara, J. F. Algorri, A. Cuadrado, V. Urruchi, J. M. Sánchez-Pena, R. Serna, and R. Vergaz, *All-optical nanometric switch based on the directional scattering of semiconductor nanoparticles*, *The Journal of Physical Chemistry C* **119** (2015), no. 33 19558–19564.

[53] K. E. Chong, I. Staude, A. James, J. Dominguez, S. Liu, S. Campione, G. S. Subramania, T. S. Luk, M. Decker, D. N. Neshev, *et. al.*, *Polarization-independent silicon metadevices for efficient optical wavefront control*, *Nano letters* **15** (2015), no. 8 5369–5374.

[54] P. P. Iyer, M. Pendharkar, and J. A. Schuller, *Electrically reconfigurable metasurfaces using heterojunction resonators*, *Advanced Optical Materials* **4** (2016), no. 10 1582–1588.

[55] C. Wang, Z. Jia, K. Zhang, Y. Zhou, R. Fan, X. Xiong, and R. Peng, *Broadband optical scattering in coupled silicon nanocylinders*, *Journal of Applied Physics* **115** (2014), no. 24 244312.

[56] D. Sikdar, W. Cheng, and M. Premaratne, *Optically resonant magneto-electric cubic nanoantennas for ultra-directional light scattering*, *Journal of Applied Physics* **117** (2015), no. 8 083101.

[57] P. Albella, T. Shibanuma, and S. A. Maier, *Switchable directional scattering of electromagnetic radiation with subwavelength asymmetric silicon dimers*, *Scientific Reports* **5** (2015).

[58] I. Sinev, I. Iorsh, A. Bogdanov, D. Permyakov, F. Komissarenko, I. Mukhin, A. Samusev, V. Valuckas, A. I. Kuznetsov, B. S. Luk'yanchuk, *et. al.*, *Polarization control over electric and magnetic dipole resonances of dielectric nanoparticles on metallic films*, *Laser & Photonics Reviews* **10** (2016), no. 5 799–806.

[59] H. Rubinsztein-Dunlop, A. Forbes, M. Berry, M. Dennis, D. L. Andrews, M. Mansuripur, C. Denz, C. Alpmann, P. Banzer, T. Bauer, *et. al.*, *Roadmap on structured light*, *Journal of Optics* **19** (2016), no. 1 013001.

[60] T. Bauer, S. Orlov, G. Leuchs, and P. Banzer, *Towards an optical far-field measurement of higher-order multipole contributions to the scattering response of nanoparticles*, *Applied Physics Letters* **106** (2015), no. 9 091108.

[61] G. Volpe, S. Cherukulappurath, R. Juanola Parramon, G. Molina-Terriza, and R. Quidant, *Controlling the optical near field of nanoantennas with spatial phase-shaped beams*, *Nano Letters* **9** (2009), no. 10 3608–3611.

[62] L. Novotny, M. Beversluis, K. Youngworth, and T. Brown, *Longitudinal field modes probed by single molecules*, *Physical Review Letters* **86** (2001), no. 23 5251.

[63] K. S. Youngworth and T. G. Brown, *Focusing of high numerical aperture cylindrical-vector beams*, *Optics Express* **7** (2000), no. 2 77–87.

[64] K. Kitamura, T. T. Xu, and S. Noda, *Investigation of electric field enhancement between metal blocks at the focused field generated by a radially polarized beam*, *Optics express* **21** (2013), no. 26 32217–32224.

[65] T. Das, P. P. Iyer, R. A. DeCrescent, and J. A. Schuller, *Beam engineering for selective and enhanced coupling to multipolar resonances*, *Physical Review B* **92** (2015), no. 24 241110.

[66] L. Wei, Z. Xi, N. Bhattacharya, and H. P. Urbach, *Excitation of the radiationless anapole mode*, *Optica* **3** (2016), no. 8 799–802.

[67] B. Richards and E. Wolf, *Electromagnetic diffraction in optical systems. ii. structure of the image field in an aplanatic system*, in *Proceedings of the Royal Society of London A: Mathematical, Physical and Engineering Sciences*, vol. 253, pp. 358–379, The Royal Society, 1959.

[68] "Lumerical, fdtd solutions." https://www.lumerical.com/tcad-products/fdtd/.

[69] R. M. Bakker, D. Permyakov, Y. F. Yu, D. Markovich, R. Paniagua-Domínguez, L. Gonzaga, A. Samusev, Y. Kivshar, B. Luk'yanchuk, and A. I. Kuznetsov, *Magnetic and electric hotspots with silicon nanodimers*, *Nano Letters* **15** (2015), no. 3 2137–2142.

[70] P. Albella, M. A. Poyli, M. K. Schmidt, S. A. Maier, F. Moreno, J. J. Sáenz, and J. Aizpurua, *Low-loss electric and magnetic field-enhanced spectroscopy with subwavelength silicon dimers*, *The Journal of Physical Chemistry C* **117** (2013), no. 26 13573–13584.

[71] U. Zywietz, M. K. Schmidt, A. B. Evlyukhin, C. Reinhardt, J. Aizpurua, and B. N. Chichkov, *Electromagnetic resonances of silicon nanoparticle dimers in the visible*, *ACS Photonics* **2** (2015), no. 7 913–920.

[72] S. Panaro, F. De Angelis, and A. Toma, *Dark and bright mode hybridization: From electric to magnetic fano resonances*, *Optics and Lasers in Engineering* **76** (2016) 64–69.

[73] A. Mirzaei and A. E. Miroshnichenko, *Electric and magnetic hotspots in dielectric nanowire dimers*, *Nanoscale* **7** (2015), no. 14 5963–5968.

[74] G. Boudarham, R. Abdeddaim, and N. Bonod, *Enhancing the magnetic field intensity with a dielectric gap antenna*, *Applied Physics Letters* **104** (2014), no. 2 021117.

[75] E. Almpanis and N. Papanikolaou, *Comparison of ag and si nanoparticle arrays: mimicking subwavelength plasmonic field concentrations with dielectric components*, *JOSA B* **33** (2016), no. 1 99–104.

[76] M. Kasperczyk, S. Person, D. Ananias, L. D. Carlos, and L. Novotny, *Excitation of magnetic dipole transitions at optical frequencies*, *Physical review letters* **114** (2015), no. 16 163903.

[77] Q. Zhan, *Cylindrical vector beams: from mathematical concepts to applications*, *Advances in Optics and Photonics* **1** (2009), no. 1 1–57.

[78] I. Alessandri and J. R. Lombardi, *Enhanced raman scattering with dielectrics*, *Chemical Reviews* (2016).

[79] G. Pirruccio, M. Ramezani, S. R.-K. Rodriguez, and J. G. Rivas, *Coherent control of the optical absorption in a plasmonic lattice coupled to a luminescent layer*, *Physical review letters* **116** (2016), no. 10 103002.

[80] W. Chen, D. C. Abeysinghe, R. L. Nelson, and Q. Zhan, *Plasmonic lens made of multiple concentric metallic rings under radially polarized illumination*, *Nano letters* **9** (2009), no. 12 4320–4325.

[81] K. Şendur, W. Challener, and O. Mryasov, *Interaction of spherical nanoparticles with a highly focused beam of light*, *Optics express* **16** (2008), no. 5 2874–2886.

[82] İ. R. Çapoğlu, A. Taflove, and V. Backman, *Generation of an incident focused light pulse in fdtd*, *Optics Express* **16** (2008), no. 23 19208–19220.

[83] İ. R. Çapoğlu, A. Taflove, and V. Backman, *Computation of tightly-focused laser beams in the fdtd method*, *Optics Express* **21** (2013), no. 1 87–101.

[84] J. C. Ranasinghesagara, C. K. Hayakawa, M. A. Davis, A. K. Dunn, E. O. Potma, and V. Venugopalan, *Rapid computation of the amplitude and phase of tightly focused optical fields distorted by scattering particles*, *JOSA A* **31** (2014), no. 7 1520–1530.

[85] W. Challener, I. Sendur, and C. Peng, *Scattered field formulation of finite difference time domain for a focused light beam in dense media with lossy materials*, *Optics express* **11** (2003), no. 23 3160–3170.

[86] K. Kitamura, K. Sakai, and S. Noda, *Finite-difference time-domain (fdtd) analysis on the interaction between a metal block and a radially polarized focused beam*, *Optics Express* **19** (2011), no. 15 13750–13756.

[87] A. Salandrino, S. Fardad, and D. N. Christodoulides, *Generalized mie theory of optical forces*, *JOSA B* **29** (2012), no. 4 855–866.

[88] J. M. Auñón and M. Nieto-Vesperinas, *Optical forces from evanescent bessel beams, multiple reflections, and kerker conditions in magnetodielectric spheres and cylinders*, *JOSA A* **31** (2014), no. 9 1984–1992.